The role of stem cell fusion in (re)programming somatic cells both in vitro and in vivo: implications for cardiac regeneration

by

Brian T. Freeman

A dissertation submitted in partial fulfillment of the requirements for the degree of

Doctor of Philosophy

(Biomedical Engineering)

at the

UNIVERSITY OF WISCONSIN-MADISON

2015

Date of final oral examination: 7/27/2015

The dissertation is approved by the following members of the Final Oral Committee:
M. Elizabeth Meyerand, Professor, Biomedical Engineering
Sean P. Palecek, Professor, Chemical and Biological Engineering
David J. Beebe, Professor, Biomedical Engineering
Peiman Hematti, Associate Professor, Medicine and Pediatrics
Timothy J. Kamp, Professor, Medicine and Public Health
Brenda M. Ogle, Associate Professor, Biomedical Engineering

Abstract

Every year hundreds of thousands of Americans will suffer a myocardial infarction, which makes it one of the most prevalent health problems in the United States. One promising therapy is the delivery of mesenchymal/multipotent stem/stromal cells (MSCs) to regions around the infarct, which has been shown to improve cardiac recovery. MSCs home to injured tissues and several mechanisms for MSC-based recovery have been proposed, including MSC differentiation into cardiac cells and the release of pro-survival signals from the MSCs. Some of these studies have reported evidence of cell fusion between stem cells and cardiac cells, but the impact of this cell fusion and subsequent (re)programming on cardiac function at the cellular and tissue scale is not well understood. This thesis describes three independent studies analyzing the affects of cell fusion between MSCs and cardiomyocytes both *in vivo* and *in vitro*. In the first study, the amount of fusion after MSC transplantation to the heart and other organ systems was quantified and fusion products were observed in the heart, liver, small intestine and stomach through fluorescent microscopy. Once MSC fusion was confirmed by the first study, the second study examined the affect MSC fusion has on the infarcted murine heart. This study found that augmenting fusion of MSCs in the infarcted heart hindered cardiac healing via decreased vascularization and immune modulation. The negative affect of cell fusion on cardiac function was unanticipated, which led to a final study that sought to uncover the transcriptional reprogramming that occurred after cell fusion by single-cell RNA-seq. The transcriptomes of fusion products

revealed extensive diversification after fusion and activation of latent pluripotency genes and oncogenes.

Table of Contents

List of Figures

microscopy) of human MSCs following two days on the TM patch and stained for MSC-marker CD105 (green) and DAPI (blue). Greater than 95% of cells imaged were CD105 positive. Regions with high intensity (CD105) indicate cells aligned with planes other than the focal plane, perhaps indicative of cells migrating into the patch. Scale bars are 50 μm. **B,** MSCs and VSV-G-transfected MSCs (vMSCs) fused with murine cells in an infarcted heart after delivery via TissueMend patch (TM). There was a significant increase in the percent of fusion products present in the TissueMend for untransfected MSCs (TM + MSCs), 22% $\pm$ 17% (10 images/area), compared to the TM only control with no cells, 2% $\pm$ 2% (10 images/area) (*, $P < 0.05$). The percent of fusion products present in the BorderZone increased as well for untransfected MSCs (14% $\pm$ 9%, 10 images/area), but it was not significantly different than the TM only control (0.2% $\pm$ 0.5%, 10 images/area). The percent of fusion products in the TissueMend and BorderZone increases (albeit not significantly) to 24% $\pm$ 16% and 23% $\pm$ 15% when the MSCs were transfected with VSV-G (TM + vMSC) prior to delivery (10 images/area)(**, $P < 0.01$, compared to the TM only control). There was no significant difference between the TM control and both MSC and vMSCs in the unhealthy heart and healthy heart regions. All percentages represent 10 randomly selected images for each region in the tissue sections. **C,** Representative images of murine heart following transplantation stained for human (red) and mouse (green) centromeres using FISH. The top row contains a field of view from the TissueMend patch; the bottom row contains a field of view from the BorderZone between the TissueMend and infarcted myocardium. Scale bars are 50 μm

Figure 3-2. **Detection of cell fusion in living mice. A,** Average bioluminescent radiance (photons/second/cm^2/steradian) of chest and abdomen of mice receiving MSCs 2 and 8 days following transplantation to the heart. **B,** Representative IVIS imaging of one control and two treated mice (Mouse 1, Mouse 3). **C,** Average bioluminescent radiance (photons/second/cm^2/steradian) of heart, stomach, small intestine, liver and kidney (n=4 mice). Signal from heart, stomach, and small intestine was significantly higher than that of corresponding control organs and kidney tissue of treated mice (** $P < 0.01$, * $P < 0.05$). **D,** Representative images for each organ. From top to bottom: photograph, bioluminescence emission, overlay. Scale bar equals 10 mm.

Figure 3-3. **Detection of cell fusion in living mice peaks at 1 week. A,** Average radiance of chest and abdomen of mice at 1, 2, 3 and 4 weeks following transplantation of MSCs to the

heart. Values were normalized to the week 1 average radiance. **B,** Representative IVIS image of a mouse at each time point.

Figure 3-4. **Frequency of fusion following delivery of vMSCs to healthy, noninfarcted, murine myocardium via TissueMend (TM) collagen-based patch.** VSV-G-transfected human MSCs (vMSCs) fused with recipient cells in the murine heart after delivery via TissueMend patch. **A,** Significantly more fusion products were detected in the TissueMend patch and BorderZone than in the healthy heart distant from the patch (** $P < 0.01$). **B,** Bright field cross section of the heart. **C,** FISH images are stained for mouse centromeres (green), human centromeres (red) and nuclei (blue). Representative fusion products, defined as dual color fluorescence within individual nuclei, are designated with a white arrowhead. Insets are magnified views of representative fusion products. Background signal in the healthy heart is due to autofluorescence of cardiac sarcomeres, this was left intentionally to appreciate position of fusion products relative to healthy myocardial tissue. Scale bar is 50 μm. **D,** Immunohistochemistry for HLA-A,B,C (green) and nuclei (blue). Scale bar is 50 μm.

Figure 3-5. Frequency of fusion following delivery of vMSCs to murine myocardium via bolus injection. A, VSV-G-transfected human MSCs (vMSCs) fused with recipient cells in the murine heart after bolus injection directly into the myocardium. Fusion hybrids were prevalent in a discrete region assumed to be associated with the point of injection (49% $\pm$ 10% fusion products). Human cells were found in regions beyond the borders of the discrete region (10% $\pm$ 11% fusion products) and were more prevalent (not significant) than fusion hybrids located in the healthy myocardium following transplantation with the TissueMend patch (3% $\pm$ 5%). **B,** Representative images of murine heart following transplantation stained for human (red) and mouse (green) centromeres using FISH. The top row contains a field of view from the Bolus injection; the bottom row contains a field of view from the Healthy Heart. Background (green) signal in the healthy heart is due to autofluorescence of cardiac sarcomeres; this was left intentionally to appreciate position of fusion products relative to healthy myocardial tissue. Scale bars are 50 μm.

Figure 3-6. Detection of fusion products in the murine small intestine using FISH. Fusion products (white arrowhead) and unfused human cells (white arrow) were detected in the murine small intestine using a human centromere probe (red) and a murine centromere probe (green).

A, Bright field cross section of the small intestine. **B,** FISH images are stained for mouse centromeres (green), human centromeres (red) and nuclei (blue). Insets are magnified views of representative fusion products. Scale bar is 50 μm. **C,** Immunohistochemistry for HLA-A,B,C (green) and nuclei (blue). Scale bar is 50 μm.

Figure 3-7. Detection of fusion hybrids in the murine stomach using FISH. Fusion products (white arrowhead) and unfused human cells (white arrow) were detected in the murine stomach using a human centromere probe (red) and a murine centromere probe (green). **A,** Bright field cross section of the stomach. **B,** FISH images are stained for mouse centromeres (green), human centromeres (red) and nuclei (blue). Insets are magnified views of representative fusion products. Scale bar is 50 μm. **C,** Immunohistochemistry for HLA-A,B,C (green) and nuclei (blue). Scale bar is 50 μm.

Figure 3-8. Detection of fusion products near the vasculature in the murine stomach. Fusion products (white arrowhead) were detected adjacent to the vasculature in the murine stomach using a human centromere probe (red) and a murine centromere probe (green) as well as an antibody for von Willebrand Factor (vWF), a marker for endothelial cells. **A,** Bright field cross section of the stomach. **B,** Immunohistochemistry for vWF (red) and nuclei (blue). Scale bar is 100 μm. **C,** FISH staining for mouse centromeres (green), human centromeres (red) and nuclei (blue). Insets are magnified views of a representative fusion product near a blood vessel (dashed line). Scale bar is 50 μm.

Figure 4-1. Detection and Augmentation of MSC Cell Fusion in vivo

(A): Schematic of the *in vivo* Cre/*LoxP* biophotonic detection system. The MSCs are transfected with a *LoxP*-stop codon-*LoxP*-luciferase plasmid prior to cell transplantation. The MSCs are transplanted into mice constitutively expressing Cre recombinase. Upon fusion between MSCs and a cell of the Cre mouse, Cre recombinase excises the *LoxP*-stop codon-*LoxP* sequence and luciferase is expressed in the fusion product. The fusion product can then emit a bioluminescent signal after the addition of the luciferin substrate. (B). Quantification of the day 7 mean luminescent signal (photons/centimeters^2/second/steradian, photons/cm^2/s/sr) for each treatment group (Sham, MSC, and MSC-VSVG). The MSC and MSC-VSVG emitted a significantly higher mean luminescent signal compared to the Sham control group (*$P < 0.05$, data is displayed as average (Avg) $\pm$ standard deviation (SD)). Three representative luminescent overlay images for each group are shown below graph.

Figure 4-2. Augmented MSC Cell Fusion Affects Function of Infarcted Myocardium
Cardiac functional improvement is displayed relative to the values at 3 days after infarction/cell delivery for (A) fractional area change (FAC) and (B) cardiac output (CO). The Sham group displayed the highest fold increase over the 28 days monitored. The augmented fusion group (MSC-VSVG) showed the lowest fold change. To demonstrate the variability between samples in the treatment groups, the mean luminescent signal for each mouse was plotted against the (C) FAC (%) or (D) CO (mL/min) for each time point. At day 7 a positive correlation emerges between mean luminescent signal (fusion) and cardiac function, but this correlation is lost at later time points.

Figure 4-3. Human MSC Retention and Vascular Response in Infarcted Murine Heart
(A). Quantification at day 56 after infarction/cell delivery of human leukocyte antigen (HLA) expression (area) normalized to DAPI signal (area) for four regions in the infarcted heart (TissueMend, BorderZone, Infarct and Healthy Heart) (5-20 images per region per sample, data displayed as Avg $\pm$ SD). (B). Mean luminescent signal for each mouse was plotted against the HLA area/DAPI area for each mouse. The MSC group showed a negative correlation between mean luminescent signal (fusion) and MSC retention. (C). Representative images for MSC and MSC-VSVG groups in the BorderZone (HLA, green and DAPI, blue) (Scale bar = 50 μm). (D). Quantification at day 56 after infarction/cell delivery of vessel density (CD31 expression area) normalized to DAPI signal (area) for four regions in the infarcted heart (5-20 images per region per sample, data displayed as Avg $\pm$ SD, *** $P < 0.001$ compared to the MSC-VSVG group). (E). Mean luminescent signal for each mouse was plotted against the CD31 area/DAPI area for each mouse. The MSC group showed a negative correlation between mean luminescent signal (fusion) and vessel density. (C). Representative images in the Healthy Heart (CD31, green and DAPI, blue) (Scale bar = 50 μm).

Figure 4-4. Immune Modulation Response to Treatments
(A). Quantification at day 56 after infarction/cell delivery of T-cell concentration (CD3 expression area) normalized to DAPI signal (area) for four regions in the infarcted heart (5-20 images per region per sample, data displayed as Avg $\pm$ SD, ** $P < 0.005$ compared to the MSC-VSVG group). (B). Mean luminescent signal for each mouse was plotted against the CD3 area/DAPI area for each mouse. (C). Representative images in the BorderZone (CD3, green and DAPI, blue) (Scale bar = 50 μm). (D). Colocalization of regulatory T-cells (CD25, red) and T-cells (CD3,

green) seen in the BorderZone of a mouse from the MSC group (DAPI, blue) (Scale bar = 50 μm).

Figure 5-1. Workflow for identification, isolation and RNA-seq of mMSC-cardiomyocyte fusion products and associated controls, Related to Experimental Procedures.
Fusion products were identified via detection of green fluorescence associated with the intact BiFC construct or dual color expression of both GFP and mCherry (and therefore cell fusion) via fluorescence microscopy, upper left panel. Merged image of bright field (to discern cell membranes) and BiFC (green). Scale bar = 50 μm. After identification, cells were removed from culture dishes and sorted for GFP^+ cells using FACS. Sorted cells were injected into the Fluidigm C1 chip and again visualized via fluorescence microscopy to ensure successful capture and to confirm cell viability (cells were also stained with DEAD cell viability assay). Cells of interest were lysed and RNA extraction and cDNA synthesis were performed on the chip. Library preparation followed using Illumina Nextera XT and then sequencing using MiSeqv3.

Figure 5-2. Induction and detection of cell fusion via the measles virus system and bimolecular fluorescence complementation (BiFC) and dual-color fluorescence, respectively. A. DNA content of HL1cm was analyzed via DAPI staining with flow cytometry and DNA content of experimental cocultures (H-F/hSLAM and F-H/hSLAM) was compared to coculture controls (no fusogen/no fusogen, H-F/no fusogen, F-H/no fusogen, and hSLAM/no fusogen) (*$p < 0.05$). Data are represented as mean $\pm$ standard deviation (SD). B. Immunocytochemistry for hemagglutinin (H) on hMSC (green) and hSLAM on HL1cm (green). Nuclei stained with DAPI (blue). Scale bar = 50 mm. C. Greater than 50% of detected fusion products contained 2 nuclei. Data are represented as mean $\pm$ SD. (*$p < 0.05$, **$p < 0.01$). D. Approximately 50% of the total nuclei of fusion products were of human origin, supporting the specificity of the system. E. Schematic for the bimolecular fluorescence complementation (BiFC) system. Fusion products were detected with fluorescence microscopy for BiFC (green). Cells were then labeled for human nuclear antigen (HNA, red, only present in the hMSC nuclei). Representative fusion products were detected with BiFC (green), HNA (red), and nuclei detected with DAPI (blue). Scale bar = 50 mm. F. Schematic for the dual color fluorescence system. Fusion products were detected with fluorescence microscopy for dual expression of GFP from HL1cm and mCherry from mMSC. Representative fusion product is shown below schematic. Scale bar = 50 mm.

Figure 5-3. Hierarchal clustering (HC) and principal component analysis (PCA) of differentially expressed genes between mMSC-cardiomyocyte fusion products and parental controls. A. A global view of differential gene expression between hybrids (BiFC_D1_F1-5, DC_D1_F1-16, and DC_D3_F1-7), parental cells (mMSC_1-15, mMSC_D1_1-5, HL1cm_1-15, and HL1cm_D1_1-5) and population controls (mMSC_PC, HL1cm_PC, and Mix_D1). Global Z-Score reflects the number of standard deviations away from the mean of expression of all genes in the display. Gene expression is shown in fragments per kilobase of exon per million fragments mapped (FPKM). Differential expression was defined as a $\log_2$ fold change of greater than 1 and a false discovery rate (FDR)-adjusted *P*-value below 0.05. B. PCA analysis of hybrids, parental cells and population controls.

Figure 5-4. Hierarchal clustering of differentially expressed genes of individual hybrids organized according to chromosome. To determine whether gain or loss of gene expression between parental cells and fusion products favored particular chromosomes we plotted differentially expressed genes as a function of chromosome number for BIFC_D1_F1-5 hybrids. Differentially expressed genes of fusion products versus HL1cms (A) or mMSCs (B) were organized into chromosomal groups and hierarchal clustering was performed. There were no specific chromosome(s) that experienced extensive increase or decrease in FPKM per gene, but BIFC_D1_F4 and BIFC_D1_F5 displayed global reduction of FPKM of many genes on most chromosomes compared to the parental controls and even the other three BiFC fusion products.

Figure 5-5. Differentially expressed genes of individual hybrids organized according to chromosome. Total number of increased FPKM values (red) or decreased FPKM values (blue) were normalized to the total number of genes on each chromosome for each fusion product (vs. HL-1cm: open bars, vs. mMSC: closed bars). Increases in FPKM values varied from chromosome to chromosome and between hybrids and, as shown in Figure 5-3, occurred most often of chromosomes 2, 11 and 17. Decrease in FPKM values was universal and not chromosome specific. (*$P < 0.05$ via LSD post-hoc analysis). Data are represented as mean $\pm$ SD.

Figure 5-6. Gene Ontology of BiFC Fusion Products and all hybrids with a unique transcriptome. *P*-value of functional annotation for differentially expressed genes (increased FPKM values (A, red) or decreased FPKM values (B, blue)) for each BiFC fusion product. C. Gene ontology analysis after combining the ten hybrids with unique transcriptomes (vs. HL1cm: open bars, vs. mMSC: closed bars). The dashed line represents a *P*-value of 0.05.

Figure 5-7. mMSC-cardiomyocyte fusion products can express a cardiomyocyte cell-like, stem cell-like or distinct transcriptome. A. HC of fusion products in relation to a set of genes related to stemness (*), adipogenic differentiation (ɵ), osteogenic differentiation (+), or chondrogenic differentiation (x). B. PCA analysis of fusion products and controls. D. HC of fusion products for a set of genes related to cardiac development (+) or contractile ability (x). E. PCA analysis of fusion products and controls. G. HC of fusion products, a population of tumor initiating cancer cells (TIC-PC), a population of nontumorigenic cancer cells (NTC-PC), and controls for a set of oncogenes and a set of tumor suppressor genes. H. PCA analysis of fusion products, cancer populations and controls for the combined oncogene tumor suppressor gene set. C, F, I. qPCR confirmation of RNA-seq data. See also Table S4 and Figure 5-8.

Figure 5-8. PCA loading plot and PCA Score plot for the cancer gene set, The score plot is a summary of the relationship between single-cell samples (or population controls, PC). The loading plot is a summary of the genes and provides a means to interpret patterns seen in the score plot. Genes in the loading plot that fall far from zero on a PC axis are those that most significantly impact on the PC score of individual samples. In this case, *Fos* and *Jun* gene expression have a high negative contribution to the PC2 score, whereas *Fas* and *Trp53* expression have a high positive contribution to PC2. Therefore, if a cell has high expression of *Fos* and *Jun*, but low expression of *Fas* and *Trp53* it will have a negative PC2 value, as seen with BiFC_D1_F4 and DC_D1_F16 and the cancer populations. Interestingly, if BiFC_D1_F4 had lower expression of oncogenes *Fos* and *Jun* and increased expression of tumor suppressor genes *Trp53* and *Fas*, it would cluster more closely with the breast cancer cells on the PCA score plot.

Figure A1-1. Schematic of Technique to Detect Cell Fusion In Vivo. If fusion between Cre-expressing mouse cells and transplanted cells expressing a floxed luciferase plasmid occurs, luciferase will be expressed. Luciferase can be detected by injecting the enzymatic substrate, D-luciferin, into the mouse and then imaging the mouse using a Xenogen Biophotonic Imaging System (Adapted from reference 19).

Figure A1-2. Sensitivity of detection of luciferase-expressing cells in cardiac tissue with biophotonic imaging. A cell line which constitutively expresses luciferase (231-LUC-D3H1, Xenogen) was delivered to the intramyocardial space of C57/Bl6 mice at various total cell numbers. Representative images of mice receiving 1 x 106, 1 x 103 and 1 x 101 cells (left to

right) are shown, imaging was conducted approximately 6 hours after injection.

Figure A1-3. Quantification of In Vivo Luminescence Indicative of Cell Fusion. MSCs were transfected with the LoxP-Stop-LoxP-Luciferase plasmid and delivered to the myocardium of Cre-expressing mice. Approximately one week and two weeks after cell delivery, Cre mice were imaged using the Xenogen Biophotonic Imaging System to measure the intensity of luminescence indicative of cell fusion. (A) Overlay of photograph and intensity of luminescence of sham and mice 1-4 (left to right) 17 days after cell delivery. (B) Intensity of luminescence of sham and mice 1-4 (left to right) 17 days after cell delivery. A region of interest was selected (yellow) corresponding to the injection site and intensity levels were determined using ImageJ (free source) software20. (C) Intensity of luminescence was normalized to the same region of interest on sham mouse for all experimental conditions. At one week, mice 3 and 4 showed positive luminescence signal suggesting spontaneous fusion of a mouse cell and transplanted MSC. The signal persisted in mouse 3 at two weeks. To determine organ-specific localization of the signal corresponding to mouse 3, the thoracic cavity was exposed and primary organs excised and imaged. (D) Overlay of photograph and intensity of luminescence of mouse 3. Note localization of intensity signal in the small intestine. (E) Intensity of luminescence of mouse 3. (F) Overlay of photograph and intensity of luminescence of sham mouse. (G) Intensity of luminescence of sham mouse.

Figure A2-1. Single-cell mMSCs express genes associated with MSC multipotency A. Hierarchal clustering (HC) of mMSCs for a set of genes related to MSC multipotency. Genes are organized either by genes expressed highly in mMSCs (red), genes expressed moderately/heterogeneously in mMSCs (pink), genes that are lowly expressed in mMSCs (blue) or housekeeping genes (green). Global Z-Score reflects the number of standard deviations away from the mean of expression in the reference. **B.** Principal component analysis (PCA) analysis of single cell mMSCs (1-16) (red), negative control single cells (HL1cm1-HL1cm5) (brown), and population controls (PC and HL1cmPC). **C.** Quantitative reverse transcriptase polymerase chain reaction (qPCR) confirmation of RNA-seq data.

Figure A2-2. Individual mMSCs express genes from multiple differentiation pathways. A. HC of single cell mMSCs and mMSC population control (mMSC-PC) for a set of genes related to osteogenesis, chondrogenesis, adipogenesis, vascular smooth muscle, neurogenesis, and housekeeping genes. **B.** PCA analysis of single cell mMSCs (1-16) and population control (PC). **C**. PCA loading plot showing individual differentiation genes represented in **B**. **D.** qPCR

confirmation of RNA-seq data. **E.** A key transcription factor was selected for each differentiation lineage and expression was normalized to *Gapdh* for each sample.

Figure A2-3. Expression of each lineage gene normalized to *Gapdh*. A. Osteogenic gene profile. **B.** Chondrogenic gene profile. **C**. Adipogenic gene profile. **D**. Vascular smooth muscle gene profile. **E**. Neurogenic gene profile.

Figure A2-4. **Single cell mMSCs exhibit minimal but measureable differences in expression of immunomodulatory genes. A.** HC of single cell mMSCs, negative control single cells (HL1cm1-5), and population controls (mMSC-PC and HL1cmPC) for a set of genes related to immunomodulatory function. **B.** PCA analysis of single cell mMSCs (1-16) and population control (PC). **C**. PCA loading plot showing individual differentiation genes represented in **B**. *Il6* expressing cells clustered together (yellow).

Figure A2-5. HC and PCA of mMSCs show transcriptome heterogeneity and gene ontology of subpopulations. A. A global view of differential gene expression between single cell mMSCs and the population control (mMSC-PC). Gene Z-Score reflects the number of standard deviations away from the mean of expression in the reference. **B.** PCA analysis of single cell mMSCs (1-16) and population control (PC). **C.** Gene onotology of five subpopulations of single-cell mMSCs (green, blue, yellow, purple and red clusters). Ontology groups are plotted with the *P* value on the y-axis. Upregulated groups have bars extending in the positive y-direction and down regulated groups have bars extending in the negative y-direction.

List of Tables

Chapter 1 Introduction

1.1. Introduction to Cell Fusion

1.1.1 Rationale

The American Heart Association reported that in 2013 over 715,000 Americans suffer a new or recurrent myocardial infarction each year [1]. One promising therapy is the delivery of MSCs to the damaged myocardium, which has been shown to improve cardiac recovery [2-8]. MSCs home to injured tissues [9,10] and several mechanisms for MSC-based recovery have been proposed. For example, MSCs may transdifferentiate into cardiac cells to replace the dead and damaged cells, [11-14]. As a second mechanism, the transplanted MSCs could act through secretion of paracrine factors that limit immune responses [15] and/or increase angiogenesis [10, 16-23]. A third possible mechanism is nuclear reprogramming via fusion between the MSCs and cells of the pericardium, epicardium, or myocardium [24]. Recent studies have uncovered evidence of cell fusion between stem cells and cardiac cells [25-30] but the impact of this cell fusion and subsequent reprogramming on cardiac function at the cellular and tissue scale is not well understood.

1.1.2 Reprogramming due to cell fusion *in vitro*

Fusion of MSCs with cardiac cell types may improve cardiac function if the fusion products adopt the phenotype and associated function of cardiac cell types including cardiomyocytes, smooth muscle cells and endothelial cells. Evidence from the literature suggests stem cells and somatic cells can give rise to fusion products with

characteristics of the somatic cell, thereby effectively programming the stem cells. For example, Blau et al. fused differentiated mouse muscle cells and human amniocytes and found that the mature cell phenotype dominated such that the amniocytes expressed human muscle proteins via exchange of cytomplasmic component[31]. Recent studies have shown that fusion of bone marrow-derived cells with hepatocytes has a therapeutic effect on the liver because the bone marrow-derived cells repopulate damaged liver tissue and adopt the biochemical functions of hepatocytes, including maintaining correct levels of serum transaminases, bilirubin and amino acids [32-34]. However, fusion of MSCs with cardiac cell types may also improve cardiac function if the fusion products adopt the phenotype and associated function of mesenchymal stem cells, such self-renewal and anti-inflammatory properties. Evidence from the literature suggests fusion products of stem cells and somatic cells can serve to effectively reprogram the somatic cell to a less mature state. For example, Cowan et al. reverted human fibroblasts to a pluripotent-like state after fusion with embryonic stem cells [36]. Tada et al. observed a similar pluripotent hybrid cell after fusing embryonic germ cells and lymphocytes [37]. Alternatively, fusion of MSCs with cardiac cell types may worsen cardiac function if the fusion products adopt a phenotype and associated function distinct from either cardiac cell types or mesenchymal stem cells. Blau et al. found heterokaryons formed from muscle cells and keratinocytes, expressed a combination of both gene profiles [38]. A similar result was seen after fusing intestinal epithelial cells and macrophages in a murine model of intestinal cancer [39] while Powell et al. found that cell fusion hybrids retained the transcriptome identity characteristic of both parental cells, but also expressed genes not activated in either

parent cell type. The activation of previously unexpressed genes is postulated to be responsible for the creation of cancer stem cells through fusion between tumor cells and bone marrow-derived cells [40, 41]. Another result of cell fusion is chromosomal instability (CIN), which is an increased and continuous rate of large chromosomal aberrations, including deletions, duplications, or translocations as well as loss or gain of whole chromosomes [40]. CIN can randomize normal diploid human cells so extensively that each cell has a unique karyotype [42]. This phenomenon is one possible explanation of the unique transcription profiles observed in the hybrid fusion products described previously [38,39].

1.1.3 Reprogramming after *In vivo* cell fusion

The biologic outcome of fusion of stem cells at the tissue and organ level (i.e., *in vivo*) has been even more challenging to discern than at the cellular scale (i.e., *in vitro*) due to the difficulty of detecting and tracking fusion products in living organisms. Studies of the liver found that cell fusion is the principal means by which bone-marrow-derived cells acquire a hepatocyte-like phenotype. *In vitro* fusion of bone marrow-derived cells with hepatocytes was detected using Southern blots and fluorescent *in situ* hybridization (FISH) on harvested tissue using probes specific for mouse donor X chromosome and the host mouse Y chromosome [33,34]. Vassilopoulos et al. also found that transplanted bone marrow regenerated the liver by cell fusion via detection of donor GFP labeled bone marrow cells in host hepatic nodules and detection of donor bone marrow cells expressing a hepatic specific profile [43]. Reprogramming after cell fusion *in vivo* was observed by Quintana-Bustamante et al., who utilized microarrays to show

that bone marrow-derived hepatocytes had a unique gene profile relative to both hematopoetic cells and hepatocytes of the host [44]. Cancer research has also provided some evidence for *in vivo* cell fusion in malignant tumors [45-47]. Cell fusion of bone-marrow derived hematopoietic cells and cardiomyocytes has been reported *in vivo*, albeit at a low frequency [48-50]. However, all of these studies only detected fusion when analyzing the tissue or protein levels after sacrificing the host animal (thus limiting studies of the kinetics and functional outcomes of fusion) and typically analysis is done in target organs and not the entire animal (thus limiting knowledge of the potential breadth of cell fusion). Lacking is a means to accurately detect fusion *in vivo* in the entire organism over time.

1.1.4 Tools for studying cell fusion

Detection of fusion, whether *in vitro* or *in vivo,* is technically challenging as fusion products often resemble fusion partners based on phenotype alone, especially if the nuclear content from the two cells merge to form a synkaryon or if the fusion product sheds one of the nuclei. The challenge of identification causes cell fusion to be overlooked in many cases. However, recent technological advances have given the scientific community a few tools to overcome these challenges. Fluorescent cytoplasmic dyes can be used to show fusion by observing a mixing of two different cellular dyes in co-culture. However, this technique is only good *in vitro* and for short term studies due to the signal being lost over time. Also, the cytoplasmic dye method is reliant on fluorescent microscopy to observe the fusion events, which can be difficult if cells are densely packed or overlapping. A second technique utilized to detect cell

fusion is bimolecular fluorescence complementation (BiFC) (**Figure 1-1)**. BiFC uses two non-fluorescent fragments of a fluorescent molecule that are attached to two separate proteins. If the two proteins interact, the two non-fluorescent fragments will interact and mature into the fluorescent molecule. The BiFC system is inducible, giving the user control of when and where the signal is observed. This is beneficial for studying cell fusion by allowing the researcher to give half the system to one cell type and the other half to a different cell type, thus the only time a signal is seen is after cell fusion and mixing of both cells cytoplasmic and nuclear content. Inducible methods such as BiFC give a high confidence level in the signal and a lower chance of seeing a false positive.

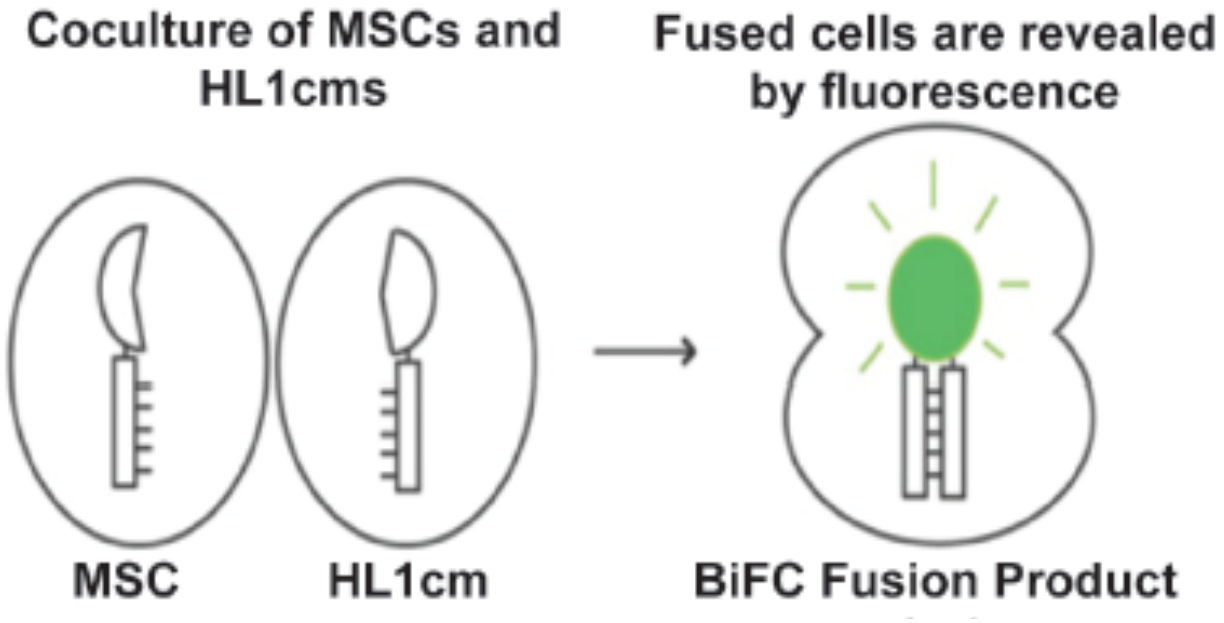

Figure 1-1. **Bimolecular Fluorescence Complementation (BiFC) method.** Schematic for the bimolecular fluorescence complementation (BiFC) system. Fusion products were detected with fluorescence microscopy for BiFC (green).

Another method to identify cell fusion utilizes genetic engineering and the Cre-*LoxP* system (**Figure 1-2)**. In the Cre-*LoxP* system, one fusion partner expresses the enzyme Cre recombinase and the other contains a reporter gene that is downstream of a stop codon flanked by *LoxP* sites. If fusion occurs and the Cre enzyme is exposed to the *LoxP* sites, the stop codon is excised and the reporter gene is then expressed. The Cre-*LoxP* method allows for detection of only true fusion events both *in vitro* and *in vivo*, however there is a delay between the event of fusion and expression and translation of the reporter. We utilize a construct encoding the firefly luciferase (*Photinus pyralis*) gene adjacent to the floxed stop codon as a method of detecting fusion *in vivo*. Also to increase the frequency of fusion, we can simultaneously transfected cells with a viral fusogen, vesicular stomatitis virus (the glycoprotein, VSVG) along with the *LoxP*-luciferase reporter plasmid. Because bioluminescence can be reliably detected in living organisms, an inducible "living" detection signal is produced that can be tracked in real time.

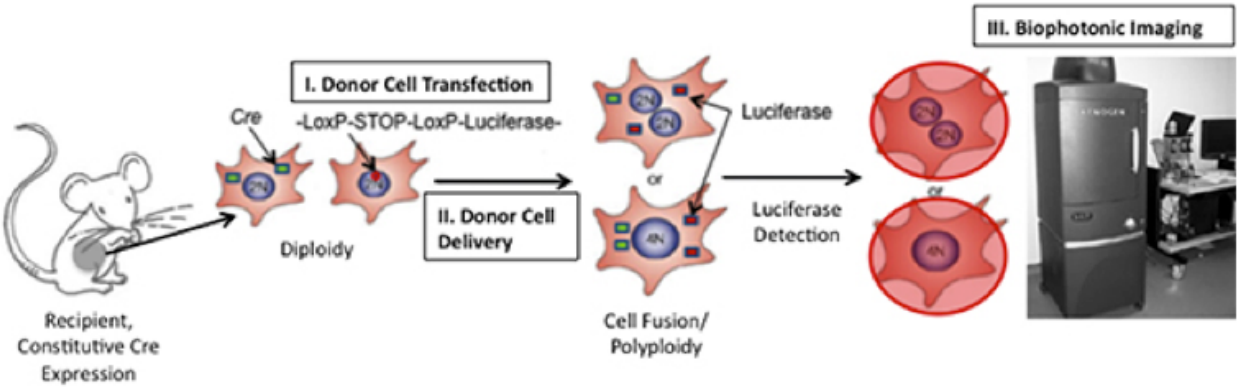

Figure 1-2. **Cre-*LoxP* biophotonic fusion detection system.** If fusion between Cre-expressing mouse cells and transplanted cells expressing a floxed luciferase plasmid occurs, luciferase will be expressed. Luciferase can be detected by injecting the enzymatic substrate, D-luciferin, into the mouse and then imaging the mouse using a Xenogen Biophotonic Imaging System.

1.1.5 Possible outcomes after MSC-cardiomyocyte fusion

The three outcomes of fusion between MSCs and cardiomyocytes are 1) the MSC phenotype could dominate resulting in a more stem cell-like transcriptional profile, 2) the cardiomyocyte phenotype could dominate resulting in a more cardiac-like transcriptional profile, or 3) a new phenotype could be formed from a mixing of the cytoplasmic and nuclear elements of the two cells (**Figure 1-3**). If a stem cell-like hybrid is formed, the hybrid would adapt MSC functionality and be able to proliferate, release positive paracrine signaling, and exhibit immunological advantages. For example, MSC cytoplasmic and nuclear elements might affect the expression of the transcription factor Meis1, which has been found to be a critical regulator of the cardiomyocytes cell cycle [51]. Meis1 becomes active by postnatal day 7 in mice and suppresses cardiomyocyte proliferative ability. However, if Meis1 expression was silenced or down regulated by MSC components after fusion, a hybrid could then proliferate and repopulate the myocardium. However, the stem cell-like hybrid could also have issues incorporating into the myocardium. Without the proper ion channels and sarcomeres, the stem cell-like hybrid might cause arrhythmias or a change in electrophysiological properties of the heart [52]. Repopulating an infarct, releasing survival paracrine signals, and decreasing rejection after transplantation would be beneficial in stem cell therapy after a myocardial infarction, but if the cells cannot integrate into the local myocardium and help the heart beat more effectively there could be adverse affects.

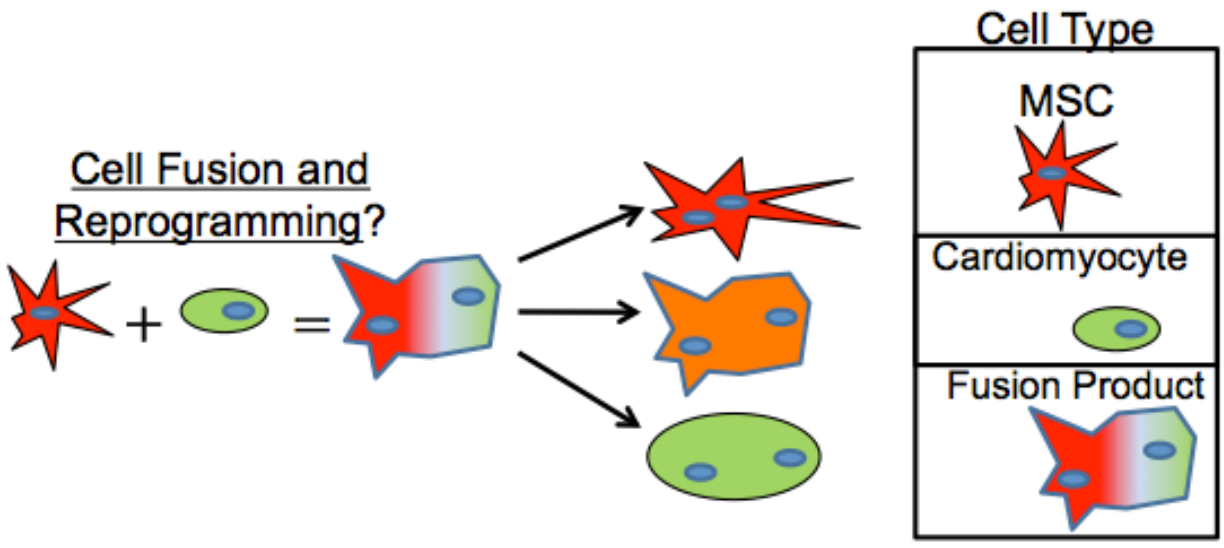

Figure 1-3. **Possible outcomes after cell fusion.** The three outcomes of fusion between MSCs and cardiomyocytes are 1) the MSC phenotype could dominate resulting in a more stem cell-like transcriptional profile (RED), 2) the cardiomyocyte phenotype could dominate resulting in a more cardiac-like transcriptional profile (GREEN), or 3) a new phenotype could be formed from a mixing of the cytoplasmic and nuclear elements of the two cells (ORANGE).

The second possible outcome of MSC-cardiomyocyte fusion involves the cardiac phenotype dominating and turning the hybrid into a cardiomyocyte-like cell. A cardiomyocyte-like hybrid has the potential to match the action potentials of the local myocardium since it would be expressing all the necessary proteins to receive and transmit the signal to surrounding cells. This integration would be useful if there is not an extensive amount of damage to the myocardium after an infarct. However, mature cardiomyocytes proliferate at a low level [53], so a cardiomyocyte-like hybrid might only have a small effect on decreasing scar size or other measurable functionality. A recent study looked at the electrophysiology of fusion products formed between human MSC and rat neonatal ventricular myocytes [54]. Shadrin et al. found that this type of fusion product produced electrically active hybrids, but they are non-contractile. If fusion

products between MSCs and myocytes are not able to contract, then perhaps increasing fusion in the heart would yield negative effects to cardiac functionality.

The final outcome of cell fusion between MSCs and cardiomyocytes is the creation of a new phenotype [38-41]. The fusion hybrid could express a combination of proteins from both cell types or a totally new set of genes unexpressed in both parental cells. It is unknown how the hybrid would affect a damaged myocardium. The fusion hybrid may express the therapeutic advantages of both parental cells and the hybrid could not only integrate into the local myocardium, but it would be able to repopulate the damaged tissue and prevent an immune response. On the contrary, the fusion hybrid may lose all of the beneficial abilities of each cell type and have a negative effect on the surrounding myocardium. One study proposed that cell fusion is a method to create emergent cell phenotypes due to state conflicts and colliding molecular systems [55]. The goal of this study is to begin to probe which of the above three cell fates is favored after fusion between MSCs and cardiomyocytes.

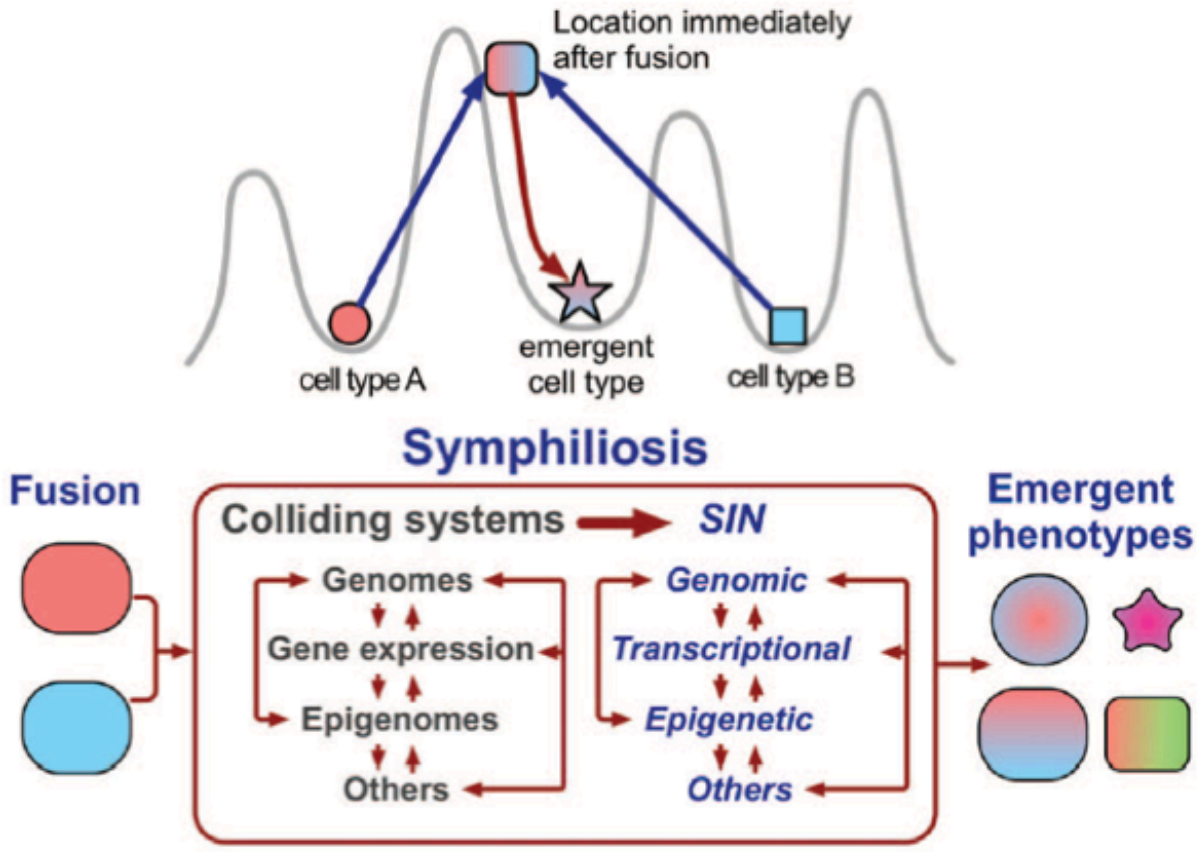

Figure 1-4. **Model describing the state conflicts and collision of merged cellular systems.** The top model is based on the notion that gene expression patterns correspond to points in the Waddington epigenetic landscape (sketched with the gray line), with the stable patterns (cell types) corresponding to the "valleys" known as attractors. Merging different cells nearly instantly creates a new pattern, which is initially an average of the two, on a slope of a "hill" in the landscape [55]. The bottom model describes how fusion of different cells causes the collision of merged cellular systems, resulting in death or leading to symphiliosis, or reconciliation. Symphiliosis is manifested by interrelated instabilities summarily named symphilial instabilities (SIN) that are a result of integrating distinct sets of parental networks into one. Symphiliosis can produce emergent phenotypes, cause death, senescence, or continue permanently. "Other" systems can include mitochondria, which have their own genome, and interactions with other cells to give just two examples [55].

Thus, in this study we aim to discern the extent to which the transcriptome of hybrids can change globally and over time, to develop better tools to study hybrid formation in the heart with stem cell transplantation and to study cell and tissue scale changes that occur as a consequence. We anticipate that the results from these investigations will increase the knowledge of the biological impacts of cell fusion and functional affects after cell transplantation.

1.2 References

1. Go A. S., Mozaffarian D., Roger V. L. et al., “Executive Summary: Heart Disease and Stroke Statistics−−2013 Update: A Report From the American Heart Association,” Circulation, vol. 127, pp. 143-152, 2013.
2. A. Abdel-Laitf et al., “Adult bone marrow-derived cells for cardiac repair: a systematic review and meta-analysis. Arch. Intern. Med., vol 167, pp. 989-997, 2007.
3. S. Chen et al., “Intracoronary transplantation of autologous bone marrow mesenchymal stem cells for ischemic cardiomyopathy due to isolated chronic occluded left anterior descending artery,” J. Invasive Cardiol., vol. 18, pp. 552-556, 2006.
4. S. Tomita, R. K. Li, R. D. Weisel et al., “Autologous transplantation of bone marrow cells improves damaged heart function,” Circulation, vol. 100, no. 19, supplement 2, pp. II247–II256, 1999.
5. L. C. Amado, A. P. Saliaris, K. H. Schuleri et al., “Cardiac repair with intramyocardial injection of allogeneic mesenchymal stem cells after myocardial infarction,” Proceedings of the National Academy of Sciences of the United States of America, vol. 102, no. 32, pp. 11474–11479, 2005.

6. S. L. Chen, W. W. Fang, F. Ye et al., “Effect on left ventricular function of intracoronary transplantation of autologous bone marrow mesenchymal stem cell in patients with acute myocardial infarction,” American Journal of Cardiology, vol. 94, no. 1, pp. 92–95, 2004.
7. J. Ma, J. Ge, S. Zhang et al., “Time course of myocardial stromal cell-derived factor 1 expression and beneficial effects of intravenously administered bone marrow stem cells in rats with experimental myocardial infarction,” Basic Research in Cardiology, vol. 100, no. 3, pp. 217–223, 2005.
8. J. G. Shake, P. J. Gruber, W. A. Baumgartner et al., “Mesenchymal stem cell implantation in a swine myocardial infarct model: engraftment and functional effects,” Annals of Thoracic Surgery, vol. 73, no. 6, pp. 1919–1926, 2002.
9. M. Mouiseddine, S. François, A. Semont et al., “Human mesenchymal stem cells home specifically to radiation-injured tissues in a non-obese diabetes/severe combined immunodeficiency mouse model,” British Journal of Radiology, vol. 80, no. 1, pp. S49–S55, 2007.
10. N. Nagaya, T. Fujii, T. Iwase et al., “Intravenous administration of mesenchymal stem cells improves cardiac function in rats with acute myocardial infarction through angiogenesis and myogenesis,” American Journal of Physiology, vol. 287, no. 6, pp. H2670–H2676, 2004.
11. H. Kawada, J. Fujita, K. Kinjo et al., “Nonhematopoietic mesenchymal stem cells can be mobilized and differentiate into cardiomyocytes after myocardial infarction,” Blood, vol. 104, no. 12, pp. 3581–3587, 2004.

12. A. Deb, S. Wang, K. A. Skelding, D. Miller, D. Simper, and N. M. Caplice, “Bone marrow-derived cardiomyocytes are present in adult human heart: a study of gender-mismatched bone marrow transplantation patients,” Circulation, vol. 107, no. 9, pp. 1247–1249, 2003.
13. S. Dimmeler, A. M. Zeiher, M. D. Schneide, “Unchain my heart: the scientific foundations of cardiac repair,” J Clin Invest., vol. 115, pp. 572-583, 2005.
14. Y. S. Yoon, A. Wecker, L. Heyd, J. S. Park et al., “Clonally expanded novel multipotent stem cells from human bone marrow regenerate myocardium after myocardial infarction,” J Clin Invest., vol. 115, pp. 326-338, 2005.
15. G. Chen, M. Nayan, M. Duong et al., “Marrow stromal cells for cell-based therapy: the role of antiinflammatory cytokines in cellular cardiomyoplasty,” Annals of Thoracic Surgery, vol. 90, no. 1, pp. 190–197, 2010.
16. H. Kamihata, H. Matsubara, T. Nishiue et al., “Implantation of bone marrow mononuclear cells into ischemic myocardium enhances collateral perfusion and regional function via side supply of angioblasts, angiogenic ligands, and cytokines,” Circulation, vol. 104, no. 9, pp. 1046–1052, 2001.
17. T. Kinnaird, E. Stabile, M. S. Burnett et al., “Marrow-derived stromal cells express genes encoding a broad spectrum of arteriogenic cytokines and promote in vitro and in vivo arteriogenesis through paracrine mechanisms,” Circulation Research, vol. 94, no. 5, pp. 678–685, 2004.
18. M. Gnecchi, H. He, O. D. Liang, L. G. Melo, F. Morello, H. Mu, N. Noiseux, L. Zhang, R. E. Pratt, J. S. Ingwall, V. J. Dzau, “Paracrine action accounts for marked protection of

ischemic heart by Akt-modified mesenchymal stem cells," Nat Med., vol. 11, pp. 367–368, 2005.

19. M. Gnecchi, H. He, N. Noiseux, O. D. Liang, L. Zhang, F. Morello, H. Mu, L. G. Melo, R. E. Pratt, J. S. Ingwall, V. J. Dzau, "Evidence supporting paracrine hypothesis for Akt-modified mesenchymal stem cell-mediated cardiac protection and functional improvement," FASEB J., vol. 20, pp. 661–669, 2006.
20. A. I. Caplan, J. E. Dennis, "Mesenchymal stem cells as trophic mediators," J Cell Biochem, vol. 98, pp. 1076–1084, 2006.
21. T. Kinnaird, E. Stabile, M. S. Burnett, C. W. Lee, S. Barr, S. Fuchs, S. E. Epstein, "Marrow-derived stromal cells express genes encoding a broad spectrum of arteriogenic cytokines and promote in vitro and in vivo arteriogenesis through paracrine mechanisms," Circ Res., vol. 94, pp. 678-685, 2004.
22. A. Linke, P. Muller, D. Nurzynska, C. Casarsa, D. Torella, A. Nascimbene, C. Castaldo, S. Cascapera, M. Bohm, F. Quaini, K. Urbanek, A. Leri, T. H. Hintze, J. Kajstura, P. Anversa, "Stem cells in the dog heart are self-renewing, clonogenic, and multipotent and regenerate infarcted myocardium, improving cardiac function," Proc Natl Acad Sci U S A, vol. 102, pp. 8966-8971, 2005.
23. J. M. Nygren, S. Jovinge, M. Breitbach et al., "Bone marrow-derived hematopoietic cells generate cardiomyocytes at a low frequency through cell fusion, but not transdifferentiation," Nature Medicine, vol. 10, no. 5, pp. 494–501, 2004.
24. A. Caplan, "Why are MSCs therapeutic? New data: new insight," J. Pathol., vol. 217, pp. 318–324, 2009.

25. H. P. Lin, C. Vincenz, K. W. Eliceiri, T. K. Kerppola, and B. M. Ogle, “Bimolecular fluorescence complementation analysis of eukaryotic fusion products,” Biology of the Cell, vol. 102, no. 9, pp. 525–537, 2010

26. K. Matsuura, H. Wada, T. Nagai et al., “Cardiomyocytes fuse with surrounding noncardiomyocytes and reenter the cell cycle,” Journal of Cell Biology, vol. 167, no. 2, pp. 351–363, 2004.

27. H. Oh, S. B. Bradfute, T. D. Gallardo et al., “Cardiac progenitor cells from adult myocardium: homing, differentiation, and fusion after infarction,” Proceedings of the National Academy of Sciences of the United States of America, vol. 100, no. 21, pp. 12313–12318, 2003.

28. S. Zhang, D. Wang, Z. Estrov et al., “Both cell fusion and transdifferentiation account for the transformation of human peripheral blood CD34-positive cells into cardiomyocytes in vivo,”Circulation, vol. 110, no. 25, pp. 3803–3807, 2004.

29. A. J. Sprangers, B. T. Freeman, N. A. Kouris, B. M. Ogle, “A Cre-Lox P Recombination Approach for the Detection of Cell Fusion,” *In Vivo. J. Vis. Exp., vol.* 59, e3581, 2012.

30. N. A. Kouris, J. A. Schaefer, M. Hatta, et al., “Directed Fusion of Mesenchymal Stem Cells with Cardiomyocytes via VSV-G Facilitates Stem Cell Programming,” Stem Cells International, vol. 2012, Article ID 414038, 13 pages, 2012.

31. H. M. Blau, C. P. Chiu, C. Webster, “Cytoplasmic activation of human nuclear genes in stable heterocaryons,” Cell, vol. 32, pp. 1171-1180, 1983.

32. E. Lagasse, H. Connors et al., “Purifiec hematopoietic stem cells can differentiate into hepatocytes *in vivo*,” Nature Medicine, vol. 6, pp. 1229-1234, 2000.

33. X. Wang, H. Willenbring, Y. Akkari, Y. Torimaru, M. Foster, M. Al-Dhalimy, E. Lagasse, M. Finegold, S. Olson and M. Grompe, "Cell fusion is the principal source of bone-marrow derived hepatocytes", Nature vol. 422(6934), pp. 897-901, 2003.
34. H. Willenbring, A. S. Bailey, M. Foster, Y, Akkari, C. Dorrell, S. Olson, M. Finegold, W. H. Fleming and M. Grompe, "Myelomonocytic cells are sufficient for therapeutic cell fusion in liver", Nature Medicine, vol. 10(7), pp. 744-8, 2004.
35. R. A. Miller, F. H. Ruddle, “Pluripotent teratocarcinoma-thymus somatic cell hybrids,” Cell, vol. 9, pp. 45-55, 1976.
36. C. A. Cowan, J. Atienza, D. A. Melton, K. Eggan, “Nuclear reprogramming of somatic cells after fusion with human embryonic stem cells,” Science, vol. 309, pp. 1369-1373, 2005.
37. M. Tada, T. Tada, L. Lefebvre, S. C. Barton, M. A. Surani, “Embryonic germ cells induce epigenetic reprogramming of somatic nucleus in hybrid cells,” EMBO J, vol. 16, pp. 6510-6520, 1997.
38. A. Palermo, R. Doyonnas, N. Bhutani, J. Pomerantz, O. Alkan, H. M. Blau, “Nuclear reprogramming in heterokaryons is rapid, extensive, and bidirectional,” FASEB J, vol. 23, pp. 1431-1440, 2009.
39. A. E. Powell, E. C. Anderson, P. S. Davies, A. D. Silk, C. Pelz, S. Impey et al., “Fusion between intestinal epithelial cells and macrophages in a cancer context results in nuclear reprogramming,” Cancer Res, vol. 71, pp. 1497–505, 2011.
40. T. Harkness, B. A. Weaver, C. M. Alexander, B. M. Ogle, “Cell fusion in tumor development: accelerated genetic evolution,” Crit Rev Oncog., vol. 18(1-2), pp. 19-42, 2013.

41. T. Dittmar, C. Nagler, B. Niggemann, K. S. Zanker, “The dark side of stem cells: Triggering cancer progression by cell fusion,” Current Molecular Medicine, Vol. 13, Number 5, pp. 735-750, 2013.
42. D. M. Duelli, H.M. Padilla-Nash, D. Berman, K.M. Murphy, T. Ried, and Y. Lazebnik, “A virus causes cancer by inducing massive chromosomal instability through cell fusion,” Curr. Biol., vol 17, pp. 431-437, 2007.
43. G. Vassilopoulos, P. Wang, D. W. Russell, “Transplanted bone marrow regenerates liver by cell fusion,” Nature, vol. 422, pp. 901-904, 2003.
44. O. Quintana-Bustamante, E. Grueso, R. Garcia-Escudero, E. Arza, A. Alvarez-Barrientos et al., “Cell Fusion Reprogramming Leads to a Specific Hepatic Expression Pattern during Mouse Bone Marrow Derived Hepatocyte Formation *In Vivo*,” PLoS ONE, vol. 7(3), 2012.
45. G. Kovacs, “Premature Chromosome Condensation: Evidence for *in vivo* cell fusion in human malignant tumors,” Int. J. Cancer., vol. 36, pp. 637-641, 1985.
46. G. Klein, U. Bregula, F. Wiener, H. Harris, “The analysis of malignancy by cell fusion,” J Cell Sci, vol. 8, pp. 659-672, 1971.
47. H. Harris, “The analysis of malignancy by cell fusion: The position in 1988,” Cancer Research, vol. 48, pp. 3302-3306, 1988.
48. S. Zhang, D. Wang, Z. Estrov, S. Raj et al., “Both cell fusion and transdifferentiation account for the transformation of human peripheral blood CD34-positive cells into cardiomyocytes *in vivo*,” Circulation, vol. 110, pp. 3803-3807, 2004.

49. J. M. Nygren, S. Jovinge, M. Breitbach et al., “Bone marrow-derived hematopoietic cells generate cardiomyocytes at a low frequency through cell fusion, but no transdifferentiation,” Nature Medicine, vol. 10, pp. 494-501, 2004.

50. M. Alvarez-Dolado, R. Pardal et al., “Fusion of bone-marrow-derived cells with purkinje neurons, cardiomyocytes and hepatocytes,” Nature, vol. 425, pp. 968-973, 2003.

51. A.I. Mahmoud, F. Kocabas, et al., “Meis1 regulates postnatal cardiomyocytes cell cycle arrest,” Nature, 497, pp. 249-253, 2013.

52. M.J. Price, C. Chou, et al., “Intravenous mesenchymal stem cell therapy early after reperfused acute myocardial infarction improves left ventricular function and alters electrophysiologic properties,” International Journal of Cardiology, vol 111(2), pp. 231-239, 2006.

53. S.E. Senyo, M.L. Steinhauser, et al., “Mammalian heart renewal by pre-existing cardiomyocytes,” Nature, 493, pp. 433-436, 2013.

54. Shadrin IY, Yoon W, Li L et al. Rapid fusion between mesenchymal stem cells and cardiomyocytes yields electrically active, non-contractile hybrid cells. Scientific reports. 5:12043. 2015.

55. Lazebnik Y. The shock of being united and symphiliosis: Another lesson from plants? Cell Cycle. 13(15):2323-2329. 2014.

Chapter 2 Objectives

2.1. Thesis Approach

In this work, I propose to examine cell fusion between MSCs and cardiomyocytes both *in vivo* and *in vitro*. We propose that when MSCs are delivered to an infarcted myocardium, MSCs will fuse with cardiac cells and improve functional properties of the infarcted heart. Furthermore, I hypothesize that fusion between MSCs and cardiomyocytes *in vitro* will result in shifts in the transcriptome of the resultant fusion product, either towards a cardiomyocytes-like profile or a mixed profile of the two cell types.

2.2 Objective 1: Develop tool to detect and quantify cell fusion *in vivo*.

In order to properly study the affects of MSC fusion in a mouse myocardial infarction model, a method to detect and quantify fusion was developed. Prior to this thesis, the methods used to detect cell fusion all involved sacrifice of the mouse and histological analysis of the tissue. This methodology allowed for fusion detection only at fixed time points and any study attempting to track fusion over time was not possible. In this thesis, a new tool for the study of fusion is proposed utilizing the Cre/*LoxP* system and bioluminescence imaging which allows for detection and quantification of fusion throughout the entire body of a live mouse.

2.3 Objective 2: Measure the impact of MSC-cardiac cell fusion on macroscale myocardial function following MSC transplantation in a murine model of myocardial

infarction and determine the mechanism of any affect by examining cellular-scale changes.

The delivery of MSCs to an ischemic heart has been a used as a therapy to improve cardiac recovery. No clear mechanism has emerged to fully explain how the MSCs help repair the infarcted heart, but researchers have proposed several possibilities. Mechanisms of MSC cardiac repair that have been studied include the secretion of paracrine factors, differentiation into cardiomyocytes to repopulate damaged tissue, and induction of neovascularization. However, fusion between MSCs and the cardiac cells may also contribute to functional outcomes, but the extent to which it may is unclear. In this objective it is proposed that fusion between MSCs and cells of the heart will affect the myocardial function in a murine model through improved engraftment of MSCs and possible programming of fusion products into a different phenotype. This hypothesis will be tested by utilizing an *in vivo* imaging system and echocardiography. Functional parameters such as percent fractional area change and cardiac output will be measured over a month in parallel with quantification of fusion in each mouse to determine how fusion affects the functionality of the heart.

2.4 Objective 3: Determine whether heterotypic cell fusion between MSCs and cardiomyocytes can drive transcriptional programming of the resultant fusion product.

Fusion of MSCs and cardiomyocytes allows exchange of cytoplasmic elements and even genetic components if nuclear fusion occurs. This could lead to altered gene and protein expression if the nuclear and cytoplasmic elements from one cell type activate genes previously unexpressed in its fusion partner. To test this possibility, we will first

co-opt viral fusogens to increase the frequency of cell fusion *in vitro*. After increasing the frequency of fusion, we will isolate the fusion products and examine the transcriptome via single-cell RNA-sequencing and compare the results to a culture of cardiomyocytes and a culture of MSCs both with and without co-culture.

Chapter 3 Tracking fusion of human mesenchymal stem cells following transplantation to the heart

Elements of this work have been published as:

Freeman BT, Kouris NA, Ogle BM. Tracking fusion of human mesenchymal stem cells following transplantation to the heart. *Stem Cells Translational Medicine*, 4 (6), 685-694. 2015.

3.1 Abstract

Evidence suggests that transplanted mesenchymal stem cells (MSCs) may aid recovery of damaged myocardium caused by a myocardial infarction. One possible mechanism for MSC-mediated recovery is (re)programming after cell fusion between transplanted MSCs and recipient cardiac cells. Here we utilize a Cre/*LoxP*-based luciferase reporter system coupled to biophotonic imaging to detect fusion of transplanted human pluripotent stem cell-derived MSCs to cells of organs of living mice. Human MSCs, with transient expression of a viral fusogen, were delivered to the murine heart via a collagen patch. Two days and one week later, living mice were probed for bioluminescence indicative of cell fusion. Cell fusion was detected at the site of delivery (heart) as well as distal tissues (stomach, small intestine, and liver). Fusion was confirmed at the cellular scale via fluorescence *in situ* hybridization (FISH) for human-specific and

mouse-specific centromeres. Human cells in organs distal to the heart were typically located near the vasculature suggesting MSCs and perhaps MSC fusion products have the ability to migrate via the circulatory system to distal organs and engraft with local cells. This study reveals previously unknown migratory patterns of delivered human MSCs and associated fusion products in the healthy murine heart. The study also sets the stage for follow-on studies to determine the functional effects of cell fusion in a model of myocardial damage or disease.

3.2 Introduction

More than 715,000 Americans suffer a new or recurrent myocardial infarction each year leading to cell death in cardiac tissue distal to the lesion and a progressive loss of cardiac function [1]. One promising therapy to recover or at least sustain cardiac function is the delivery of MSCs to the damaged myocardium [2-8]. MSCs home to injured tissues [9, 10] and several mechanisms for MSC-based recovery have been proposed. First, MSCs may differentiate into cardiac cells to replace the dead and damaged cells [11-14]. Alternatively, the transplanted MSCs could act through secretion of paracrine factors that limit immune responses [15] and/or increase angiogenesis [10, 16-22]. A third possible mechanism is nuclear (re)programming via fusion between the MSCs and cells of the pericardium, epicardium, or myocardium [23]. Recent studies have uncovered evidence of cell fusion between stem cells and cardiac cells [24-29] but the impact of cell fusion and subsequent (re)programming on cardiac function at the cellular and tissue scale is not well understood.

The biologic outcome of fusion of stem cells at the tissue and organ level has been even more challenging to discern than at the cellular scale due to the difficulty of detecting and tracking fusion products in living organisms. To date, all methods to assess fusion *in vivo* have relied on tissue procurement and histologic analysis. For example, to study the contribution of fusion of bone marrow-derived cells to liver regeneration, female mice expressing green fluorescent protein (GFP) in all hematopoietic-derived cells were used as bone marrow donors (GFP^+ cells) for male mice with liver injury. Fusion in this case was defined as binucleated, GFP+ cells with one Y chromosome observed in histologic tissue sections. The authors showed that bone marrow-derived hepatocytes had a unique gene profile relative to both hematopoietic cells and hepatocytes of the host, suggesting reprogramming after cell fusion [30, 31]. Cell fusion of bone marrow derived hematopoietic cells and cardiomyocytes has also been reported *in vivo*, albeit at a low frequency [23, 29, 32]. However, as with the liver, these studies rely on tissue analysis after sacrificing the host animal (thus limiting studies of the kinetics and outcomes of fusion) and typically analysis is done in target organs and not the entire animal (thus limiting knowledge of the potential breadth of cell fusion).

Lacking is a means to accurately detect fusion *in vivo* in the entire organism over time. To address this gap, we previously developed a molecular approach wherein bioluminescence is induced upon fusion [28]. We utilize a construct encoding the firefly luciferase (*Photinus pyralis*) gene adjacent to a floxed stop codon. When cells expressing this gene fuse with cells expressing the Cre recombinase protein, the *LoxP*

sites are cleaved, excising the stop signal thereby allowing transcription of luciferase. To increase the frequency of fusion, we simultaneously transfect the cells with a viral fusogen, vesicular stomatitus virus (the glycoprotein, VSV-G), along with the *LoxP*-luciferase reporter plasmid [33, 34]. Because bioluminescence can be reliably detected in living organisms, an inducible "living" detection signal is produced that can be tracked in real time.

Here we utilize this Cre/*LoxP*-based molecular approach to detect fusion of transplanted cells to cells of organs of living mice. Using this approach, we found that human mesenchymal stem cells delivered to the murine heart via a collagen-based patch can fuse after delivery and that hybrids formed in this way can be detected *in vivo* in the target organ and in surrounding organ systems. We confirmed the inducible fusion detection system with fluorescence *in situ* hybridization (FISH) for human and mouse centromeres and immunohistochemistry for human leukocyte antigen (HLA-A,B,C). This paper illustrates the potential of this molecular methodology applied to the study of fusion in living organisms especially with cellular transplantation. In addition, we show for the first time the substantial dissemination of human mesenchymal stem cells and human-mouse hybrid cells to stomach and small intestine following transplantation to a healthy murine heart. Follow-on studies will investigate functional effects of cell fusion in a small animal model of myocardial damage or disease.

3.3 Materials and Methods

3.3.1Transgenic Mice

We utilized C57BL/6 mice (Jackson Laboratory, Bar Harbor, ME) (5 mice, **Figure 3-1** only) or transgenic mice that constitutively express Cre recombinase (B6.C-Tg(CMV-cre)1Cgn/J, Jackson Laboratory, Bar Harbor, ME) such that deletion of *LoxP*-flanked genes occurs in all tissues, including germ cells. The Cre gene is under transcriptional control of the cytomegalovirus(CMV) minimal promoter and is X-linked. The Cre sequence was introduced to BALB/cJ derived BALB/c-I embryonic stem (ES) cells. The resulting mice were backcrossed to the BALB/c background for 8 generations and then backcrossed to the C57BL/6J background for 10 generations [35]. Only male Cre mice (4 mice, 2 months of age) were used for **Figures 3-2 through 3-6** in the study due to a false positive signal detected when imaging these female transgenic mice (data not shown).

3.3.2 Cell Culture

Human MSCs derived from human embryonic stem cells (hMSCs from WA-01 or WA-09 (Figure 1 only), a gift of Dr. Peiman Hematti of University of Wisconsin-Madison) were expanded and cultured as previously described [36]. Briefly, hMSCs were cultured on a 0.1% gelatin (Sigma Aldrich, St. Louis, MO) pretreated flask containing α-minimum essential medium (MEM) complete. Alpha-MEM-complete consisted of α-MEM (Invitrogen, Carlsbad, CA), 10% fetal bovine serum (Hyclone, Logan, UT), 0.1 mM nonessential amino acids (Invitrogen), and 2mM L-glutamine (Invitrogen). hMSC cultures were allowed to grow to 60-70% confluence and were replated at a concentration of 1,500 cells/cm^2. These human ESC-derived MSCs have cell surface

markers, differentiation potential, and immunological properties *in vitro* that are similar to adult BM-derived MSCs [36].

3.3.3 Gene Transfer

hMSCs were transiently transfected with viral fusogen VSV-G [24, 37] to promote cell-cell fusion. In addition, they were simultaneously transfected with the luciferase gene adjacent to a floxed stop codon (p231 pCMVe-betaAc-STOP-luc, Addgene, Cambridge, MA) [28]. Transfection was accomplished using the Neon Transfection System (Invitrogen, Carlsbad, CA) as previously described [38]. All recombinant DNA research was conducted according to NIH guidelines and in accord with the University of Wisconsin-Madison and University of Minnesota-Twin Cities Institutional Biosafety Committee.

3.3.4 Myocardial Infarction and Cell Delivery

Mice underwent an infarction procedure by left coronary artery ligation (**Figure 3-1** only) as is routinely performed in the University of Wisconsin Cardiovascular Physiology Core Facility [28, 39, 40]. All animal procedures were performed in accordance with the guidelines of the American Association for Laboratory Animal Science and the University of Wisconsin-Madison Animal Care and Use Committee.

3.3.5 Delivery of Transfected hMSCs via the TissueMend Matrix to the Murine Myocardium

Co-transfected hMSCs were delivered to the myocardium of mice two days after infarction (**Figure 3-1** only) or to a healthy heart (**Figures 3-2 through 3-6**) via a collagen patch (TissueMend, TEI Biosciences, Boston, MA) as previously described [24, 39]. TissueMend matrices (2 x 2 x 0.8 mm) were placed in a 24-well plate (Falcon, Fischer Scientific, Pittsburgh, PA) and hydrated with α-MEM-complete culture medium. Following electroporation, hMSCs were seeded on the TissueMend sections at a concentration of 1×10^6 cells/mL (**Figure 3-1A)**. Medium was changed at 24 and 48 h, at which point the TissueMend matrix containing approximately 1×10^5 transfected hMSCs was attached to the myocardium with a single suture (7-0 prolene Ethicon, Johnson & Johnson, New Brunswick, NJ) at each corner of the matrix. A matrix was placed such that it was in contact with both the infarct and the peri-infarct regions of the myocardium (**Figure 3-1** only) [24, 39]. In the follow up study, two matrices were placed on a healthy, noninfarted mouse heart such that they were in contact with the myocardium (**Figures 3-2 through 3-6**).

3.3.6 Bioluminescence Imaging

Recipient mice constitutively expressed Cre recombinase, therefore when transplanted human MSCs fused with cells of the recipient, the *LoxP* sites were cleaved and the stop signal excised, allowing expression of luciferase. Luciferase expression was detected two and eight days after cell transplantation in living mice with an IVIS (*In vivo* Illuminescence System, IVIS Spectrum, Caliper Life Sciences, Hopkinton, MA) imaging system as previously described [28]. Average radiance was determined by measuring

the emitted photons per second per cm^2 per steradian of each organ with the Living Image In Vivo Imaging Software (PerkinElmer, Waltham, MA).

3.3.7 Optical Analysis of Heart/Tissue Explants

Murine hearts, stomachs, small intestines, livers, and kidneys were harvested eight days after matrix implantation to determine the incidence of fusion at the cellular level. Following excision, hearts were bisected longitudinally through the matrix and other organs were bisected longitudinally near the site of the bioluminescent signal. The tissues were immediately placed into 10% buffered formalin (pH = 7.2; Fisher Scientific, Pittsburgh, PA) for 24 h followed by 24 h of fresh 10% buffered formalin, and a final 24 h incubation in 70% ethanol. Samples were further processed for paraffin embedding and sectioning as previously described [41]. A tissue digestion kit with all human centromere probe (Platinum*Bright*550) and all mouse centromere probe (Platinum*Bright*495) (Kreatech, Amsterdam, the Netherlands) was used to performed FISH on sections [24]. Samples were processed by the Cytogenetics Laboratory (WiCell Research Institute, Madison, WI) according to manufacturer's protocol. Briefly, slides with paraffin embedded sections were baked for 4 h at 56°C. Specimens were incubated with pepsin (Fischer Scientific, Pittsburgh, PA) for 70 min for tissue digestion prior to sequential hybridization of the human probe followed by the mouse probe. After hybridization, slides were stained with DAPI (Sigma Aldrich, St. Louis, MO). Images were acquired with a 60X UPlanSApo (NA = 1.35 Oil), DAPI, Green, and Orange filters, on an Olympus BX41 Upright Fluorescence Microscope (Olympus Valley, PA), and analyzed with FISHView Version 5.5 software (Applied Spectral Imaging, Vista, CA). In

the studies with a myocardial infarction (**Figure 3-1** only), three different hearts were stained with FISH and 10 images per region were analyzed (approximately 40 to 150 cells per image depending on the heart region). Control mice received either the TissueMend patch (without cells) or the TissueMend patch with untransfected MSCs following induction of infarction as described above. In the cases without myocardial infarction, three different hearts were stained with FISH and 6 images per region were analyzed (approximately 20 to 100 cells per image depending on heart region). The small intestine and stomach from the mouse with the highest abdominal bioluminescence emission were stained with FISH and at least 8 images per organ were analyzed (approximately 100 cells per image). Fusion events were defined as nuclei with positive staining for both human centromeres (red) and mouse centromeres (green). The frequency of fusion was quantified for each image and defined as the number of fusion events divided by the total number of nuclei and reported as a percentage (% Fusion Products).

For immunohistochemistry (IHC) analysis, organ sections were deparaffinized by incubating at 60^{o}C for 1 hour and then washed for 6 minutes in Xylene twice. The sections were rehydrated by dipping sections 15 times each in 100% ethanol, 100% ethanol, 95% ethanol, and then finally ultrapure water. Antigen retrieval was accomplished by incubating the sections for 20 minutes at 37^{o}C in 0.5% pepsin (Fischer Scientific, Pittsburgh, PA) in 5mM HCl. The sections were removed and allowed to cool for 10 minutes at room temperature. Sections were rinsed in 1X PBS twice for 3 minutes. Sections were incubated with 1:10 dilution of Unconjugated AffiniPure Fab

Fragment Goat Anti-Mouse IgG (H+L) (Jackson ImmunoResearch Labs, West Grove, PA) in PBS for 1 hour at room temperature. Sections were rinsed again in 1X PBS twice for 3 minutes. A 1:50 dilution of the anti-HLA-A,B,C (EMR8-5, MBL International, Woburn, MA) antibody or a 1:25 dilution of anti-von Willebrand Factor (F8/86, Thermo Fisher, Minneapolis, MN) was made with dilution buffer containing 5% Bovine Serum Albumin (Hyclone, Logan, UT), 2% goat serum (MP Biomedical, Solon, OH), 1% glycine (Sigma Aldrich, St. Louis, MO), and 0.1% triton-X (MP Biomedical, Solon, OH). 40 µL of this antibody solution were placed on each tissue section overnight at 4^{o}C. Sections were washed with 1X PBS and incubated for 45 minutes at 4^{o}C with 40 µL of a 1:200 dilution of the secondary antibody (AF647 goat anti-mouse, Invitrogen, Carlsbad, CA) in dilution buffer. Sections were washed with 1X PBS and mounted using DABCO/DAPI solution composed of 5% DABCO (Sigma Aldrich, St. Louis, MO) and 0.01% DAPI (Sigma Aldrich, St. Louis, MO) in a mixture of 50% glycerol (Fischer Scientific, Pittsburgh, PA) and 50% 2XPBS on a microscope coverslip sealed with nail polish. Fluorescence emission was detected on an IX71 inverted deconvolution fluorescence microscope (Olympus). Images were acquired with a 20X UPlanFluor objective (NA = 0.5), using Slidebook software (Intelligent Imaging Innovations Denver, CO, USA) and analyzed with ImageJ (Fiji; open source software, http://pacific.mpi-cbg.de/wiki/index.php/Fiji). Background fluorescence was determined using a secondary antibody only control.

To confirm that MSCs retained their phenotype after seeding onto the TissueMend patch and prior to transplantation, MSCs were seeded onto TissueMend patches at a

concentration of 1 x 10^6 cells per mL and allowed to attach overnight. Medium was changed at 24 h and 48 h, at which point the cells were fixed with 4% paraformaldehyde for 15 minutes and then washed twice with 1X PBS. A 1:25 dilution of goat anti-CD105 (GKY02, R&D Systems, Minneapolis, MN, USA) was made with dilution buffer containing 5% Bovine Serum Albumin (Hyclone, Logan, UT), 2% goat serum (MP Biomedical, Solon, OH), 1% glycine (Sigma Aldrich, St. Louis, MO), and 0.1% triton-X (MP Biomedical, Solon, OH). 200 µL of this antibody solution was placed on patches seeded with MSCs overnight at 4^{o}C. The patches seeded with MSCs were washed with 1X PBS and incubated for 45 minutes at 4^{o}C with 200 µL of a 1:200 dilution of the secondary antibody (AF488 donkey anti-goat, Invitrogen, Carlsbad, CA) in dilution buffer. Patches seeded with MSCs were washed with 1X PBS and stained with DABCO/DAPI solution. Fluorescence emission was detected using a multiphoton fluorescence microscope (Prairie Technologies, Madison, WI). Images were acquired with a 40X objective (NA = 0.80), using Prairie View 5.0 software and analyzed with ImageJ. Background fluorescence was determined using a secondary antibody only control.

3.3.8 Statistical Analysis

Statistical analyses were performed by ANOVA with Tukey's Honest Significant Difference (HSD) *post hoc* test for multiple comparisons or Student's *t*-test for two independent samples, where *P* values lower than 0.05 were considered to be significant. Data were analyzed with SigmaPlot (Systat Software Inc, San Jose, CA).

3.4 Results

3.4.1 Fusion of MSCs occurs both spontaneously and with the aid of viral fusogens following transplantation to the murine heart

Previously, we have shown that fusion of transplanted MSCs with recipient cells occurs spontaneously in the murine heart [24]. In this case, a myocardial infarction was induced in C57BL/6 mice and then treated with either a TissueMend patch without cells (TM only) or a TissueMend patch with human MSCs (TM+MSCs). MSCs seeded on the patch and incubated for two days prior to transplantation maintained expression of CD105 (>95% of cells imaged; **Figure 3-1A**). Mice were sacrificed after three weeks and the hearts of each were fixed and sectioned. Histological sections were probed using FISH for human-specific and mouse-specific centromeres and all nuclei containing both probes were considered fusion products. Fusion products were identified in the TissueMend patch, BorderZone (area between patch and myocardium), unhealthy heart (the infarct scar), and healthy heart (areas distant from the infarct). Recently we have conducted a more comprehensive quantitative analysis of these tissues by systematically counting 10 images, selected randomly for each region. In each region the percentage of fusion products was determined by dividing the number of fusion products by the total number of cells imaged. We detected substantial numbers of fusion products in the TissueMend patch group, (TM+MSCs, 22% $\pm$ 17%), relative to the TM only control (2% $\pm$ 2%, $P < 0.05$, **Figure 3-1B** and **Table 3-1**). A similar result was observed in the BorderZone group, (TM+MSCs, 14% $\pm$ 9%; group TM only, 0.2% $\pm$ 0.5%). Representative images of the TissueMend and BorderZone regions can be seen in **Figure 3-1C** (inset shows magnified view).

A

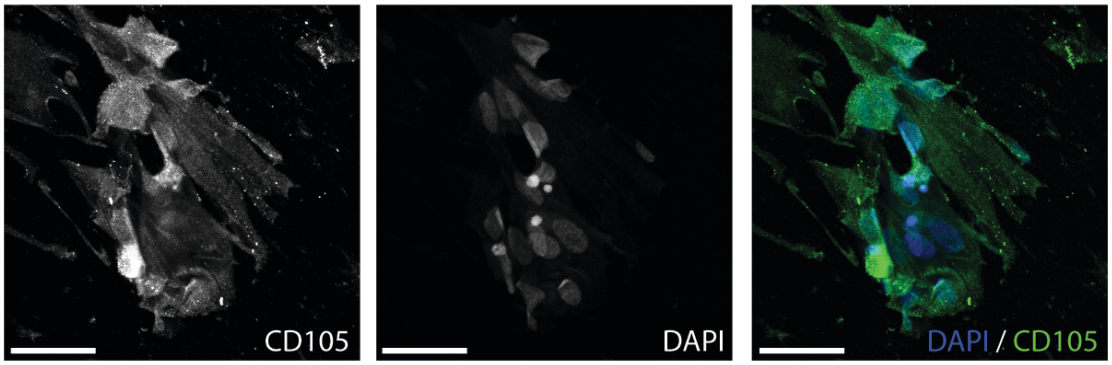
CD105
DAPI
DAPI / CD105

B

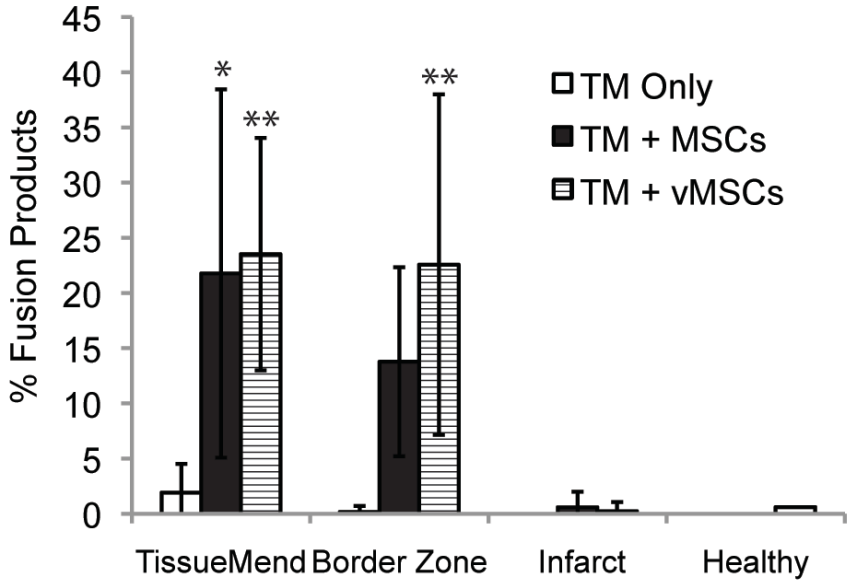
% Fusion Products
45
40
35
30
25
20
15
10
5
0
*
**
**
TM Only
TM + MSCs
TM + vMSCs
TissueMend
Border Zone
Infarct
Healthy

C

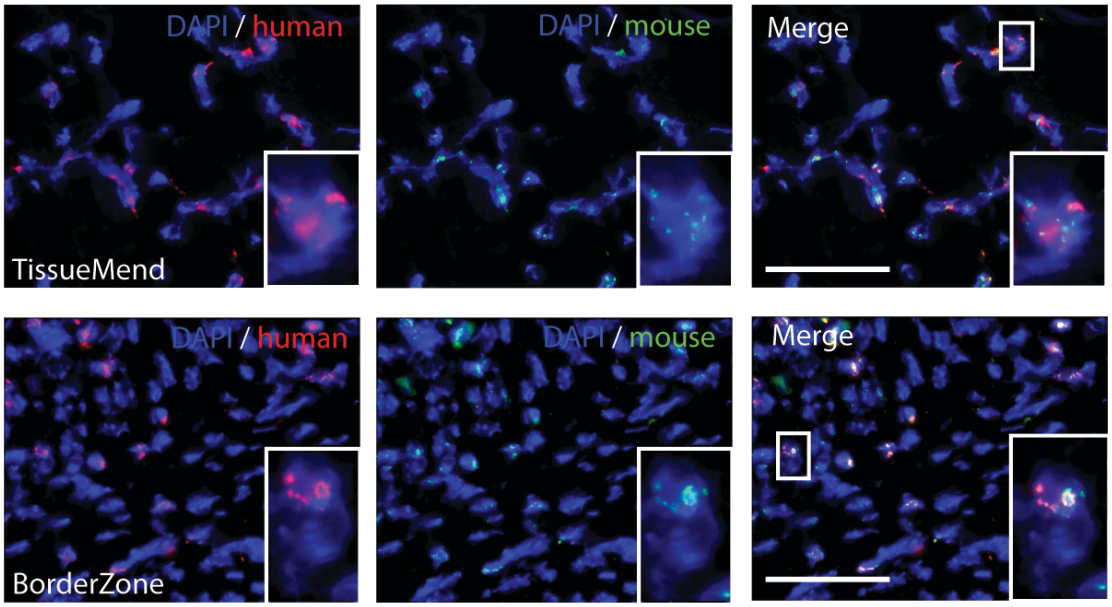
DAPI / human
DAPI / mouse
Merge
TissueMend
DAPI / human
DAPI / mouse
Merge
BorderZone

Figure 3-1. **Frequency of fusion following delivery of MSCs to infarcted murine heart via TissueMend (TM) collagen-based patch**. **A,** Representative optical section (multiphoton microscopy) of human MSCs following two days on the TM patch and stained for MSC-marker CD105 (green) and DAPI (blue). Greater than 95% of cells imaged were CD105 positive. Regions with high intensity (CD105) indicate cells aligned with planes other than the focal plane, perhaps indicative of cells migrating into the patch. Scale bars are 50 μm. **B,** MSCs and VSV-G-transfected MSCs (vMSCs) fused with murine cells in an infarcted heart after delivery via TissueMend patch (TM). There was a significant increase in the percent of fusion products present in the TissueMend for untransfected MSCs (TM + MSCs), 22% $\pm$ 17% (10 images/area), compared to the TM only control with no cells, 2% $\pm$ 2% (10 images/area) (*, $P < 0.05$). The percent of fusion products present in the BorderZone increased as well for untransfected MSCs (14% $\pm$ 9%, 10 images/area), but it was not significantly different than the TM only control (0.2% $\pm$ 0.5%, 10 images/area). The percent of fusion products in the TissueMend and BorderZone increases (albeit not significantly) to 24% $\pm$ 16% and 23% $\pm$ 15% when the MSCs were transfected with VSV-G (TM + vMSC) prior to delivery (10 images/area)(**, $P < 0.01$, compared to the TM only control). There was no significant difference between the TM control and both MSC and vMSCs in the unhealthy heart and healthy heart regions. All percentages represent 10 randomly selected images for each region in the tissue sections. **C,** Representative images of murine heart following transplantation stained for human (red) and mouse (green) centromeres using FISH. The top row contains a field of view from the TissueMend patch; the bottom row contains a field of view from the BorderZone between the TissueMend and infarcted myocardium. Scale bars are 50 μm.

Treatment	Location	% Fusion Products of Total Cells	% Unfused Human Cells of Total Human Cells
TM Only (No Cells)	TissueMend	2% ± 2%	10.0% ± 0.2%
	BorderZone	0.2% ± 0.5%	0% ± 0%
	Infarct	0% ± 0%	0% ± 0%
	Healthy	0% ± 0%	0% ± 0%
TM + MSCs	TissueMend	22% ± 17%	3% ± 9%
	BorderZone	14% ± 9%	3% ± 6%
	Infarct	0.6% ± 1%	14% ± 20%
	Healthy	0% ± 0%	0% ± 0%
TM + vMSCs (with VSVG)	TissueMend	24% ± 16%	3% ± 6%
	BorderZone	23% ± 15%	2% ± 3%
	Infarct	0.2% ± 0.6%	0% ± 0%
	Healthy	0.6% ± 1%	0% ± 0%

Table 3-1. Fusion in regions of the heart for different treatments. TM = TissueMend, MSCS = human Mesenchymal Stem Cells, vMSCs = Transfected human Mesenchymal Stem Cells, VSVG = Vesicular Stomatitis Virus-Glycoprotein

In the same study, we asked whether transfection of MSCs with the fusogen of the vesicular stomatitis virus (VSV-G) prior to transplantation augments fusion. The percent of fusion products in the TissueMend patch and BorderZone was higher (though not

statistically higher) with addition of the fusogen (24% ± 16% and 23% ± 15%, **Figure 3-1B** and **Table 3-1**). Based on this augmented analysis of tissues of previous studies and in an effort to realize as much cell fusion as possible in a healthy mouse model, we elected to implement our *in vivo* tracking method using MSCs transfected with the VSV-G viral fusogen. Of note, the current study could have been conducted without the fusogen (as is the case for most preclinical and clinical MSC grafts).

3.4.2 Cell fusion can be detected at the delivery site and at distal organs in living mice

To test the hypothesis that cell fusion between hMSCs and cells of the heart occurs and can be detected in living animals, we transplanted hMSCs expressing viral fusogen VSV-G and floxed luciferase to the healthy murine myocardium. To determine whether transplanted cells could fuse with the cells of the ventricle and persist for at least a week, live animal imaging for bioluminescence (and therefore cell fusion) was conducted at two and eight days after transplantation. Interestingly, bioluminescence was detected both in the chest region and the mid/lower abdomen (**Figure 3-2A, B**) suggesting transplanted cells could fuse with recipient cells both in the heart (chest region) and also in organs distal to the heart (abdominal region). The average radiance was unchanged or increasing from 2 to 8 days suggesting either fusion can occur over an extended period or that cells that fuse early after transplantation are capable of proliferation. A similar increase in average radiance due to MSC proliferation *in vivo* has recently been shown to occur in mice who received MSCs injected subcutaneously [42].


A
Chest
Abdomen
Average Radiance [p s-1cm-2 sr-1]
1200
1000
800
600
400
200
0
4000
3500
3000
2500
2000
1500
1000
500
0
2
8
Day
Mouse 1
Mouse 2
Mouse 3

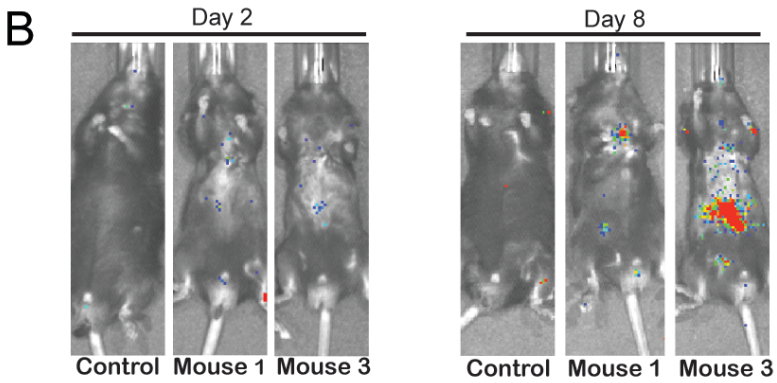
B
Day 2
Day 8
Control
Mouse 1
Mouse 3
Control
Mouse 1
Mouse 3

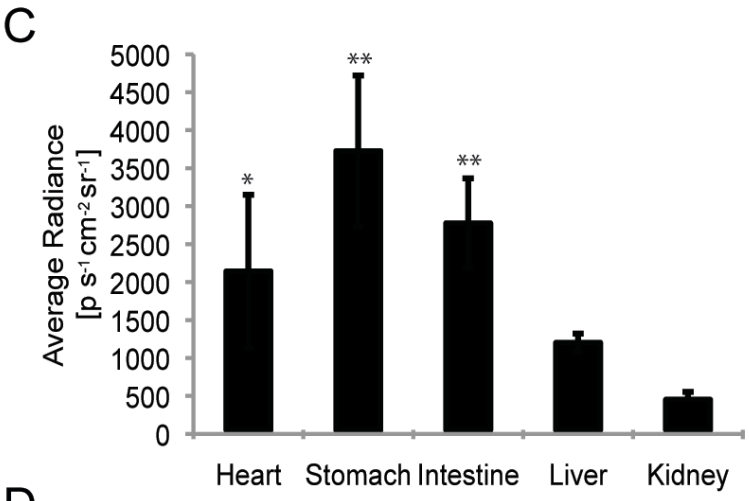
C
Average Radiance [p s-1 cm-2 sr-1]
5000
4500
4000
3500
3000
2500
2000
1500
1000
500
0
*
**
**
Heart
Stomach
Intestine
Liver
Kidney

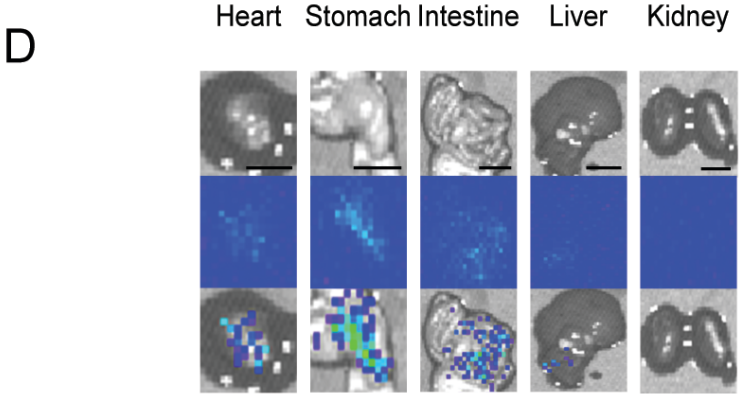
D

Figure 3-2. Detection of cell fusion in living mice. A, Average bioluminescent radiance (photons/second/cm^2/steradian) of chest and abdomen of mice receiving MSCs 2 and 8 days following transplantation to the heart. **B,** Representative IVIS imaging of one control and two treated mice (Mouse 1, Mouse 3). **C,** Average bioluminescent radiance (photons/second/cm^2/steradian) of heart, stomach, small intestine, liver and kidney (n=4 mice). Signal from heart, stomach, and small intestine was significantly higher than that of corresponding control organs and kidney tissue of treated mice (** $P < 0.01$, * $P < 0.05$). **D,** Representative images for each organ. From top to bottom: photograph, bioluminescence emission, overlay. Scale bar equals 10 mm.

At eight days bioluminescence peaks before dropping off (**Figure 3-3)**, therefore mice were euthanized and the heart and organs in the vicinity of the bioluminescent signal were extracted and imaged independently. A distinct bioluminescent emission was detected in the excised heart of all (n = 4) mice receiving transplanted cells (2090 $\pm$ 1008 photons/second/cm^2/steradian (p/s/cm^2/sr), $P < 0.05$ when compared to average radiance in non bioluminescent organs (e.g., kidney), (**Figure 3-2C, D**). Interestingly, bioluminescence was also detected in the stomach and small intestine of transplanted mice, at levels similar to that observed in the heart. The stomach had the highest emission (3673 $\pm$ 996.8 p/s/cm^2/sr), while the small intestine emission was slightly lower (2723 $\pm$ 590.6 p/s/cm^2/sr), (n=4 mice, $P < 0.01$ when compared to average radiance in non bioluminescent organs (e.g., kidney)). Some of the mice receiving cell transplants also exhibited low levels of bioluminescence in the liver (1149 $\pm$ 119.0 p/s/cm^2/sr) (n=4, not significant when compared to average radiance in non bioluminescent organs (e.g., kidney)). Other distal organs exhibited no bioluminescence (e.g., kidneys, spleen and lungs) and were not excised for quantification. However, the kidneys were used as a negative control organ for comparison (399.4 $\pm$ 102.1 p/s/cm^2/sr). The detected

luciferase activity is a reflection of the number of cells expressing luciferase and therefore a reflection of the relative number of cell fusion events.

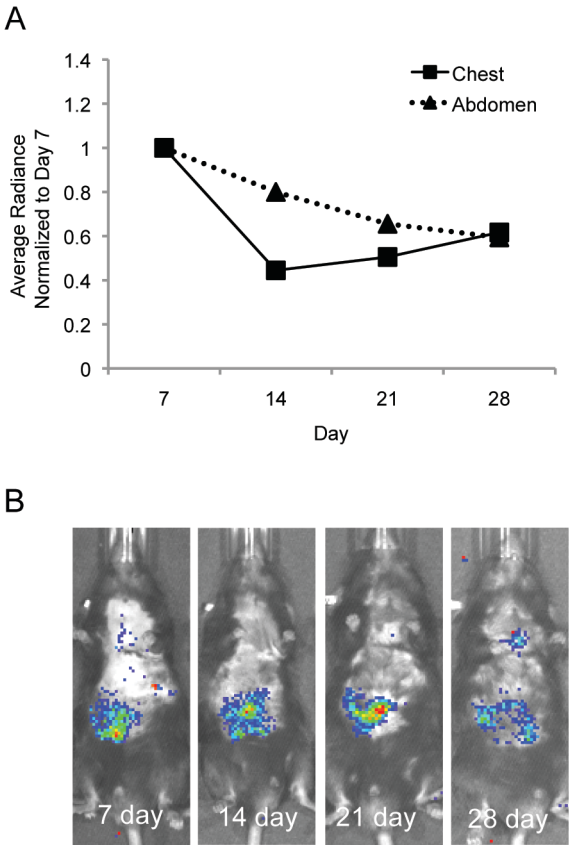

Figure 3-3. **Detection of cell fusion in living mice peaks at 1 week. A,** Average radiance of chest and abdomen of mice at 1, 2, 3 and 4 weeks following transplantation of MSCs to the heart. Values were normalized to the week 1 average radiance. **B,** Representative IVIS image of a mouse at each time point.

3.4.3 Confirmation of hMSC-mouse cell fusion at the cellular level

To assess fusion at the cellular level, Fluorescence *In Situ* Hybridization (FISH) was used to distinguish centromeres of the donor (human) from those of the recipient (mouse). Cells exhibiting fluorescence signals indicative of both human and mouse centromeres were considered fusion products. Using this criterion, fusion products

were detected and quantified in organs emitting a bioluminescent signal. In the heart, fusion products were 52% ± 24% of total cells imaged in the collagen patch (n = 17 fields of view containing fusion products of interest, 358 total cells) and 44% ± 27% of total cells imaged in scar-like tissue (BorderZone) between the patch and damaged myocardium (n = 17 fields of view containing fusion products of interest, 1693 total cells) (**Figure 3-4A** and **Table 3-2**). A few fusion products were localized to the healthy heart (3% ± 5% of total cells imaged, n=4 fields of view containing fusion products of interest, 553 total cells). The background fluorescence signal (green) in the healthy heart image is due to autofluorescence of cardiac sarcomeres (cytoplasmic), which did not interfere with the nuclear staining of the centromeres (**Figure 3-4C**). The result was not a function of the TissueMend delivery vehicle as similar results were obtained following bolus injection of vMSCs directly to the myocardium (**Figure 3-5**).

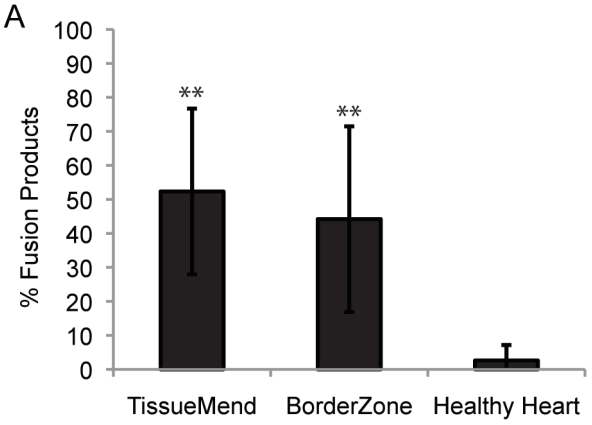

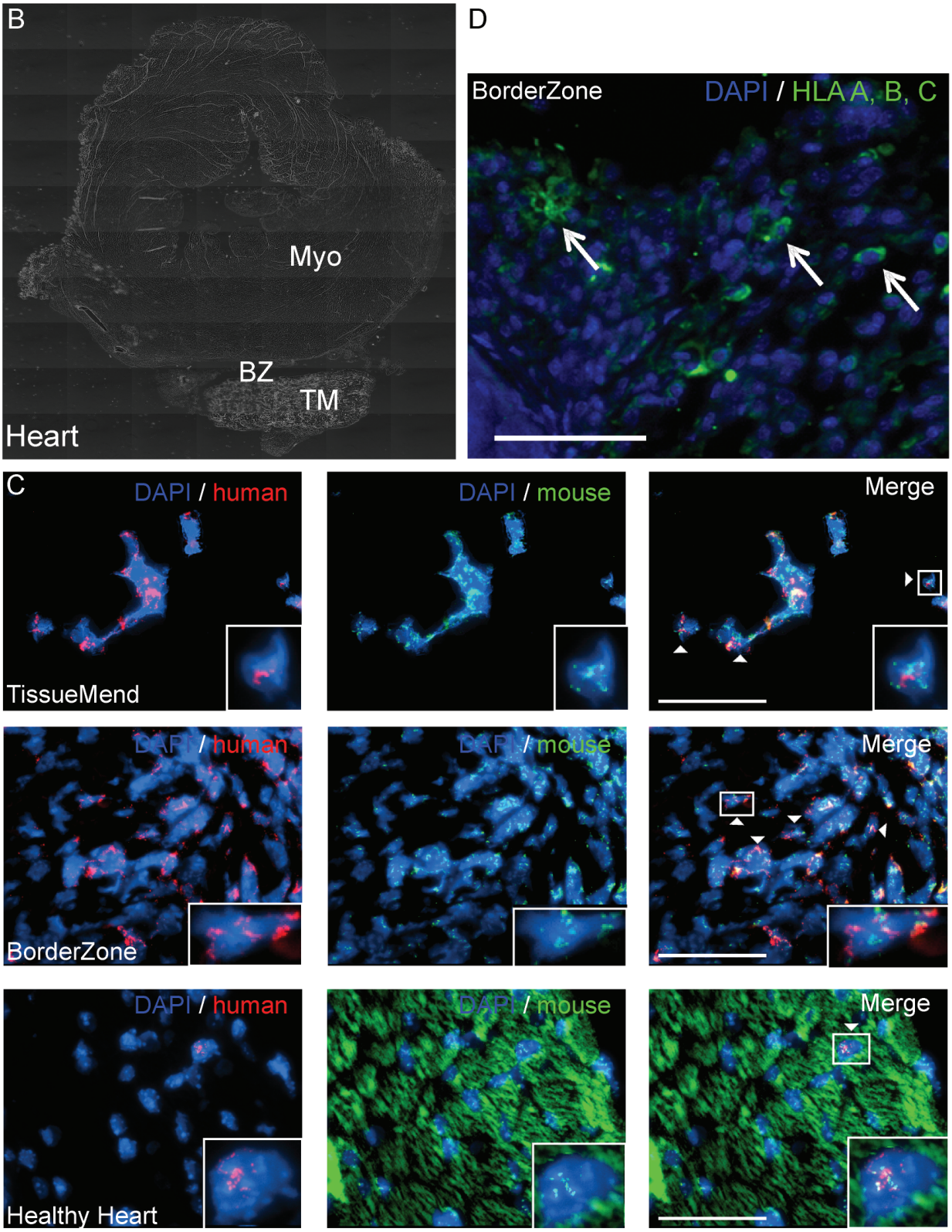
B
Myo
BZ
TM
Heart
D
BorderZone
DAPI / HLA A, B, C
C
DAPI / human
DAPI / mouse
Merge
TissueMend
DAPI / human
DAPI / mouse
Merge
BorderZone
DAPI / human
DAPI / mouse
Merge
Healthy Heart

Figure 3-4. **Frequency of fusion following delivery of vMSCs to healthy, noninfarcted, murine myocardium via TissueMend (TM) collagen-based patch.** VSV-G-transfected human MSCs (vMSCs) fused with recipient cells in the murine heart after delivery via TissueMend patch. **A,** Significantly more fusion products were detected in the TissueMend patch and BorderZone than in the healthy heart distant from the patch (** $P < 0.01$). **B,** Bright field cross section of the heart. **C,** FISH images are stained for mouse centromeres (green), human centromeres (red) and nuclei (blue). Representative fusion products, defined as dual color fluorescence within individual nuclei, are designated with a white arrowhead. Insets are magnified views of representative fusion products. Background signal in the healthy heart is due to autofluorescence of cardiac sarcomeres, this was left intentionally to appreciate position of fusion products relative to healthy myocardial tissue. Scale bar is 50 μm. **D,** Immunohistochemistry for HLA-A,B,C (green) and nuclei (blue). Scale bar is 50 μm.

Organ	**% Fusion Products of Total Cells**	**% Unfused Human Cells of Total Human Cells**	**% Fusion Products of Total Human Cells**
Heart – TissueMend	52% ± 24%	7% ± 8%	93% ± 8%
Heart – BorderZone	44% ± 27%	9% ± 9%	91% ± 9%
Heart – Healthy Heart	3% ± 5%	0% ± 0%	100% ± 0%
Stomach	5% ± 5%	12.5% ± 28%	87.5% ± 28%
Small Intestine	11% ± 5%	7.1% ± 11%	92.9% ± 11%

Table 3-2. Frequency of Fusion in organs and tissues of mice following transplantation of MSCs expressing viral fusogens (vMSCs)

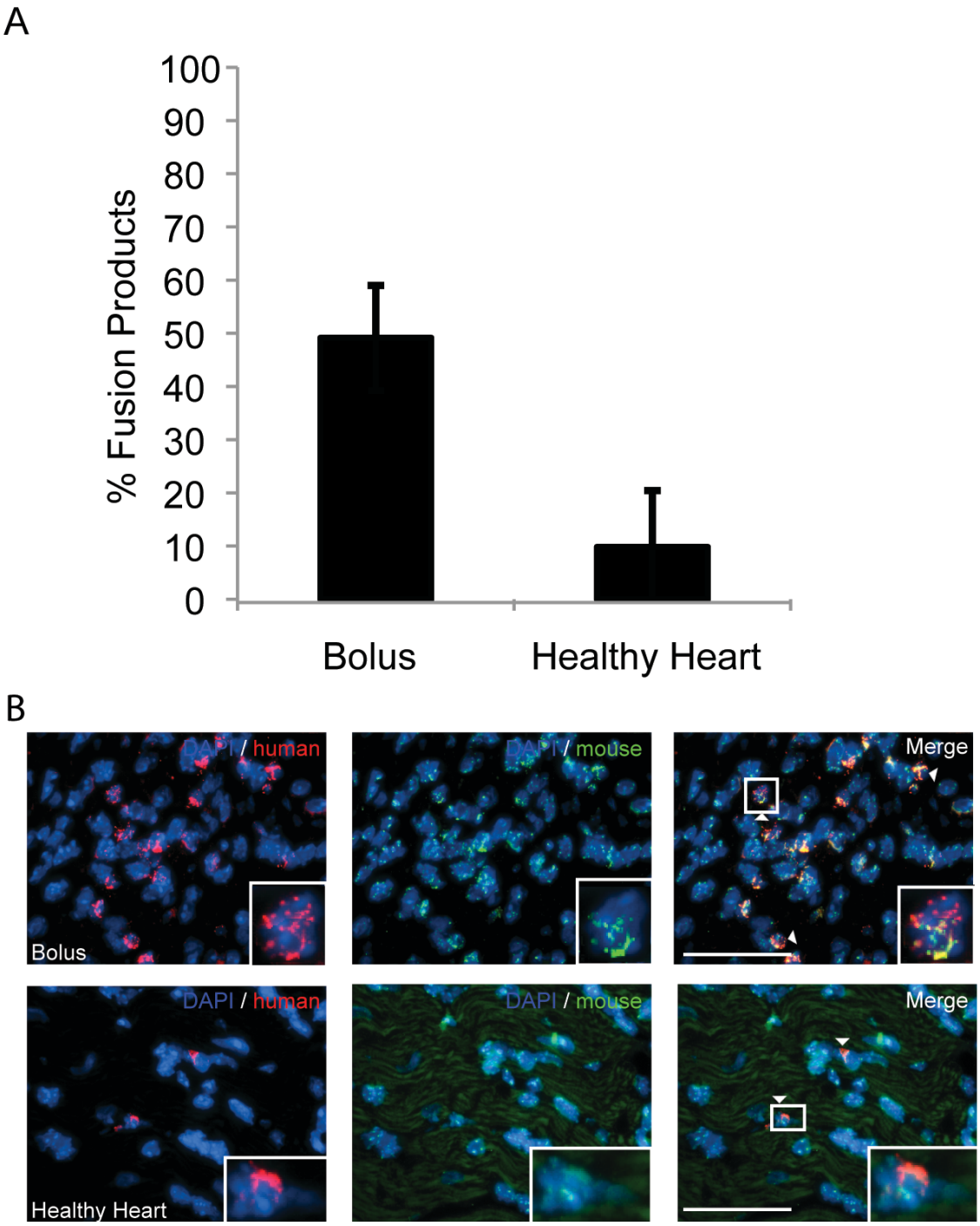

Figure 3-5: **Frequency of fusion following delivery of vMSCs to murine myocardium via bolus injection. A,** VSV-G-transfected human MSCs (vMSCs) fused with recipient cells in the murine heart after bolus injection directly into the myocardium. Fusion hybrids were prevalent in a discrete region assumed to be associated with the point of injection (49% $\pm$ 10% fusion products). Human cells were found in regions beyond the borders of the discrete region (10% $\pm$ 11% fusion products) and were more prevalent (not significant) than fusion hybrids located in

the healthy myocardium following transplantation with the TissueMend patch (3% ± 5%). **B,** Representative images of murine heart following transplantation stained for human (red) and mouse (green) centromeres using FISH. The top row contains a field of view from the Bolus injection; the bottom row contains a field of view from the Healthy Heart. Background (green) signal in the healthy heart is due to autofluorescence of cardiac sarcomeres; this was left intentionally to appreciate position of fusion products relative to healthy myocardial tissue. Scale bars are 50 μm.

The small intestine exhibited extensive fusion (11% ± 5% of total cells imaged, n=8 fields of view containing fusion products of interest, 880 total cells), with most of the fusion products localized to the lamina propria of the villi (34% ± 18% of cells in lamina propria, 222 total cells) (**Figure 3-6** and **Table 3-2**). No fusion products were detected in the epithelium of the small intestinal villi (n = 72 villi). Unfused human cells were seen in the small intestine (7.1% of human cells detected via FISH, n = 8 fields of view, 98 total human cells). In the stomach, fusion products were 5% ± 5% of total cells imaged (n=14 fields of view containing fusion products of interest, 913 total cells) and fusion products were primarily detected in regions close to the vasculature (**Figure 3-7, 3-8** and **Table 3-2**). Unfused human cells were seen in the stomach (12.5% of human cells detected via FISH, n = 14 fields of view, 32 total human cells). These results confirm the bioluminescent emission detected in the live animals in a variety of organs.

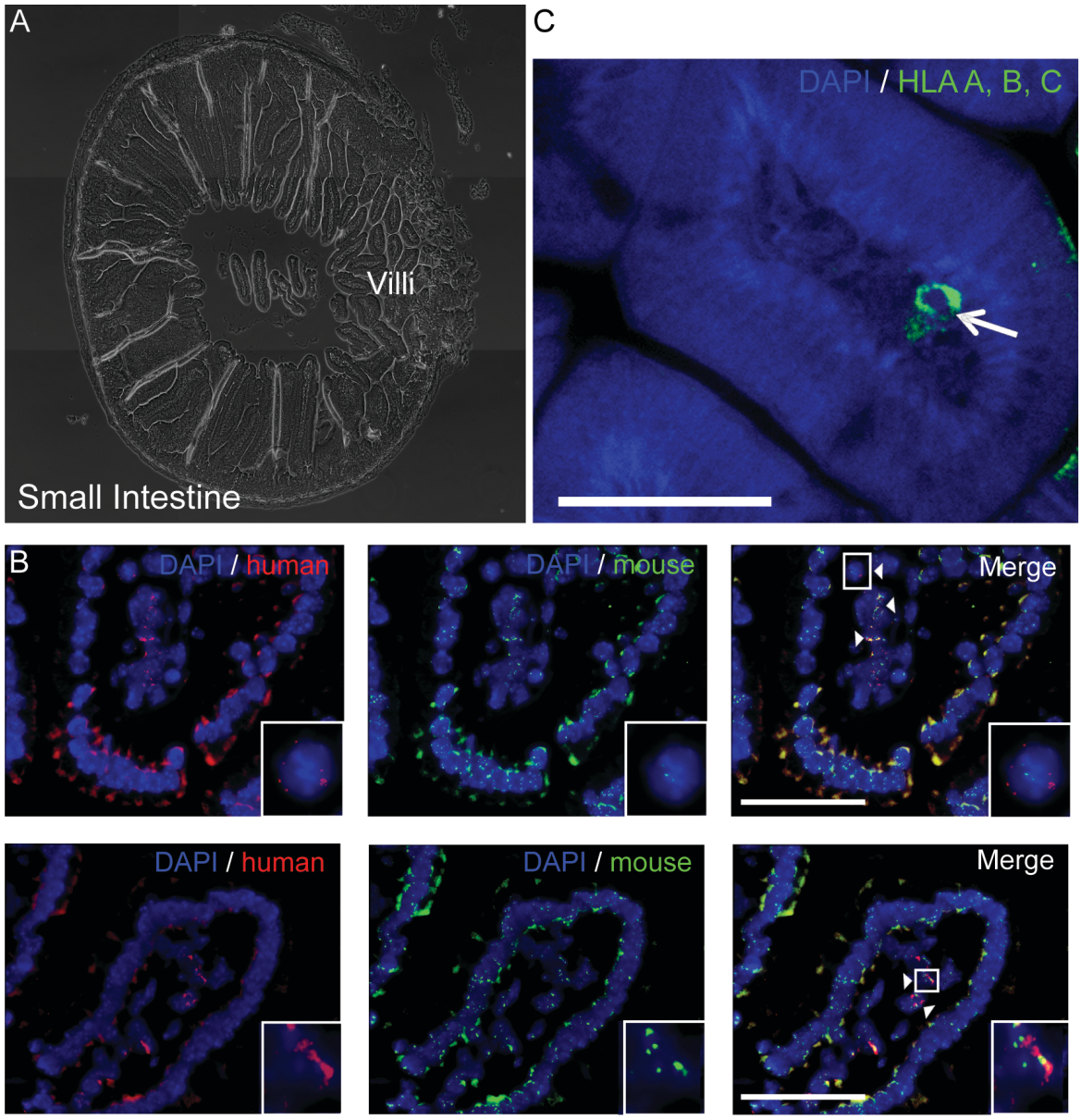

Figure 3-6: Detection of fusion products in the murine small intestine using FISH. Fusion products (white arrowhead) and unfused human cells (white arrow) were detected in the murine small intestine using a human centromere probe (red) and a murine centromere probe (green). **A,** Bright field cross section of the small intestine. **B,** FISH images are stained for mouse centromeres (green), human centromeres (red) and nuclei (blue). Insets are magnified views of representative fusion products. Scale bar is 50 μm. **C,** Immunohistochemistry for HLA-A,B,C (green) and nuclei (blue). Scale bar is 50 μm.

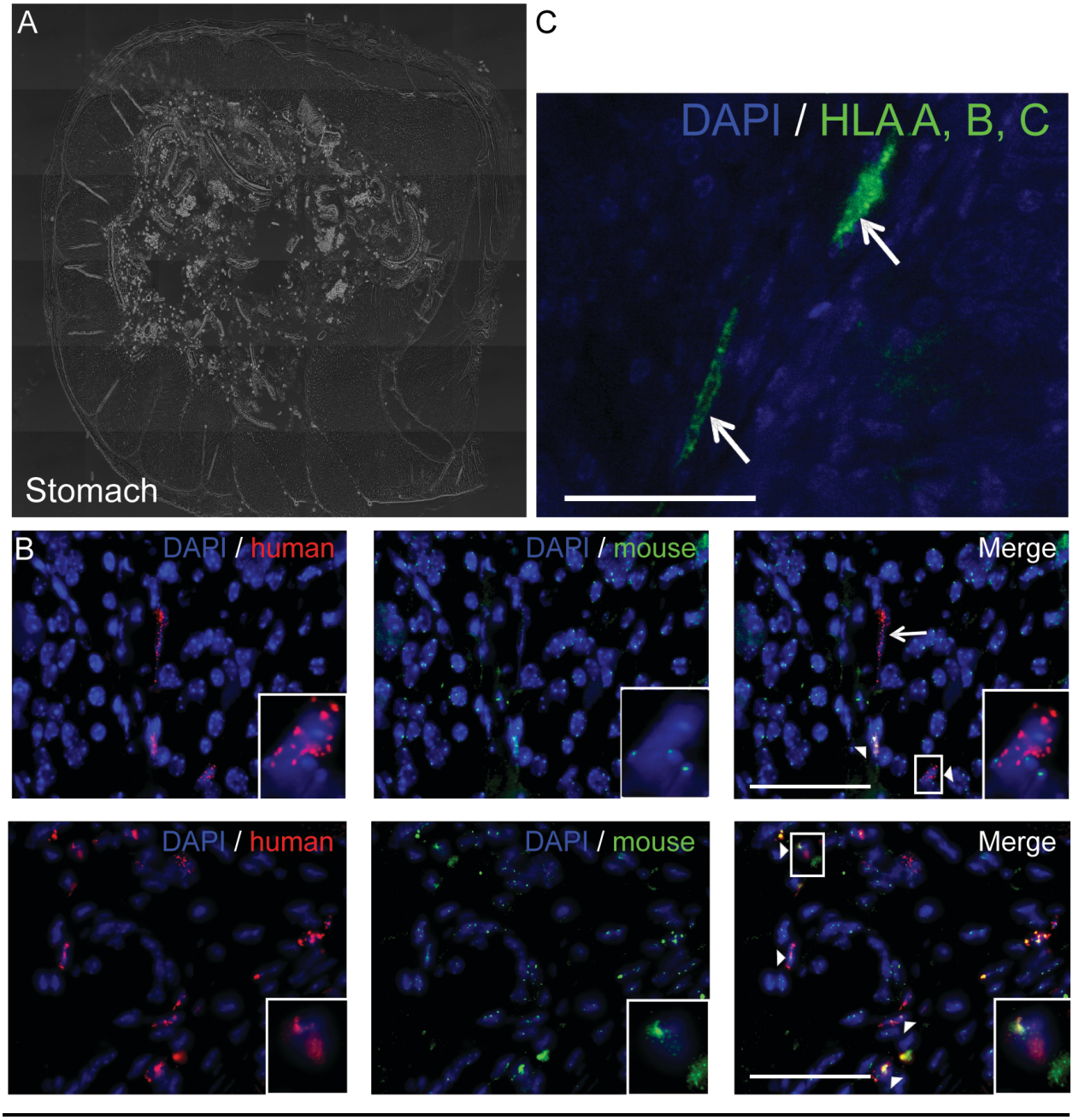

Figure 3-7: Detection of fusion hybrids in the murine stomach using FISH. Fusion products (white arrowhead) and unfused human cells (white arrow) were detected in the murine stomach using a human centromere probe (red) and a murine centromere probe (green). **A,** Bright field cross section of the stomach. **B,** FISH images are stained for mouse centromeres (green), human centromeres (red) and nuclei (blue). Insets are magnified views of representative fusion products. Scale bar is 50 μm. **C,** Immunohistochemistry for HLA-A,B,C (green) and nuclei (blue). Scale bar is 50 μm.

3.4.4 HLA A,B,C expressing cells are detected at delivery site and distal organs

To further confirm the translocation of human MSCs from the site of delivery (the heart) to the small intestine and stomach, IHC was conducted with an anti-HLA A,B,C antibody. Using this method, human cells were found in tissues harboring a bioluminescent signal (**Figure 3-4D, 3-6C, 3-7C**). As with the FISH analysis in the heart, the human cells were concentrated in the collagen patch and in the scar-like tissue between the patch and damaged myocardium. The small intestine proved difficult to probe due to high levels of autofluorescence. However, a few human cells expressing high levels of HLA A,B,C (at an intensity level above background) were detected in the lamina propria. In the stomach, human cells were observed in regions near blood vessel-like structures, similar to what was seen in the FISH analysis. These results further confirm the movement of human MSCs from the mouse heart to the small intestine and stomach.

3.4.5 Detection of fusion products near the vasculature in the murine stomach

To test whether the observed fusion products were located near blood vessels in a distal organ, the stomach was stained with an anti-von Willebrand Factor (vWF) antibody, a marker for endothelial cells. By staining a stomach section adjacent to the section used for FISH analysis, the location of the fusion products relative to the blood vessels could be ascertained. Fusion products were usually found near vWF positive cells (**Figure 3-8)**. One fusion product (**Figure 3-8**, inset) was located directly next to a blood vessels (dashed line). This result supports the possibility that human cells or human cell hybrids transit via the vasculature to distal organs.

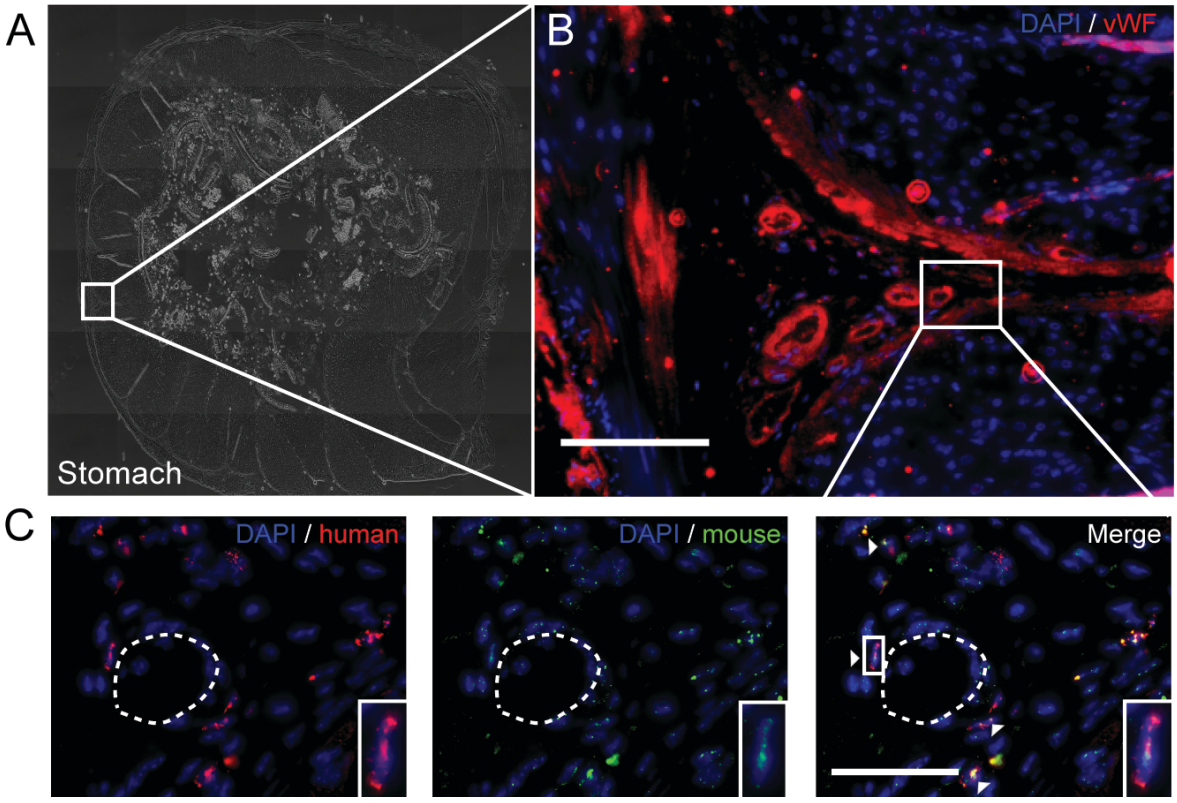

Figure 3-8: Detection of fusion products near the vasculature in the murine stomach. Fusion products (white arrowhead) were detected adjacent to the vasculature in the murine stomach using a human centromere probe (red) and a murine centromere probe (green) as well as an antibody for von Willebrand Factor (vWF), a marker for endothelial cells. **A,** Bright field cross section of the stomach. **B,** Immunohistochemistry for vWF (red) and nuclei (blue). Scale bar is 100 μm. **C,** FISH staining for mouse centromeres (green), human centromeres (red) and nuclei (blue). Insets are magnified views of a representative fusion product near a blood vessel (dashed line). Scale bar is 50 μm.

3.5 Discussion

In this study, we took advantage of a Cre/*LoxP*-based molecular approach to detect fusion of hMSCs following transplantation to the heart. In this way, we were able to determine the presence of fusion in the heart and in other tissues and organ systems of the mouse. We found (i) fusion of hMSCs with cells of the mouse can occur at the

delivery site and at distal organs, (ii) fusion is not a prerequisite nor does it appear to hinder movement of hMSCs away from the delivery site since unfused human cells were found in the stomach and small intestine, and (iii) fusion products in distal organs were localized around vasculature. This is the first study to specifically track fusion of MSCs after transplantation and to do so at the whole organism scale.

Migration of MSCs has been indentified in studies conducted to monitor homing and engraftment of MSCs. MSC migration in disease models or injured tissue has been reported in tumors [43], arthritic joints [44], middle cerebral artery occlusion [45], and myocardial infarction [46, 47]. In a disease model for Chagas disease, which affects heart function, MSCs injected intravenously migrated to a limited degree to the heart and to a greater extent to the liver, lungs, and spleen [48]. Similarly, other studies show that the majority of MSCs injected to the venous system were found in the liver, lung, and spleen [47, 49]. We also observed hMSC fusion products in the liver, though most hMSC fusion products were detected in the heart, stomach and intestine. This difference from previous studies could reflect the delivery method or the fact that transplanted cells expressed a viral fusogen. In our study hMSCs were delivered on a myocardial patch rather than an intravenous injection as used in other studies. hMSC fusion products in the heart were found primarily in the collagen patch and in scar-like tissue between the patch and damaged myocardium. Homing of hMSCs or hMSC fusion products of our study may also have been impacted by the expression of fusogen, VSV-G. The fusogen may enable fusion of hMSCs with circulating cells thereby altering their migratory properties and subsequent tissue targets. Also, our analysis of tissue

sections followed detection of fusion at the organ level. Thus it is possible we missed organs that contained only human cells or that contained fused human cells at levels too low to detect with our approach.

Interestingly, hMSC fusion products in organs distal to the heart (i.e., stomach and small intestine) were found primarily near the vasculature, suggesting blood vessels were the likely path for mobility. Another possibility is that hMSCs remained in tissues where the fusogen was most likely to be active (pH of approximately 5.5) and therefore most likely to fuse with recipient cells. Similarly, the proximity of cells of the stomach to acidic digestion conditions may also activate the fusogen, stimulating fusion. Yet unclear is whether hMSCs fuse with cells of the murine heart, then migrate or migrate first to fuse with cells of distal tissues. Of note, unfused hMSCs were detected in the stomach and small intestine, suggesting that hMSCs migrate to and infiltrate the distal organs without fusion. Also unclear is what cell type(s) of the recipient serve as fusion partners. Possible candidates include those previously reported to fuse with transplanted MSCs, 1) cardiomyocytes of the heart [23, 29, 32],and 2) hepatocytes of the liver [30, 31]. In addition, macrophages may fuse with transplanted MSCs as they have well-defined fusion machinery used to fuse with other macrophages for the formation of giant cells [50].

The detection of fusion products was made possible by combining an inducible, Cre/*LoxP*-based molecular strategy with whole animal imaging using the IVIS system. The Cre/*LoxP* system utilizes the enzyme Cre recombinase, which only cuts at *LoxP*

sites, to excise the floxed stop codon from the *LoxP*-luciferase construct thus expressing the reporter only when both the Cre recombinase enzyme (mouse cells) and *LoxP*-luciferase plasmid (hMSCs) are present in the same cell. This inducible method ensures detection of only true fusion products (and their progeny) both *in vitro* and *in vivo.* Also, the IVIS system allows imaging of bioluminescence intensity of the entire animal, not just regions of interest. We used this macro scale imaging technology to detect fusion in locations that were not necessarily expected following delivery of our transfected cells. In addition, imaging was conducted while the animal was still alive, which makes imaging of successive time points possible. A more in depth study of the kinetics of fusion *in vivo* will be an important next step applying this approach. In the current study, the *LoxP*-luciferase plasmid was expressed transiently thus the signal is lost once the plasmid is degraded within the cell, which occurs about one week after transfection. If the *LoxP*-luciferase construct was redesigned to be expressed for a longer period or if it were incorporated into the genome, the kinetics experiment could be performed to examine long-term survival (greater than 1 week) and migration of the fusion products.

The Cre/*LoxP* -based approach, as well as the IVIS system, is limited in certain ways. First, the inducible Cre/*LoxP* system detects only true fusion products, however the generation of a signal requires time to remove the stop codon, then transcription and translation of the reporter gene. This temporal delay prevents detection of fusion immediately after the event. As a result, the actual frequency of cell fusion is likely to be underrepresented in our findings. Second, the detection limit of the IVIS system for

internal organs including the heart is approximately 10,000 cells [28]. The resolution limit makes finding very rare events nearly impossible. For example, hMSC fusion products might have been present in other distal organs in the mouse, but if the threshold was not above the background level, fusion would be undetectable. Recent developments in the field of live animal imaging could help address this limitation. For example, a 100-fold stronger synthetic luciferase substrate has been engineered that increases the sensitivity of the system and theoretically decreases the detection threshold to less than 100 events [51].

3.6 Conclusions

In conclusion, this study establishes the efficacy of utilizing a bioluminescent Cre/LoxP system, in conjunction with whole animal imaging, to examine cell fusion following transplantation in live animals. Not only were we able to detect fusion events in live mice, our results suggest that hMSCs, and possibly hMSC fusion products, have the ability to migrate to distal organs and engraft with local cells. This knowledge is important for the clinical transplantation of hMSCs, as it appears hMSCs can home, reside and possibly fuse in unanticipated organs of the recipient, which could cause potential complications in a patient. Similarly while cell fusion occurs at a much lower level without a fusogen, hMSCs are able to spontaneously fuse with other cells [52, 53], therefore additional information about cell fusion and its role in regeneration is essential when assessing the clinical potential and possible side effects of cell transplantation. The work presented here provides not only additional insights into MSC cell fusion and translocation but also establishes a technological platform for further study of cell fusion

in vivo with other types of cellular grafts. These results also provide rationale for future studies to determine how hMSC fusion products affect the functional profile of a diseased murine heart and the mechanisms that govern the functional capacity of fusion products.

3.7 Acknowledgements

The authors would like to thank Jayne Squirrel and Sean Palecek for critical comments on the paper; Erik M. McIntire, Seth M. Taapken, and Karen D. Montgomery of the WiCell Research Institute Cytogenetics Department, Timothy A. Hacker, Guoqing Song, Jill Koch of the University of Wisconsin Cardiovascular Physiology Core Facility, Mohammed Farhoud for technical assistance with IVIS imaging, Philip Jung of the University of Minnesota for assistance with multiphoton imaging and LeAnn Oseth for assistance with FISH imaging in the Cytogenomics Shared Resource at the University of Minnesota with support from the comprehensive Masonic Cancer Center NIH Grant #P30 CA077598.

3.8 References

1. Go AS, Mozaffarian D, Roger VL et al. Executive summary: heart disease and stroke statistics--2013 update: a report from the American Heart Association. Circulation. 2013;127:143-152.
2. Abdel-Latif A, Bolli R, Tleyjeh IM et al. Adult bone marrow-derived cells for cardiac repair: a systematic review and meta-analysis. Arch Intern Med. 2007;167:989-997.

3. Amado LC, Saliaris AP, Schuleri KH et al. Cardiac repair with intramyocardial injection of allogeneic mesenchymal stem cells after myocardial infarction. Proc Natl Acad Sci U S A. 2005;102:11474-11479.

4. Chen S, Liu Z, Tian N et al. Intracoronary transplantation of autologous bone marrow mesenchymal stem cells for ischemic cardiomyopathy due to isolated chronic occluded left anterior descending artery. J Invasive Cardiol. 2006;18:552-556.

5. Chen SL, Fang WW, Ye F et al. Effect on left ventricular function of intracoronary transplantation of autologous bone marrow mesenchymal stem cell in patients with acute myocardial infarction. Am J Cardiol. 2004;94:92-95.

6. Ma J, Ge J, Zhang S et al. Time course of myocardial stromal cell-derived factor 1 expression and beneficial effects of intravenously administered bone marrow stem cells in rats with experimental myocardial infarction. Basic Res Cardiol. 2005;100:217-223.

7. Shake JG, Gruber PJ, Baumgartner WA et al. Mesenchymal stem cell implantation in a swine myocardial infarct model: engraftment and functional effects. Ann Thorac Surg. 2002;73:1919-1925; discussion 1926.

8. Tomita S, Li RK, Weisel RD et al. Autologous transplantation of bone marrow cells improves damaged heart function. Circulation. 1999;100:II247-256.

9. Mouiseddine M, Francois S, Semont A et al. Human mesenchymal stem cells home specifically to radiation-injured tissues in a non-obese diabetes/severe combined immunodeficiency mouse model. Br J Radiol. 2007;80 Spec No 1:S49-55.

10. Nagaya N, Fujii T, Iwase T et al. Intravenous administration of mesenchymal stem cells improves cardiac function in rats with acute myocardial infarction through angiogenesis and myogenesis. Am J Physiol Heart Circ Physiol. 2004;287:H2670-2676.

11. Deb A, Wang S, Skelding KA et al. Bone marrow-derived cardiomyocytes are present in adult human heart: A study of gender-mismatched bone marrow transplantation patients. Circulation. 2003;107:1247-1249.

12. Dimmeler S, Zeiher AM, Schneider MD. Unchain my heart: the scientific foundations of cardiac repair. J Clin Invest. 2005;115:572-583.

13. Kawada H, Fujita J, Kinjo K et al. Nonhematopoietic mesenchymal stem cells can be mobilized and differentiate into cardiomyocytes after myocardial infarction. Blood. 2004;104:3581-3587.

14. Yoon YS, Wecker A, Heyd L et al. Clonally expanded novel multipotent stem cells from human bone marrow regenerate myocardium after myocardial infarction. J Clin Invest. 2005;115:326-338.

15. Chen G, Nayan M, Duong M et al. Marrow stromal cells for cell-based therapy: the role of antiinflammatory cytokines in cellular cardiomyoplasty. Ann Thorac Surg. 2010;90:190-197.

16. Caplan AI. Why are MSCs therapeutic? New data: new insight. J Pathol. 2009;217:318-324.

17. Caplan AI, Dennis JE. Mesenchymal stem cells as trophic mediators. J Cell Biochem. 2006;98:1076-1084.

18. Gnecchi M, He H, Liang OD et al. Paracrine action accounts for marked protection of ischemic heart by Akt-modified mesenchymal stem cells. Nat Med. 2005;11:367-368.

19. Gnecchi M, He H, Noiseux N et al. Evidence supporting paracrine hypothesis for Akt-modified mesenchymal stem cell-mediated cardiac protection and functional improvement. FASEB J. 2006;20:661-669.

20. Kamihata H, Matsubara H, Nishiue T et al. Implantation of bone marrow mononuclear cells into ischemic myocardium enhances collateral perfusion and regional function via side supply of angioblasts, angiogenic ligands, and cytokines. Circulation. 2001;104:1046-1052.

21. Kinnaird T, Stabile E, Burnett MS et al. Marrow-derived stromal cells express genes encoding a broad spectrum of arteriogenic cytokines and promote in vitro and in vivo arteriogenesis through paracrine mechanisms. Circ Res. 2004;94:678-685.

22. Linke A, Muller P, Nurzynska D et al. Stem cells in the dog heart are self-renewing, clonogenic, and multipotent and regenerate infarcted myocardium, improving cardiac function. Proc Natl Acad Sci U S A. 2005;102:8966-8971.

23. Nygren JM, Jovinge S, Breitbach M et al. Bone marrow-derived hematopoietic cells generate cardiomyocytes at a low frequency through cell fusion, but not transdifferentiation. Nat Med. 2004;10:494-501.

24. Kouris NA, Schaefer JA, Hatta M et al. Directed Fusion of Mesenchymal Stem Cells with Cardiomyocytes via VSV-G Facilitates Stem Cell Programming. Stem Cells Int. 2012;2012:414038.

25. Lin HP, Vincenz C, Eliceiri KW et al. Bimolecular fluorescence complementation analysis of eukaryotic fusion products. Biol Cell. 2010;102:525-537.

26. Matsuura K, Wada H, Nagai T et al. Cardiomyocytes fuse with surrounding noncardiomyocytes and reenter the cell cycle. J Cell Biol. 2004;167:351-363.

27. Oh H, Bradfute SB, Gallardo TD et al. Cardiac progenitor cells from adult myocardium: homing, differentiation, and fusion after infarction. Proc Natl Acad Sci U S A. 2003;100:12313-12318.

28. Sprangers AJ, Freeman BT, Kouris NA et al. A Cre-Lox P recombination approach for the detection of cell fusion in vivo. J Vis Exp. 2012:e3581.

29. Zhang S, Wang D, Estrov Z et al. Both cell fusion and transdifferentiation account for the transformation of human peripheral blood CD34-positive cells into cardiomyocytes in vivo. Circulation. 2004;110:3803-3807.

30. Quintana-Bustamante O, Alvarez-Barrientos A, Kofman AV et al. Hematopoietic mobilization in mice increases the presence of bone marrow-derived hepatocytes via in vivo cell fusion. Hepatology. 2006;43:108-116.

31. Quintana-Bustamante O, Grueso E, Garcia-Escudero R et al. Cell fusion reprogramming leads to a specific hepatic expression pattern during mouse bone marrow derived hepatocyte formation in vivo. PLoS One. 2012;7:e33945.

32. Alvarez-Dolado M, Pardal R, Garcia-Verdugo JM et al. Fusion of bone-marrow-derived cells with Purkinje neurons, cardiomyocytes and hepatocytes. Nature. 2003;425:968-973.

33. Jeetendra E, Robison CS, Albritton LM et al. The membrane-proximal domain of vesicular stomatitis virus G protein functions as a membrane fusion potentiator and can induce hemifusion. J Virol. 2002;76:12300-12311.

34. Sun X, Belouzard S, Whittaker GR. Molecular architecture of the bipartite fusion loops of vesicular stomatitis virus glycoprotein G, a class III viral fusion protein. J Biol Chem. 2008;283:6418-6427.

35. Schwenk F, Baron U, Rajewsky K. A cre-transgenic mouse strain for the ubiquitous deletion of loxP-flanked gene segments including deletion in germ cells. Nucleic Acids Res. 1995;23:5080-5081.

36. Trivedi P, Hematti P. Derivation and immunological characterization of mesenchymal stromal cells from human embryonic stem cells. Exp Hematol. 2008;36:350-359.

37. Takada A, Robison C, Goto H et al. A system for functional analysis of Ebola virus glycoprotein. Proc Natl Acad Sci U S A. 1997;94:14764-14769.

38. Sprangers AJ, Freeman BT, Ogle BM. Electroporation Can Efficiently Transfect hESC-Derived Mesenchymal Stem Cells without Inducing Differentiation. The Open Stem Cell Journal. 2011;3:62-66.

39. Kouris NA, Squirrell JM, Jung JP et al. A nondenatured, noncrosslinked collagen matrix to deliver stem cells to the heart. Regen Med. 2011;6:569-582.

40. Michael LH, Entman ML, Hartley CJ et al. Myocardial ischemia and reperfusion: a murine model. Am J Physiol. 1995;269:H2147-2154.

41. Ogle BM, Butters KA, Plummer TB et al. Spontaneous fusion of cells between species yields transdifferentiation and retroviral transfer in vivo. FASEB J. 2004;18:548-550.

42. Preda MB, Ronningen T, Burlacu A et al. Remote transplantation of mesenchymal stem cells protects the heart against ischemia-reperfusion injury. Stem Cells. 2014.

43. Kidd S, Spaeth E, Dembinski JL et al. Direct evidence of mesenchymal stem cell tropism for tumor and wounding microenvironments using in vivo bioluminescent imaging. Stem Cells. 2009;27:2614-2623.

44. Sutton EJ, Henning TD, Boddington S et al. In vivo magnetic resonance imaging and optical imaging comparison of viable and nonviable mesenchymal stem cells with a bifunctional label. Mol Imaging. 2010;9:278-290.

45. Jang KS, Lee KS, Yang SH et al. In vivo Tracking of Transplanted Bone Marrow-Derived Mesenchymal Stem Cells in a Murine Model of Stroke by Bioluminescence Imaging. J Korean Neurosurg Soc. 2010;48:391-398.

46. Kraitchman DL, Heldman AW, Atalar E et al. In vivo magnetic resonance imaging of mesenchymal stem cells in myocardial infarction. Circulation. 2003;107:2290-2293.

47. Kraitchman DL, Tatsumi M, Gilson WD et al. Dynamic imaging of allogeneic mesenchymal stem cells trafficking to myocardial infarction. Circulation. 2005;112:1451-1461.

48. Jasmin, Jelicks LA, Koba W et al. Mesenchymal bone marrow cell therapy in a mouse model of chagas disease. Where do the cells go? PLoS Negl Trop Dis. 2012;6:e1971.

49. Gholamrezanezhad A, Mirpour S, Bagheri M et al. In vivo tracking of 111In-oxine labeled mesenchymal stem cells following infusion in patients with advanced cirrhosis. Nucl Med Biol. 2011;38:961-967.

50. Takeda Y, Tachibana I, Miyado K et al. Tetraspanins CD9 and CD81 function to prevent the fusion of mononuclear phagocytes. J Cell Biol. 2003;161:945-956.

51. Evans MS, Chaurette JP, Adams ST, Jr. et al. A synthetic luciferin improves bioluminescence imaging in live mice. Nat Methods. 2014;11:393-395.

52. Spees JL, Olson SD, Ylostalo J et al. Differentiation, cell fusion, and nuclear fusion during ex vivo repair of epithelium by human adult stem cells from bone marrow stroma. Proc Natl Acad Sci U S A. 2003;100:2397-2402.

53. Terada N, Hamazaki T, Oka M et al. Bone marrow cells adopt the phenotype of other cells by spontaneous cell fusion. Nature. 2002;416:542-545.

Chapter 4 Viral-mediated fusion of human mesenchymal stem cells with murine cells of the infarcted heart hinders cardiac healing via decreased vascularization and immune modulation

Elements of this work will be published as:

Freeman BT, Ogle BM. Viral-mediated fusion of human mesenchymal stem cells with murine cells of the infarcted heart hinders cardiac healing via decreased vascularization and immune modulation. *(*Submitted)

4.1 Abstract

Cell fusion can occur between mesenchymal stem cells (MSCs) transplanted to improve cardiac function and cells of the recipient. The therapeutic benefit or detriment of resultant cell hybrids is unknown. Here we augment fusion of transplanted MSCs with recipient cardiac cell types via viral fusogens to determine how cardiac function is impacted and via which mechanism(s). Using a Cre/LoxP-based luciferase reporter system coupled to biophotonic imaging and echocardiography, we found that augmenting fusion with the vesicular stomatitis virus glycoprotein (VSVG) increased the amount of fusion in the recipient mouse heart, but led to diminished cardiac function. Specifically, MSCs transfected with VSVG (MSC-VSVG) had the lowest mean fold increase in fractional area change (FAC) and cardiac output (CO) over the first 28 days after infarction and cell transplantation. And although the amount of fusion detected had a positive correlation with FAC and CO at day 7, this effect was lost by day 28. The decrease in cardiac function seen with MSC-VSVG treatment vs. MSC alone (no

fusogen) or sham treatment (surgery only) was associated with decreased MSC retention, altered immune cell responsiveness and reduced vascularization in the healthy heart. Thus fusion of donor MSCs can be augmented in the heart after transplantation, but the increase in fusion appears to hinder the cardiac healing response. This outcome garners consideration in the context of cellular transplantation to damaged tissues, those with viral infection or other microenvironmental conditions that might promote fusion.

Non-standard Abbreviations and Acronyms

MSC: mesenchymal stem cells

IVIS: *in vivo* imaging system

VSVG: vesicular stomatitis virus-glycoprotein

FAC: fractional area change

CO: cardiac output

TissueMend: collagen based cell delivery patch

BorderZone: area between infarcted murine heart and patch

4.2 Introduction

One of the most prevalent health issues in first world countries continues to be myocardial infarctions[1]. Mesenchymal/multipotent stem/stromal cell (MSC) therapy has been viewed as a promising treatment to solve this issue[2-8]. MSCs have the ability to home to injured tissues[9, 10], secrete paracrine factors that allow for immune evasion[11-13] and/or increase angiogenesis[10, 14-20]. In the course of these studies, many have

observed fusion between MSCs and cardiac cells[21-36] and new ones from SC paper]. However, the impact of cell fusion in this scenario and subsequent reprogramming on cardiac function at the cellular and tissue scale is not well understood.

Fusion of MSCs with cardiac cell types may improve cardiac function if the fusion products adopt the phenotype and associated function of cardiac cell types including cardiomyocytes, smooth muscle cells and endothelial cells. Evidence from the literature suggests stem cells and somatic cells can give rise to fusion products with characteristics of the somatic cell, thereby effectively programming the stem cells. For example, Blau et al. fused differentiated mouse muscle cells and human amniocytes and found that the mature cell phenotype dominated such that the amniocytes expressed human muscle proteins via exchange of cytoplasmic components[37]. Recent studies have shown that fusion of bone marrow-derived cells with hepatocytes has a therapeutic effect on the liver because the bone marrow-derived cells repopulate damaged liver tissue and adopt the biochemical functions of hepatocytes, including maintaining correct levels of serum transaminases, bilirubin and amino acids[38-43].

Fusion of MSCs with cardiac cell types could also improve cardiac function if the fusion products adopt the phenotype and associated function of mesenchymal stem cells, such self-renewal, pro-angiogenic propensity and anti-inflammatory effects. Evidence from the literature suggests fusion products of stem cells and somatic cells can serve to effectively reprogram the somatic cell to a less mature state. For example, Cowan et al. reverted human fibroblasts to a pluripotent-like state after fusion with embryonic stem

cells[44]. Tada et al. observed a similar pluripotent hybrid cell after fusing embryonic germ cells and lymphocytes[45].

Alternatively, fusion of MSCs with cardiac cell types may hinder cardiac function if the fusion products adopt a phenotype and associated function distinct from either cardiac cell types or mesenchymal stem cells. Blau et al. found heterokaryons formed from muscle cells and keratinocytes, expressed a combination of both gene profiles[46]. A similar result was seen after fusing intestinal epithelial cells and macrophages in a murine model of intestinal cancer in that cell fusion hybrids retained the transcriptome identity characteristic of both parental cells, but also expressed genes not activated in either parent cell type[47]. The activation of previously unexpressed genes is postulated to be responsible for the creation of cancer stem cells through fusion between tumor cells and bone marrow-derived cells[48-50].

In the present study, we use a Cre/*LoxP*-based molecular approach to detect fusion of transplanted MSCs to cells of living mice and we utilize echocardiography to determine how MSC fusion affects cardiac function. Using this approach, we found that human mesenchymal stem cells delivered to the murine heart via a collagen-based patch fuse after delivery and that augmented fusion of MSCs via viral fusogen appears to have a detrimental affect on cardiac function. This negative outcome was associated with decreased MSC retention, vascularization in the healthy heart and immune modulation 56 days after transplantation.

4.3 Materials and Methods

4.3.1 Transgenic Mice

We used transgenic mice that constitutively express Cre recombinase (B6.C-Tg[CMV-cre]1Cgn/J; Jackson Laboratory, Bar Harbor, ME) (15 total mice, 5 per treatment group, 2 months old), such that deletion of *LoxP*-flanked genes occurs in all tissues, including germ cells. The *Cre* gene is under transcriptional control of the cytomegalovirus (CMV) minimal promoter and is X-linked. The Cre sequence was introduced to BALB/cJ derived BALB/c-I embryonic stem cells (ESCs). The resulting mice were backcrossed to the BALB/c background for 8 generations and then backcrossed to the C57BL/6J background for 10 generations[51]. Only male Cre mice were used in the study owing to a false-positive signal detected when imaging the female transgenic mice (data not shown).

4.3.2 Cell Culture

Human MSCs derived from human embryonic stem cells (MSCs from WA-01, a gift from Dr. Peiman Hematti, University of Wisconsin-Madison, Madison, WI) were expanded and cultured, as previously described[52]. In brief, MSCs were cultured on a 0.1% gelatin (Sigma-Aldrich, St. Louis, MO) pretreated flask containing α-minimum essential medium (MEM)-complete. Complete α-MEM consisted of α-MEM (Invitrogen, Carlsbad, CA), 10% fetal bovine serum (HyClone Laboratories, Logan, UT), 0.1 mM nonessential amino acids (Invitrogen), and 2 mM L-glutamine (Invitrogen). hMSC cultures were allowed to grow to 60%–70% confluence and were replated at a concentration of 1,500 cells per cm^2. These human ESC-derived MSCs have cell surface markers,

differentiation potential, and immunologic properties in vitro that are similar to those of adult BM-derived MSCs[52].

4.3.3 Gene Transfer

MSCs were transiently transfected with viral fusogen VSV-G[21, 53] to promote cell-cell fusion (MSC-VSVG) or no fusogen (MSC). In addition, MSCs were simultaneously transfected with the luciferase gene adjacent to a floxed stop codon (p231 pCMVe-betaAc-STOP-luc; Addgene, Cambridge, MA)[24]. Transfection was accomplished using the Neon Transfection System (Invitrogen), as previously described[54]. All recombinant DNA research was conducted according to NIH guidelines and in accordance with the University of Wisconsin-Madison and University of Minnesota-Twin Cities institutional biosafety committees.

4.3.4 Myocardial Infarction and Cell Delivery

Mice underwent an infarction procedure by left coronary artery ligation, such as is routinely performed at the University of Wisconsin Cardiovascular Physiology Core Facility[24, 55, 56]. Transfected MSCs (MSC or MSC-VSVG) were delivered to the myocardium of mice immediately after infarction via a collagen patch (TissueMend; TEI Biosciences, Boston, MA), as previously described[21, 55, 57]. A control (Sham) was performed with only the infarction and no patch delivery. TissueMend matrices (2 × 2 × 0.8 mm) were placed in a 24-well plate (Falcon; Thermo Fisher Scientific, Pittsburgh, PA) and hydrated with α-MEM-complete culture medium. After electroporation, MSCs were seeded on the TissueMend sections at a concentration of 1×10^6 cells per milliliter.

The medium was changed at 24 and 48 hours, at which point the TissueMend matrix, containing $\sim 1 \times 10^5$ transfected MSCs, was attached to the myocardium with a single suture (7-0 Prolene; Ethicon, Johnson & Johnson, New Brunswick, NJ) at each corner of the matrix. A matrix was placed such that it was in contact with both the infarct and the peri-infarct regions of the myocardium[21, 55, 57]. All animal procedures were performed in accordance with the guidelines of the American Association for Laboratory Animal Science and the University of Wisconsin-Madison and the University of Minnesota-Twin Cities Animal Care and Use Committee.

4.3.5 Bioluminescent Imaging

Recipient mice constitutively expressed Cre recombinase; therefore, when transplanted human MSCs fused with cells of the recipient, the *LoxP* sites were cleaved, and the stop signal was excised, allowing expression of luciferase. Luciferase expression was detected 7 days after cell transplantation in living mice using an in vivo imaging system (IVIS) (IVIS Spectrum; Caliper Life Sciences, Hopkinton, MA), as previously described[24, 57]. The average radiance was determined by measuring the emitted photons per second per cm^2 per steradian of the heart region using the Living Image In Vivo Imaging Software (PerkinElmer, Life and Analytical Sciences, Waltham, MA).

4.3.6 Echocardiography

Mice underwent echocardiography 3 days post-infarction/cell delivery to obtain a baseline measurement of each mouse's cardiac function. Further echocardiography was repeated at 7, 14 and 28 days after infarction/cell delivery to track mouse cardiac

health over time. Transthoracic echocardiography was performed by using an Visual Sonics 770 ultrasonograph with a 30-MHz transducer (RMV 707B) (Visual Sonics, Toronto). Mice were lightly anesthestized with isoflurane (1%) and maintained on a heated platform. Two-dimensionally guided M-mode images of the long axis of the LV were acquired with the probe in different 3 planes, 1) sagittal plane, 2) 45% to the sagittal plane and 3) frontal plane. Images were recorded and the LV endocardial area traced at end-diastole and systole. Volumes were calculated from these areas and function expressed as fractional area change (FAC, %) and cardiac output (CO, mL/min). All parameters were measured over at least three consecutive cycles. Echnocardiography was performed with the assistance of Jill Koch and Tim Hacker of the University of Wisconsin Cardiovascular Physiology Core Facility.

4.3.7 Fluorescence Microscopy

Murine hearts were harvested 8 weeks after cell delivery to determine the amount of MSC retention, vascularization and immune response at the cellular level. After excision, the hearts were bisected longitudinally through the matrix. The hearts were immediately placed into 10% buffered formalin (pH 7.2; Thermo Fisher Scientific) for 24 hours, followed by 24 hours of fresh 10% buffered formalin, and a final 24-hour incubation in 70% ethanol. The samples were further processed for paraffin embedding and sectioning, as previously described[58]. For immunohistochemistry (IHC) analysis, heart sections were deparaffinized by incubating at 60°C for 1 hour and then washed for 6 minutes in Xylene twice. The sections were rehydrated by dipping the sections 15 times each in 100% ethanol, 100% ethanol, 95% ethanol, and, finally, ultrapure water. Antigen

retrieval was accomplished either by incubating the sections for 20 minutes at 37°C in 0.5% pepsin (Thermo Fischer Scientific) in 5 mM HCl for human leukocyte antigen (HLA) (monoclonal mouse anti-HLA-A,B,C; EMR8-5; MBL International Corp., Woburn, MA) or by incubating the sections for 25 minutes at 95°C in citrate buffer (10 mM sodium citrate (Fisher Scientific), pH 6, 0.01% Triton-X 100 (Sigma-Aldrich)) for CD31 (polyclonal rabbit anti-PECAM-1(CD31); M-185 sc-28188; Santa Cruz Biotechnology, Santa Cruz, CA), CD3 (monoclonal mouse anti-CD3; F7.2.38; Dako, Carpinteria, CA) and CD25 (monoclonal rat anti-mouse CD25; 7D4 (RUO); BD Pharmingen, San Jose, CA). The sections were removed and allowed to cool for 10 minutes at room temperature. The sections were rinsed in 1x phosphate-buffered saline (PBS) twice for 3 minutes. A 1:25 dilution of the anti-HLA-A,B,C antibody, a 1:50 dilution of anti-CD31 or a 1:25 dilution of anti-CD3 was made with dilution buffer containing 5% bovine serum albumin (HyClone), 2% goat serum (MP Biomedical, Solon, OH), 1% glycine (Sigma-Aldrich), and 0.1% triton-X (MP Biomedical). Next, 40 µl of this antibody solution was placed on each tissue section overnight at 4°C. The sections were washed with 1x PBS and incubated for 45 minutes at 4°C with 40 µl of a 1:200 dilution of the secondary antibody (AF647 goat anti-mouse for HLA and CD3 or AF647 goat anti-rabbit for CD31; Invitrogen) in dilution buffer. The sections were washed with 1x PBS and mounted using 1,4-diazabicyclo[2.2.2]octane (Dabco)/DAPI solution composed of 5% Dabco (Sigma-Aldrich) and 0.01% DAPI (Sigma-Aldrich) in a mixture of 50% glycerol (Thermo Fischer Scientific) and 50% 2× PBS on a microscope coverslip sealed with nail polish. Fluorescence emission was detected using an IX71 inverted deconvolution fluorescence microscope (Olympus, Center Valley, PA). The images were acquired with

a 10x or 20x UPlanFluor objective (NA = 0.5), using Metamorph software (Molecular Devices, Sunnyvale, CA) and analyzed using ImageJ (Fiji; open source software, http://pacific.mpi-cbg.de/wiki/index.php/Fiji). All hearts were stained for each antibody, and 5-20 images per region were quantified for positive expression with the number depending on the size of the region in each heart. Background fluorescence was determined using a secondary antibody-only control to set a threshold for antibody detection.

4.3.8 Statistical Analysis

Statistical analyses were performed using analysis of variance with Tukey's honest significant difference post hoc test for multiple comparisons or Student's t test for 2 independent samples; $P < 0.05$ was considered significant. Data were analyzed with SigmaPlot (Systat Software Inc, San Jose, CA, http://www.systat.com).

4.4 Results

4.4.1 Detection and Augmentation of MSC Cell Fusion in vivo

Previously, we showed that fusion of MSCs occurs both spontaneously and with the aid of exogenously supplied viral fusogens after transplantation to the murine heart[21, 55, 57]. In this study, we once again utilized a Cre/*LoxP*-based luciferase inducible reporter system coupled to biophotonic imaging to detect and quantify fusion between transplanted MSCs and cells of mice constitutively expressing Cre recombinase (**Figure 4-1A and 4-1B**). The transplanted MSCs (both MSC and MSC-VSVG) were transfected with a *LoxP*-stop codon-*LoxP*–luciferase construct such that luciferase expression is

limited to hybrids between donor and recipient cells (**Figure 4-1A**). Importantly, this imaging method is non-invasive and fusion can be quantified without sacrificing the mice. Seven days following myocardial infarction and MSC cell transplantation via collagen patch (TissueMend) to the heart, bioluminescence was measured for mice with no treatment (Sham, 5 mice), mice receiving MSCs with no fusogen (MSC, 5 mice), and mice receiving MSCs transfected with the VSVG fusogen (MSC-VSVG, 5 mice). The sham mice were used as a negative control to determine the background bioluminescent signal (2591 $\pm$ 884.9 photons per second per cm^2 per steradian (p s^{-1} cm^{-2} sr^{-1})). This signal in the sham mice represents the background luminescence. Fusion was increased in both the MSC (3818 $\pm$ 762.6 p s^{-1} cm^{-2} sr^{-1}) and MSC-VSVG (4557 $\pm$ 1317 p s^{-1} cm^{-2} sr^{-1}) groups compared to the Sham mice (* $P < 0.05$, compared to the Sham group) (**Figure 4-1B**). The highest amount of bioluminescent signal, and thus fusion, was observed in the MSC-VSVG (not significant compared to MSC group). These data demonstrate a trend towards enhanced fusion between MSCs and cardiac cell types via expression of viral fusogens in MSCs.

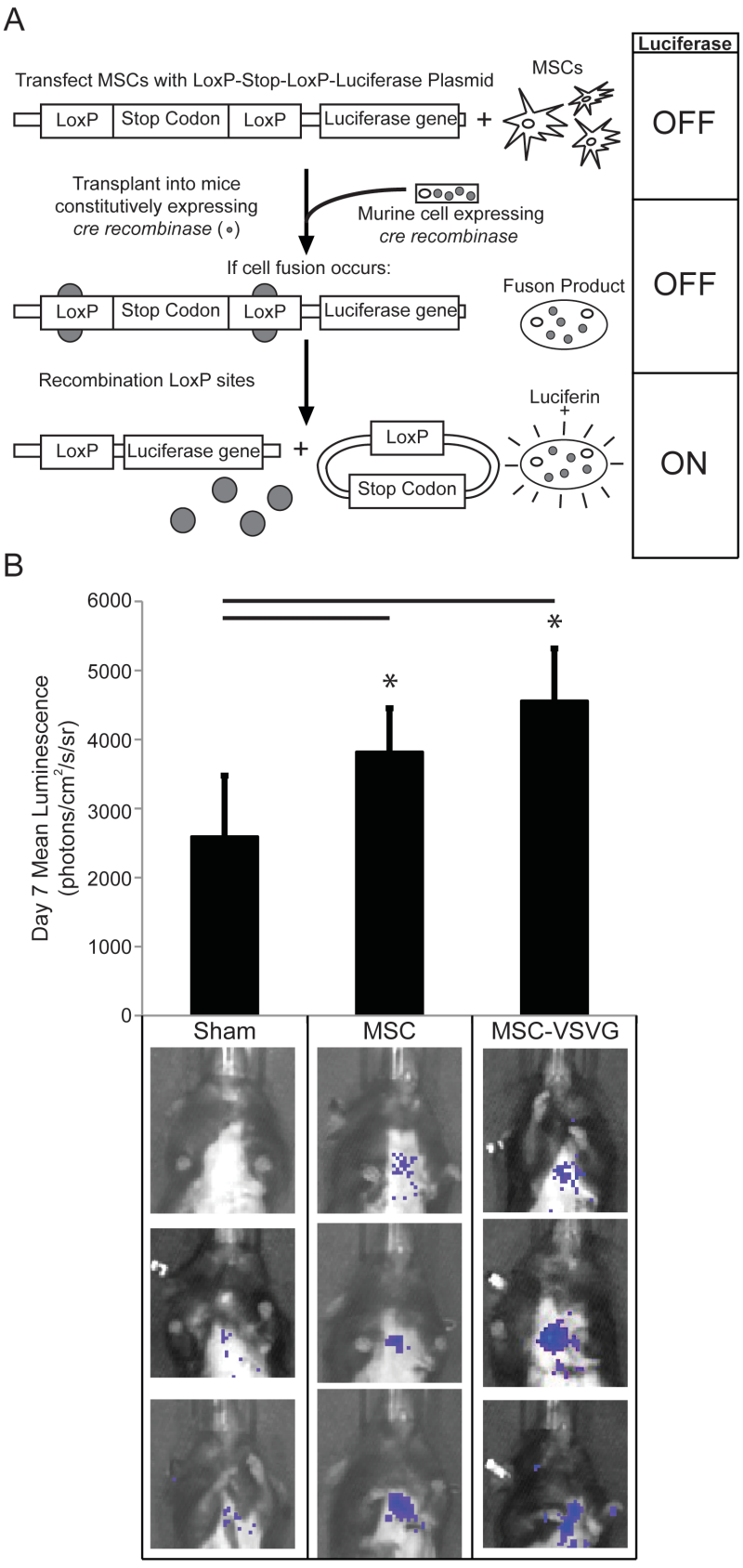
A
Luciferase
Transfect MSCs with LoxP-Stop-LoxP-Luciferase Plasmid
MSCs
LoxP
Stop Codon
LoxP
Luciferase gene
+
OFF
Transplant into mice
constitutively expressing
cre recombinase (•)
Murine cell expressing
cre recombinase
If cell fusion occurs:
Fuson Product
LoxP
Stop Codon
LoxP
Luciferase gene
OFF
Recombination LoxP sites
Luciferin
LoxP
Luciferase gene
+
LoxP
Stop Codon
ON
B
Day 7 Mean Luminescence
(photons/cm2/s/sr)
6000
5000
4000
3000
2000
1000
0
*
*
Sham
MSC
MSC-VSVG

Figure 4-1. Detection and Augmentation of MSC Cell Fusion in vivo

(A): Schematic of the *in vivo* Cre/*LoxP* biophotonic detection system. The MSCs are transfected with a *LoxP*-stop codon-*LoxP*-luciferase plasmid prior to cell transplantation. The MSCs are transplanted into mice constitutively expressing Cre recombinase. Upon fusion between MSCs and a cell of the Cre mouse, Cre recombinase excises the *LoxP*-stop codon-*LoxP* sequence and luciferase is expressed in the fusion product. The fusion product can then emit a bioluminescent signal after the addition of the luciferin substrate. (B). Quantification of the day 7 mean luminescent signal (photons/centimeters^2/second/steradian, photons/cm^2/s/sr) for each treatment group (Sham, MSC, and MSC-VSVG). The MSC and MSC-VSVG emitted a significantly higher mean luminescent signal compared to the Sham control group (*P < 0.05, data is displayed as average (Avg) $\pm$ standard deviation (SD)). Three representative luminescent overlay images for each group are shown below graph.

4.4.2 Augmented MSC Cell Fusion Affects Function of Infarcted Myocardium

To determine the impact of MSC cell fusion on cardiac function, the mice also underwent echocardiography at day 3, 7, 14 and 28 after infarction and cell delivery. Fractional area change (%) and cardiac output (mL/min) were measured at each time point for all 15 mice involved in this study. The FAC and CO measurements were normalized to the day 3 time point to discern the relative improvement of each group (Sham, MSC, MSC-VSVG) from the initial injury. The Sham group showed the largest improvement at day 28 (2.23 $\pm$ 2.06 fold increase in FAC and 3.02 $\pm$ 2.80 fold increase in CO), but there was high variability from mouse to mouse (**Figure 4-2A and 4-2B**). Interestingly, at day 28 the MSC (1.31 $\pm$ 0.48 fold increase in FAC and 1.99 $\pm$ 1.29 fold increase in CO) and MSC-VSVG (0.86 $\pm$ 0.48 fold change in FAC and 1.81 $\pm$ 1.41 fold increase in CO) groups had a lower average fold change for both FAC and CO compared to the Sham group, with the augmented fusion group MSC-VSVG having the lowest relative improvement (**Figure 4-2A and 4-2B**). These results coupled with the

observed increase in fusion from the bioluminescent data of the MSC and MSC-VSVG groups (**Figure 4-1B**) suggests that MSC fusion with cells of the mouse heart could be detrimental to the healing process in the mouse heart following myocardial infarction. However, the variability was also substantial in the MSC and MSC-VSVG groups and there were no significant differences between any group at any time point. To better probe these outcomes, a focused analysis was performed where the bioluminescent signal at day 7 for each mouse was plotted against the FAC (**Figure 4-2C**) and CO (**Figure 4-2D**) for each mouse at each time point to determine if any trends emerged. At day 7, a positive correlation was observed between bioluminescent signal (fusion) and cardiac function (FAC and CO) for both MSC and MSC-VSVG mice. However, this trend was mostly lost over time as the positive correlation decreased at later time points (day 14 and day 28). The MSC group with no fusogen did exhibit a positive correlation through day 14, but the strength of the correlation was decreased in FAC (R^2 = 0.516 at day 7 to R^2 = 0.155 at day 14) and CO (R^2 = 0.420 at day 7 to R^2 = 0.113 at day 14). Due to the high level of variability observed between mice within the same treatment group in this study as well as the loss of effect seen in the correlations, the number of mice was capped at five per group so that an in depth analysis could be performed to determine the mechanism behind the differences in cardiac functionality.

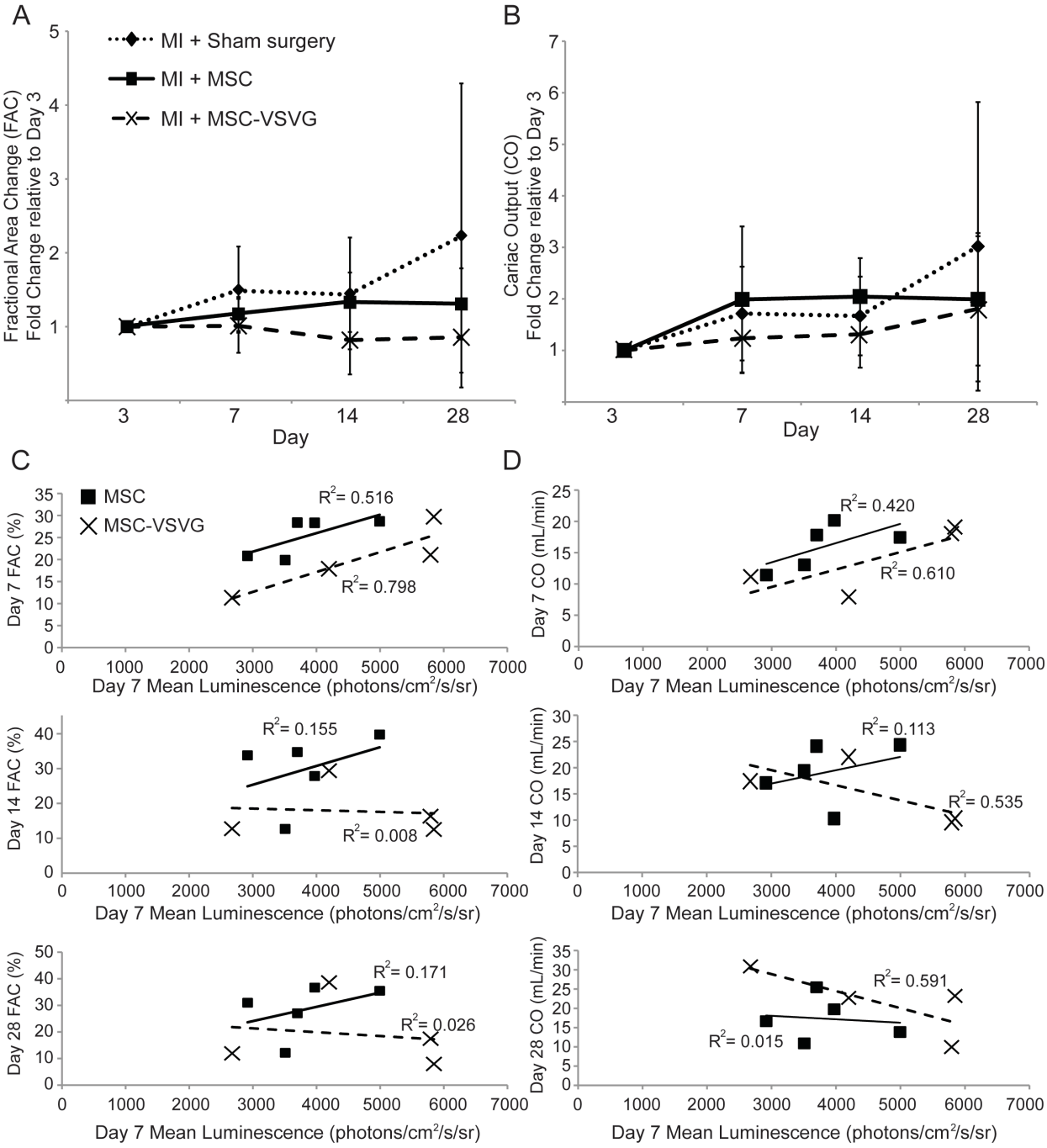

Figure 4-2. Augmented MSC Cell Fusion Affects Function of Infarcted Myocardium

Cardiac functional improvement is displayed relative to the values at 3 days after infarction/cell delivery for (A) fractional area change (FAC) and (B) cardiac output (CO). The Sham group displayed the highest fold increase over the 28 days monitored. The augmented fusion group (MSC-VSVG) showed the lowest fold change. To demonstrate the variability between samples

in the treatment groups, the mean luminescent signal for each mouse was plotted against the (C) FAC (%) or (D) CO (mL/min) for each time point. At day 7 a positive correlation emerges between mean luminescent signal (fusion) and cardiac function, but this correlation is lost at later time points.

4.4.3 Human MSC Retention in Infarcted Murine Heart

To assess if retention of the transplanted MSCs over time played a part in the observed differences between the MSC and MSC-VSVG groups, the hearts of the infarcted mice were explanted, fixed, sectioned at day 56 and probed for human leukocyte antigen (HLA) (**Figure 4-3A through 4-3C**) via immunofluorescence. The analysis of the heart tissues was separated into four regions (TissueMend patch, borderzone between the patch and heart, infarcted heart tissue and healthy heart tissue) to more accurately portray the spatial location in the tissue. The area of HLA positive signal was normalized to the area of DAPI signal to account for the difference in cell density in a given region. The MSC group showed the highest retention of human cells in the BorderZone (0.526 $\pm$ 1.06 HLA area/DAPI area), but human cells were also observed in the BorderZone of the MSC-VSVG group (0.252 $\pm$ 0.449 HLA area/DAPI area) albeit to a lesser extent than the MSC group (not significant) (**Figure 4-3A**). Also of note, the MSC group has a small negative correlation between bioluminescence signal and HLA area/DAPI area (R^2 = 0.502) (**Figure 4-3B**). This suggests that the spontaneous fusion (i.e., not triggered by viral fusogen added *ex vivo*) observed in the MSC group could hinder cell retention.

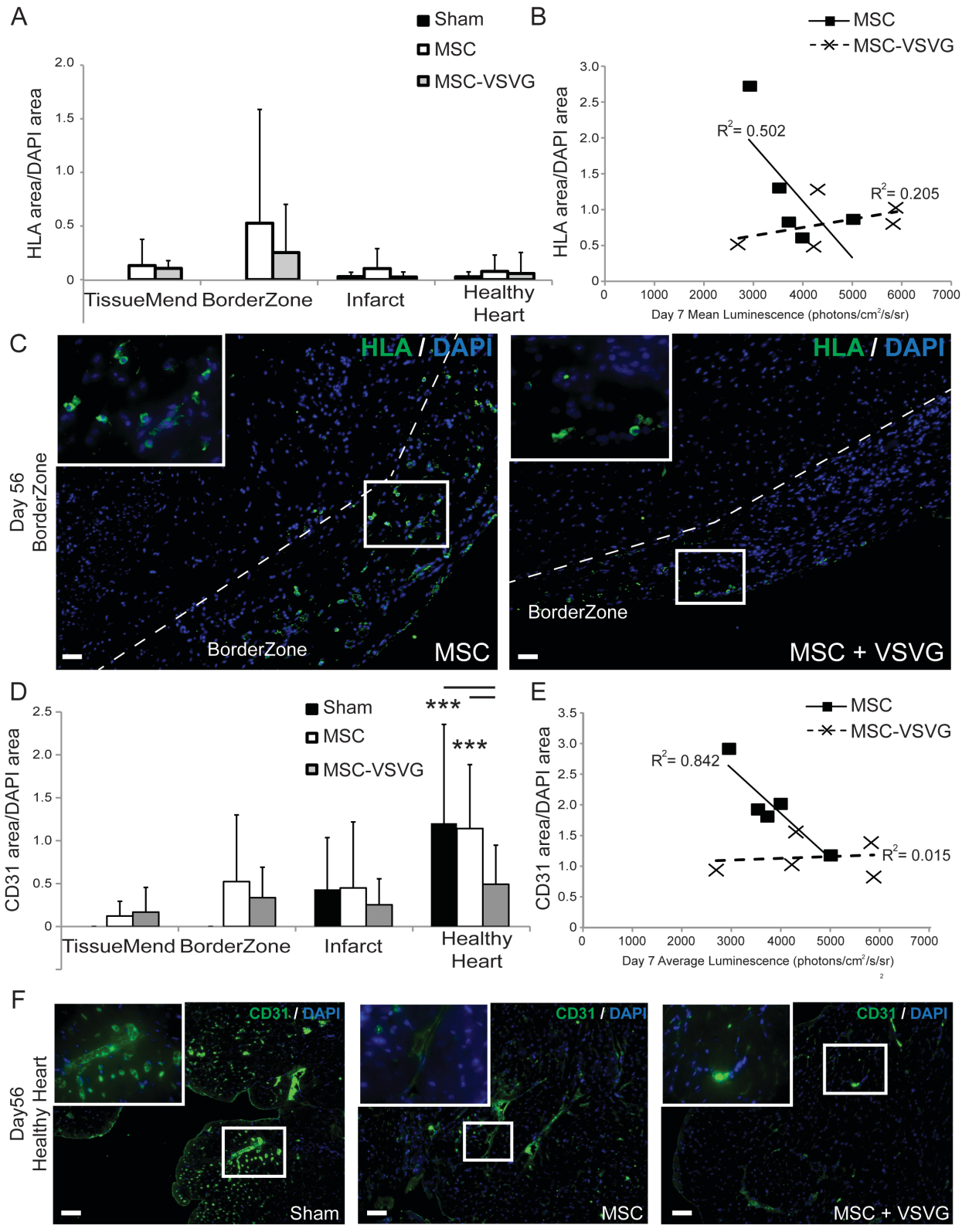

Figure 4-3. Human MSC Retention and Vascular Response in Infarcted Murine Heart

(A). Quantification at day 56 after infarction/cell delivery of human leukocyte antigen (HLA) expression (area) normalized to DAPI signal (area) for four regions in the infarcted heart (TissueMend, BorderZone, Infarct and Healthy Heart) (5-20 images per region per sample, data displayed as Avg $\pm$ SD). (B). Mean luminescent signal for each mouse was plotted against the HLA area/DAPI area for each mouse. The MSC group showed a negative correlation between mean luminescent signal (fusion) and MSC retention. (C). Representative images for MSC and MSC-VSVG groups in the BorderZone (HLA, green and DAPI, blue) (Scale bar = 50 μm). (D). Quantification at day 56 after infarction/cell delivery of vessel density (CD31 expression area) normalized to DAPI signal (area) for four regions in the infarcted heart (5-20 images per region region per sample, data displayed as Avg $\pm$ SD, *** $P < 0.001$ compared to the MSC-VSVG group). (E). Mean luminescent signal for each mouse was plotted against the CD31 area/DAPI area for each mouse. The MSC group showed a negative correlation between mean luminescent signal (fusion) and vessel density. (C). Representative images in the Healthy Heart (CD31, green and DAPI, blue) (Scale bar = 50 μm).

4.4.4 Vascular and Immune Response to Treatments

In the face of similar or nearly similar retention rates of MSCs with and without augmented cell fusion, we sought to determine whether altered MSC function at the cellular level could account for differences in tissue-level function. Specifically, we probed for angiogenic stimulation and immune modulation. Vessel density in the four different heart regions was probed via CD31 expression (fluorescence area) normalized to cell number via DAPI (fluorescence area)(**Figure 4-3D through 4-3F**). Vessel density was similar in the TissueMend, BorderZone, and infarct regions between the different treatments. However, the Sham and MSC groups had significantly higher CD31 area/DAPI area (1.20 $\pm$ 1.15 and 1.14 $\pm$ 0.744, respectively) compared to the CD31 area/DAPI area in the MSC-VSVG group (0.493 $\pm$ 0.455) (***$P < 0.001$) (**Figure 4-3D**). The MSC group again exhibited a negative correlation between bioluminescent signal and CD31 area/DAPI area (**Figure 4-3E**) (R^2 = 0.842). This trend could imply

that fused MSCs lose some ability to promote angiogenesis in an infarcted heart. The healthy region of the infarcted heart typically has to compensate for the loss of contractile tissue (which would require more energy) and the increase in vessel density observed in the Sham and MSC groups might be an attempt to supply the healthy tissue with more metabolites to match the demand due to the increased workload. However, if fused MSCs lost their innate paracrine ability to promote angiogenesis or were reprogrammed to prevent angiongenesis, the vessel density of the healthy heart could not be increased. The loss of vessel density in the healthy heart region might explain why the MSC-VSVG group had the lowest FAC and CO improvement.

Immune modulation to the treatments was analyzed via staining for T-cells (CD3 expression area) and normalizing the data to area of DAPI signal (**Figure 4-4A through 4-4C**). Adaptive immunity was probed since the time point was far later than typical innate immune activation and since MSCs have been shown to modulate T cell function *in vitro* and *in vivo*. CD3 positive cells were rare in the Sham treatment, which was expected due to the lack of transplanted cells. CD3 positive cells were also rare for the MSC and MSC-VSVG groups in the TissueMend, infarcted heart and healthy heart. Unexpectedly, the MSC group had significantly more CD3 area/DAPI area (0.540 $\pm$ 0.704) compared to the MSC-VSVG (0.185 $\pm$ 0.244) (**$P < 0.005$) (**Figure 4-4A**), but there were no correlations observed for the MSC group when assessing individual mice (**Figure 4-4B**). This result was not anticipated since the MSC-VSVG group exhibited diminished tissue level function as well as the fact that these cells express a cell surface fusogen, which was expected to trigger a larger immune response than the MSC group

with no fusogen. One potential explanation for this observation could be that all or a portion of the T-cells detected in the MSC group are regulatory T-cells, which suppress or downregulate induction and proliferation of effector T-cells. Multiple studies have shown that transplanted human MSCs have the ability to expand regulatory T-cell populations while inhibiting allostimulated T-cell proliferation[59, 60]. This could also be the reason for the higher concentration of HLA positive cells remaining the MSC group compared to the MSC-VSVG group, since the regulatory T-cells might prevent clearance of the foreign human MSCs. To determine if regulatory T-cells were the cause of the T-cell population in the MSC group, the mouse with the highest CD3 concentration underwent immunofluorescent staining for CD25. CD25 positive cells were observed in the BorderZone in regions that also stained positive for CD3 (**Figure 4-4D**). However, only a fraction (< 33%) of the CD3 positive cells were detected colocalized with CD25 positive staining. Thus increased blood vessel density and higher levels of regulatory T-cells and CD3 positive cells than the augmented MSC-VSVG fusion group further demonstrates the potential loss of paracrine or immunomodulatory function of MSCs after fusing.

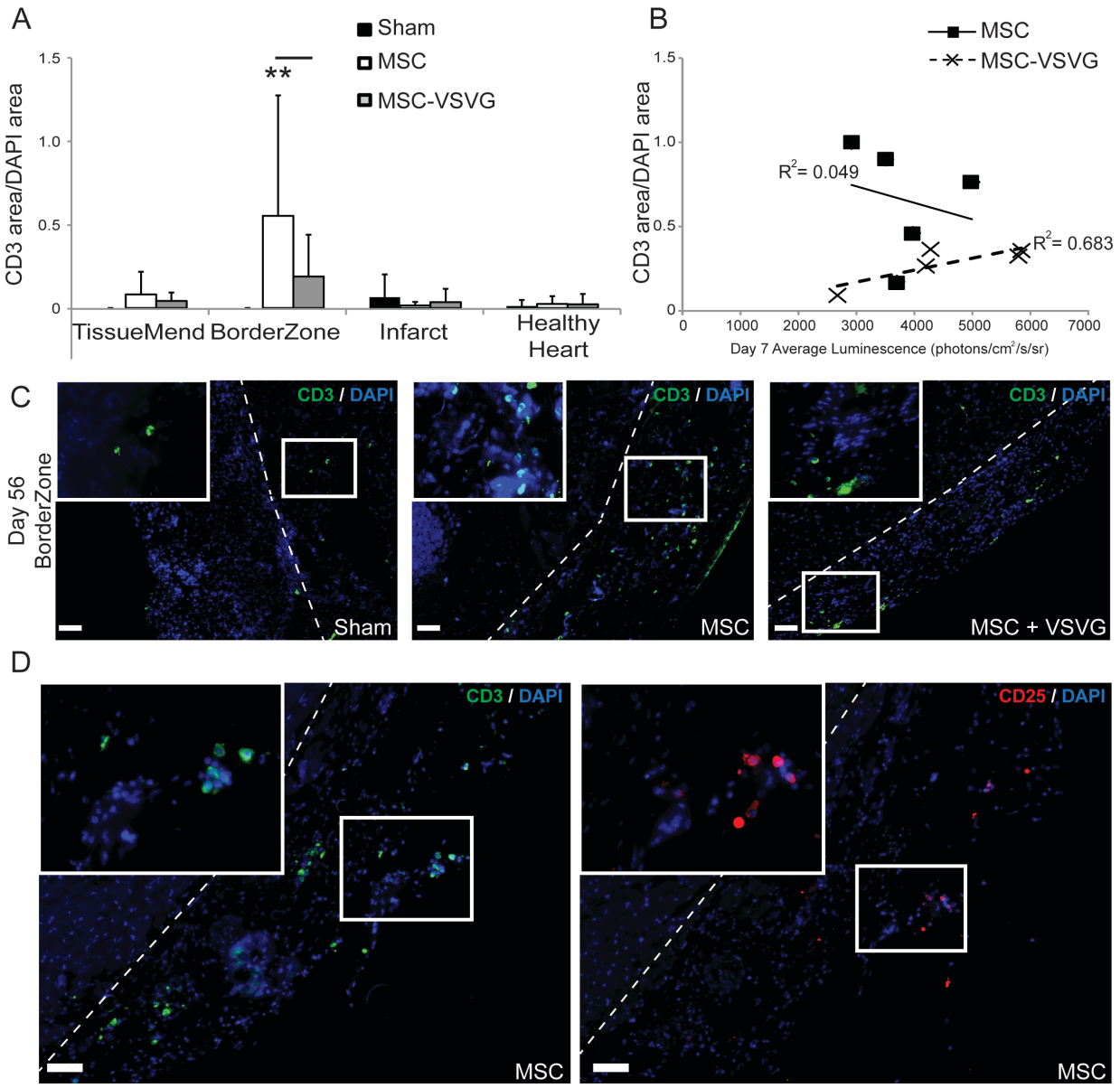

Figure 4-4. Immune Modulation Response to Treatments

(A). Quantification at day 56 after infarction/cell delivery of T-cell concentration (CD3 expression area) normalized to DAPI signal (area) for four regions in the infarcted heart (5-20 images per region region per sample, data displayed as Avg ± SD, ** $P < 0.005$ compared to the MSC-VSVG group). (B). Mean luminescent signal for each mouse was plotted against the CD3 area/DAPI area for each mouse. (C). Representative images in the BorderZone (CD3, green and DAPI, blue) (Scale bar = 50 μm). (D). Colocalization of regulatory T-cells (CD25, red) and T-cells (CD3, green) seen in the BorderZone of a mouse from the MSC group (DAPI, blue) (Scale bar = 50 μm).

4.5 Discussion

The aim of this study was to discern the affect of MSC fusion after transplantation on cardiac recovery following myocardial infarction. Three different treatment groups were utilized to help test this aim: a sham treatment, a traditional MSC transplantation, and a treatment wherein fusion was augmented in MSCs by the fusogen VSVG. Fusion was observed in both the MSC and MSC-VSVG group with the MSC-VSVG group showing the highest level of fusion. Unexpectedly, the Sham group demonstrated the highest average fold increase in cardiac function (FAC and CO) with the augmented fusion group performing the worst for cardiac recovery after an infarction. As noted earlier, fusion of MSC with parenchymal cells has been shown to aid in recovery of function in other tissues especially in the case of the liver[38-41, 43], but up to this point it was still unknown how MSC fusion in the heart could affect cardiac function. Our group and others have observed fusion of MSC in the heart, although most report a low level of fusion (<1% of transplanted cells) and thus the affect of the fusion on overall cardiac function was minimal[26, 34]. Here we report a decrease in function in the treatment group in which fusion was directly augmented. To our knowledge this is the first study to directly study the relationship between MSC fusion and cardiac function.

High variability in functional outcomes between groups, especially with fusion, led to a shift in our study design from tissue outcomes and therefore more mice (here we report five per study group) to per mouse correlative analyses and more in depth analysis of cellular-scale outcomes. This led our group to separate each mouse in the study and

directly compare the amount of fusion detected in each mouse to the FAC and CO observed during the course of the study. Within one week of infarction and transplantation, we observed a positive correlation between the amount of fusion and cardiac functional parameters. However, this correlation was lost at later time points in the study. This suggests that perhaps MSC fusion after transplantation may have a transient positive affect due to increased cell retention at the site of injury as well as increased immune evasion due to the acquisition of mouse major histocompatibility complexes after fusion. This positive affect appears to be short lived, since the sham treatment is observed to bypass both MSC treatments at day 28. Especially in the case of the augmented fusion group (MSC-VSVG), it appears that forcing the MSCs to fuse hinders the MSC's ability to promote healing. This is in line with very recent *in vitro* studies in which human MSCs that fused with rat neonatal ventricular myocytes downregulated sarcomeric structures and acquired a non-proliferative and non-contractile phenotype[61]. The loss of contractility and proliferation of fusion products between human MSCs and myocytes seen in this *in vitro* study helps to explain our *in vivo* observations that MSC fusion reduces the improvement of fractional area change and cardiac output in the infarcted heart.

After observing a decrease in cardiac function associated with MSC fusion, this study sought to understand the mechanism for the decreased function on the cellular level with a focus on MSC retention, vascularization, and immune modulation. The MSC group with no fusogen had a higher average level of MSC retention in the BorderZone (thought not significant), higher vessel density in the healthy heart as well as a higher

concentration of T-cells in the BorderZone than the MSC-VSVG group with the VSVG fusogen. These results could explain why the augmented fusion treatment saw reduced tissue-level function compared to the Sham group. Forcing MSCs to fuse via VSVG, while seeming to be positive at 7 days after transplantation, appear to prevent the MSCs from aiding in recovery at later time points. This could be due to the MSCs undergoing reprogramming after fusion and thus causing the MSCs to lose their innate abilities such as angiogenesis and immune modulation. The reprogrammed MSCs in the MSC-VSVG group might have lost essential paracrine capabilities, which rendered them less effective in promoting tissue repair. One might speculate that fusion "forced" via viral fusogen is artificial and therefore is not relevant *in vivo.* However, it is well-documented that viral infection can facilitate fusion *in vivo*[21, 55, 62-68]*.* In fact, it is possible that viral infection may have been the cause of all or a portion of the "spontaneous" fusion observed in the MSC group. Indeed, the MSC group saw a negative correlation between amount of fusion and MSC retention as well as vascularization after 56 days. This spontaneous fusion seen in the MSC group appears to negatively affect the MSC's ability to promote healing in the infarcted myocardium. The mice in the MSC group with no fusogen that exhibited the highest amount of MSC retention and vascularization were the mice with the lowest observed fusion levels. Interestingly, the MSC group with no fusogen showed an increase in CD3 positive T-cells compared to the MSC-VSVG group. The MSC-VSVG group was expected to have the highest immune response due to the introduction of a foreign surface protein, but this was not what was detected. CD3 cells in the MSC group were found to colocalize with CD25 positive regulatory T-cells in

parts the BorderZone. These regulatory T-cells might be the cause of higher MSC retention and improved cardiac functional response seen in the MSC group.

4.6 Conclusions

Taken in whole, this study is the first to examine how MSC fusion after cell transplantation affects cardiac function following myocardial infarction. The negative impact observed, even with the small number of mice tested, should be considered for future clinical trials. MSC transplantation has been shown to be an effective treatment when cell fusion is reported at low levels. However, if cell fusion is somehow increased due to viral infection or environmental conditions after transplantation, the treatment could result in a loss of function and a negative prognosis (especially in the infarcted heart).

4.7 References

1. Mozaffarian D, Benjamin EJ, Go AS, Arnett DK, Blaha MJ, Cushman M, de Ferranti S, Despres JP, Fullerton HJ, Howard VJ, Huffman MD, Judd SE, Kissela BM, Lackland DT, Lichtman JH, Lisabeth LD, Liu S, Mackey RH, Matchar DB, McGuire DK, Mohler ER, 3rd, Moy CS, Muntner P, Mussolino ME, Nasir K, Neumar RW, Nichol G, Palaniappan L, Pandey DK, Reeves MJ, Rodriguez CJ, Sorlie PD, Stein J, Towfighi A, Turan TN, Virani SS, Willey JZ, Woo D, Yeh RW, Turner MB, American Heart Association Statistics C, Stroke Statistics S. Heart disease and stroke statistics--2015 update: A report from the american heart association. *Circulation*. 2015;131:e29-322

2. Abdel-Latif A, Bolli R, Tleyjeh IM, Montori VM, Perin EC, Hornung CA, Zuba-Surma EK, Al-Mallah M, Dawn B. Adult bone marrow-derived cells for cardiac repair: A systematic review and meta-analysis. *Archives of internal medicine*. 2007;167:989-997

3. Amado LC, Saliaris AP, Schuleri KH, St John M, Xie JS, Cattaneo S, Durand DJ, Fitton T, Kuang JQ, Stewart G, Lehrke S, Baumgartner WW, Martin BJ, Heldman AW, Hare JM. Cardiac repair with intramyocardial injection of allogeneic mesenchymal stem cells after myocardial infarction. *Proceedings of the National Academy of Sciences of the United States of America*. 2005;102:11474-11479

4. Chen S, Liu Z, Tian N, Zhang J, Yei F, Duan B, Zhu Z, Lin S, Kwan TW. Intracoronary transplantation of autologous bone marrow mesenchymal stem cells for ischemic cardiomyopathy due to isolated chronic occluded left anterior descending artery. *The Journal of invasive cardiology*. 2006;18:552-556

5. Chen SL, Fang WW, Ye F, Liu YH, Qian J, Shan SJ, Zhang JJ, Chunhua RZ, Liao LM, Lin S, Sun JP. Effect on left ventricular function of intracoronary transplantation of autologous bone marrow mesenchymal stem cell in patients with acute myocardial infarction. *The American journal of cardiology*. 2004;94:92-95

6. Ma J, Ge J, Zhang S, Sun A, Shen J, Chen L, Wang K, Zou Y. Time course of myocardial stromal cell-derived factor 1 expression and beneficial effects of intravenously administered bone marrow stem cells in rats with experimental myocardial infarction. *Basic research in cardiology*. 2005;100:217-223

7. Shake JG, Gruber PJ, Baumgartner WA, Senechal G, Meyers J, Redmond JM, Pittenger MF, Martin BJ. Mesenchymal stem cell implantation in a swine myocardial infarct model: Engraftment and functional effects. *The Annals of thoracic surgery*. 2002;73:1919-1925; discussion 1926

8. Tomita S, Li RK, Weisel RD, Mickle DA, Kim EJ, Sakai T, Jia ZQ. Autologous transplantation of bone marrow cells improves damaged heart function. *Circulation*. 1999;100:II247-256

9. Mouiseddine M, Francois S, Semont A, Sache A, Allenet B, Mathieu N, Frick J, Thierry D, Chapel A. Human mesenchymal stem cells home specifically to radiation-injured tissues in a non-obese diabetes/severe combined immunodeficiency mouse model. *The British journal of radiology*. 2007;80 Spec No 1:S49-55

10. Nagaya N, Fujii T, Iwase T, Ohgushi H, Itoh T, Uematsu M, Yamagishi M, Mori H, Kangawa K, Kitamura S. Intravenous administration of mesenchymal stem cells improves cardiac function in rats with acute myocardial infarction through angiogenesis and myogenesis. *American journal of physiology. Heart and circulatory physiology*. 2004;287:H2670-2676

11. Ankrum JA, Ong JF, Karp JM. Mesenchymal stem cells: Immune evasive, not immune privileged. *Nature biotechnology*. 2014;32:252-260

12. Chen G, Nayan M, Duong M, Asenjo JF, Ge Y, Chiu RC, Shum-Tim D. Marrow stromal cells for cell-based therapy: The role of antiinflammatory cytokines in cellular cardiomyoplasty. *The Annals of thoracic surgery*. 2010;90:190-197

13. Caplan AI. Why are mscs therapeutic? New data: New insight. *The Journal of pathology*. 2009;217:318-324

14. Caplan AI, Dennis JE. Mesenchymal stem cells as trophic mediators. *Journal of cellular biochemistry*. 2006;98:1076-1084

15. Gnecchi M, He H, Liang OD, Melo LG, Morello F, Mu H, Noiseux N, Zhang L, Pratt RE, Ingwall JS, Dzau VJ. Paracrine action accounts for marked protection of ischemic heart by akt-modified mesenchymal stem cells. *Nature medicine*. 2005;11:367-368

16. Gnecchi M, He H, Noiseux N, Liang OD, Zhang L, Morello F, Mu H, Melo LG, Pratt RE, Ingwall JS, Dzau VJ. Evidence supporting paracrine hypothesis for akt-modified mesenchymal stem cell-mediated cardiac protection and functional improvement. *FASEB journal : official publication of the Federation of American Societies for Experimental Biology*. 2006;20:661-669

17. Kamihata H, Matsubara H, Nishiue T, Fujiyama S, Tsutsumi Y, Ozono R, Masaki H, Mori Y, Iba O, Tateishi E, Kosaki A, Shintani S, Murohara T, Imaizumi T, Iwasaka T. Implantation of bone marrow mononuclear cells into ischemic myocardium enhances collateral perfusion and regional function via side supply of angioblasts, angiogenic ligands, and cytokines. *Circulation*. 2001;104:1046-1052

18. Kinnaird T, Stabile E, Burnett MS, Lee CW, Barr S, Fuchs S, Epstein SE. Marrow-derived stromal cells express genes encoding a broad spectrum of arteriogenic cytokines and promote in vitro and in vivo arteriogenesis through paracrine mechanisms. *Circulation research*. 2004;94:678-685

19. Linke A, Muller P, Nurzynska D, Casarsa C, Torella D, Nascimbene A, Castaldo C, Cascapera S, Bohm M, Quaini F, Urbanek K, Leri A, Hintze TH, Kajstura J, Anversa P. Stem cells in the dog heart are self-renewing, clonogenic, and multipotent and regenerate infarcted myocardium, improving cardiac function. *Proceedings of the National Academy of Sciences of the United States of America*. 2005;102:8966-8971

20. Nygren JM, Jovinge S, Breitbach M, Sawen P, Roll W, Hescheler J, Taneera J, Fleischmann BK, Jacobsen SE. Bone marrow-derived hematopoietic cells generate cardiomyocytes at a low frequency through cell fusion, but not transdifferentiation. *Nature medicine*. 2004;10:494-501

21. Kouris NA, Schaefer JA, Hatta M, Freeman BT, Kamp TJ, Kawaoka Y, Ogle BM. Directed fusion of mesenchymal stem cells with cardiomyocytes via vsv-g facilitates stem cell programming. *Stem cells international*. 2012;2012:414038

22. Matsuura K, Wada H, Nagai T, Iijima Y, Minamino T, Sano M, Akazawa H, Molkentin JD, Kasanuki H, Komuro I. Cardiomyocytes fuse with surrounding noncardiomyocytes and reenter the cell cycle. *The Journal of cell biology*. 2004;167:351-363

23. Oh H, Bradfute SB, Gallardo TD, Nakamura T, Gaussin V, Mishina Y, Pocius J, Michael LH, Behringer RR, Garry DJ, Entman ML, Schneider MD. Cardiac progenitor cells from adult myocardium: Homing, differentiation, and fusion after infarction. *Proceedings of the National Academy of Sciences of the United States of America*. 2003;100:12313-12318

24. Sprangers AJ, Freeman BT, Kouris NA, Ogle BM. A cre-lox p recombination approach for the detection of cell fusion in vivo. *Journal of visualized experiments : JoVE*. 2012:e3581

25. Zhang S, Wang D, Estrov Z, Raj S, Willerson JT, Yeh ET. Both cell fusion and transdifferentiation account for the transformation of human peripheral blood cd34-positive cells into cardiomyocytes in vivo. *Circulation*. 2004;110:3803-3807

26. Alvarez-Dolado M, Pardal R, Garcia-Verdugo JM, Fike JR, Lee HO, Pfeffer K, Lois C, Morrison SJ, Alvarez-Buylla A. Fusion of bone-marrow-derived cells with purkinje neurons, cardiomyocytes and hepatocytes. *Nature*. 2003;425:968-973

27. Andrade J, Lam JT, Zamora M, Huang C, Franco D, Sevilla N, Gruber PJ, Lu JT, Ruiz-Lozano P. Predominant fusion of bone marrow-derived cardiomyocytes. *Cardiovascular research*. 2005;68:387-393

28. Deb A, Wang S, Skelding KA, Miller D, Simper D, Caplice NM. Bone marrow-derived cardiomyocytes are present in adult human heart: A study of gender-mismatched bone marrow transplantation patients. *Circulation*. 2003;107:1247-1249

29. He XQ, Chen MS, Li SH, Liu SM, Zhong Y, McDonald Kinkaid HY, Lu WY, Weisel RD, Li RK. Co-culture with cardiomyocytes enhanced the myogenic conversion of mesenchymal stromal cells in a dose-dependent manner. *Molecular and cellular biochemistry*. 2010;339:89-98

30. Kawada H, Fujita J, Kinjo K, Matsuzaki Y, Tsuma M, Miyatake H, Muguruma Y, Tsuboi K, Itabashi Y, Ikeda Y, Ogawa S, Okano H, Hotta T, Ando K, Fukuda K.

Nonhematopoietic mesenchymal stem cells can be mobilized and differentiate into cardiomyocytes after myocardial infarction. *Blood*. 2004;104:3581-3587

31. Kruglyakov PV, Sokolova IB, Zin'kova NN, Viide SK, Aleksandrov GV, Petrov NS, Polyntsev DG. In vitro and in vivo differentiation of mesenchymal stem cells in the cardiomyocyte direction. *Bulletin of experimental biology and medicine*. 2006;142:503-506

32. Noiseux N, Gnecchi M, Lopez-Ilasaca M, Zhang L, Solomon SD, Deb A, Dzau VJ, Pratt RE. Mesenchymal stem cells overexpressing akt dramatically repair infarcted myocardium and improve cardiac function despite infrequent cellular fusion or differentiation. *Molecular therapy : the journal of the American Society of Gene Therapy*. 2006;14:840-850

33. Terada N, Hamazaki T, Oka M, Hoki M, Mastalerz DM, Nakano Y, Meyer EM, Morel L, Petersen BE, Scott EW. Bone marrow cells adopt the phenotype of other cells by spontaneous cell fusion. *Nature*. 2002;416:542-545

34. van Berlo JH, Kanisicak O, Maillet M, Vagnozzi RJ, Karch J, Lin SC, Middleton RC, Marban E, Molkentin JD. C-kit+ cells minimally contribute cardiomyocytes to the heart. *Nature*. 2014;509:337-341

35. Yang WJ, Li SH, Weisel RD, Liu SM, Li RK. Cell fusion contributes to the rescue of apoptotic cardiomyocytes by bone marrow cells. *Journal of cellular and molecular medicine*. 2012;16:3085-3095

36. Yoon YS, Wecker A, Heyd L, Park JS, Tkebuchava T, Kusano K, Hanley A, Scadova H, Qin G, Cha DH, Johnson KL, Aikawa R, Asahara T, Losordo DW. Clonally expanded novel multipotent stem cells from human bone marrow

regenerate myocardium after myocardial infarction. *The Journal of clinical investigation*. 2005;115:326-338

37. Blau HM, Chiu CP, Webster C. Cytoplasmic activation of human nuclear genes in stable heterocaryons. *Cell*. 1983;32:1171-1180

38. Lagasse E, Connors H, Al-Dhalimy M, Reitsma M, Dohse M, Osborne L, Wang X, Finegold M, Weissman IL, Grompe M. Purified hematopoietic stem cells can differentiate into hepatocytes in vivo. *Nature medicine*. 2000;6:1229-1234

39. Wang X, Willenbring H, Akkari Y, Torimaru Y, Foster M, Al-Dhalimy M, Lagasse E, Finegold M, Olson S, Grompe M. Cell fusion is the principal source of bone-marrow-derived hepatocytes. *Nature*. 2003;422:897-901

40. Willenbring H, Bailey AS, Foster M, Akkari Y, Dorrell C, Olson S, Finegold M, Fleming WH, Grompe M. Myelomonocytic cells are sufficient for therapeutic cell fusion in liver. *Nature medicine*. 2004;10:744-748

41. Willenbring H, Grompe M. Delineating the hepatocyte's hematopoietic fusion partner. *Cell cycle*. 2004;3:1489-1491

42. Quintana-Bustamante O, Grueso E, Garcia-Escudero R, Arza E, Alvarez-Barrientos A, Fabregat I, Garcia-Bravo M, Meza NW, Segovia JC. Cell fusion reprogramming leads to a specific hepatic expression pattern during mouse bone marrow derived hepatocyte formation in vivo. *PloS one*. 2012;7:e33945

43. Vassilopoulos G, Wang PR, Russell DW. Transplanted bone marrow regenerates liver by cell fusion. *Nature*. 2003;422:901-904

44. Cowan CA, Atienza J, Melton DA, Eggan K. Nuclear reprogramming of somatic cells after fusion with human embryonic stem cells. *Science*. 2005;309:1369-1373

45. Tada M, Tada T, Lefebvre L, Barton SC, Surani MA. Embryonic germ cells induce epigenetic reprogramming of somatic nucleus in hybrid cells. *The EMBO journal*. 1997;16:6510-6520

46. Palermo A, Doyonnas R, Bhutani N, Pomerantz J, Alkan O, Blau HM. Nuclear reprogramming in heterokaryons is rapid, extensive, and bidirectional. *FASEB journal : official publication of the Federation of American Societies for Experimental Biology*. 2009;23:1431-1440

47. Powell AE, Anderson EC, Davies PS, Silk AD, Pelz C, Impey S, Wong MH. Fusion between intestinal epithelial cells and macrophages in a cancer context results in nuclear reprogramming. *Cancer research*. 2011;71:1497-1505

48. Dittmar T, Nagler C, Niggemann B, Zanker KS. The dark side of stem cells: Triggering cancer progression by cell fusion. *Current molecular medicine*. 2013;13:735-750

49. Harkness T, Weaver BA, Alexander CM, Ogle BM. Cell fusion in tumor development: Accelerated genetic evolution. *Critical reviews in oncogenesis*. 2013;18:19-42

50. Wei HJ, Nickoloff JA, Chen WH, Liu HY, Lo WC, Chang YT, Yang PC, Wu CW, Williams DF, Gelovani JG, Deng WP. Foxf1 mediates mesenchymal stem cell fusion-induced reprogramming of lung cancer cells. *Oncotarget*. 2014;5:9514-9529

51. Schwenk F, Baron U, Rajewsky K. A cre-transgenic mouse strain for the ubiquitous deletion of loxp-flanked gene segments including deletion in germ cells. *Nucleic acids research*. 1995;23:5080-5081

52. Trivedi P, Hematti P. Derivation and immunological characterization of mesenchymal stromal cells from human embryonic stem cells. *Experimental hematology*. 2008;36:350-359

53. Takada A, Robison C, Goto H, Sanchez A, Murti KG, Whitt MA, Kawaoka Y. A system for functional analysis of ebola virus glycoprotein. *Proceedings of the National Academy of Sciences of the United States of America*. 1997;94:14764-14769

54. Sprangers AJ, Freeman BT, Ogle BM. Electroporation can efficiently transfect hesc-derived mesenchymal stem cells without inducing differentiation. *Open Stem Cell Journal*. 2011:62-66

55. Kouris NA, Squirrell JM, Jung JP, Pehlke CA, Hacker T, Eliceiri KW, Ogle BM. A nondenatured, noncrosslinked collagen matrix to deliver stem cells to the heart. *Regenerative medicine*. 2011;6:569-582

56. Michael LH, Entman ML, Hartley CJ, Youker KA, Zhu J, Hall SR, Hawkins HK, Berens K, Ballantyne CM. Myocardial ischemia and reperfusion: A murine model. *The American journal of physiology*. 1995;269:H2147-2154

57. Freeman BT, Kouris NA, Ogle BM. Tracking fusion of human mesenchymal stem cells after transplantation to the heart. *Stem cells translational medicine*. 2015;4:685-694

58. Ogle BM, Butters KA, Plummer TB, Ring KR, Knudsen BE, Litzow MR, Cascalho M, Platt JL. Spontaneous fusion of cells between species yields transdifferentiation and retroviral transfer in vivo. *FASEB journal : official publication of the Federation of American Societies for Experimental Biology*. 2004;18:548-550

59. Aggarwal S, Pittenger MF. Human mesenchymal stem cells modulate allogeneic immune cell responses. *Blood*. 2005;105:1815-1822

60. Selmani Z, Naji A, Zidi I, Favier B, Gaiffe E, Obert L, Borg C, Saas P, Tiberghien P, Rouas-Freiss N, Carosella ED, Deschaseaux F. Human leukocyte antigen-g5 secretion by human mesenchymal stem cells is required to suppress t lymphocyte and natural killer function and to induce cd4+cd25highfoxp3+ regulatory t cells. *Stem cells*. 2008;26:212-222

61. Shadrin IY, Yoon W, Li L, Shepherd N, Bursac N. Rapid fusion between mesenchymal stem cells and cardiomyocytes yields electrically active, non-contractile hybrid cells. *Scientific reports*. 2015;5:12043

62. Clavel F, Charneau P. Fusion from without directed by human immunodeficiency virus particles. *Journal of virology*. 1994;68:1179-1185

63. Duelli D, Lazebnik Y. Cell-to-cell fusion as a link between viruses and cancer. *Nature reviews. Cancer*. 2007;7:968-976

64. Gao P, Zheng J. High-risk hpv e5-induced cell fusion: A critical initiating event in the early stage of hpv-associated cervical cancer. *Virology journal*. 2010;7:238

65. Hu L, Plafker K, Vorozhko V, Zuna RE, Hanigan MH, Gorbsky GJ, Plafker SM, Angeletti PC, Ceresa BP. Human papillomavirus 16 e5 induces bi-nucleated cell formation by cell-cell fusion. *Virology*. 2009;384:125-134

66. Joag SV, Li Z, Foresman L, Stephens EB, Zhao LJ, Adany I, Pinson DM, McClure HM, Narayan O. Chimeric simian/human immunodeficiency virus that causes progressive loss of cd4+ t cells and aids in pig-tailed macaques. *Journal of virology*. 1996;70:3189-3197

67. Karlsson GB, Halloran M, Schenten D, Lee J, Racz P, Tenner-Racz K, Manola J, Gelman R, Etemad-Moghadam B, Desjardins E, Wyatt R, Gerard NP, Marcon L, Margolin D, Fanton J, Axthelm MK, Letvin NL, Sodroski J. The envelope glycoprotein ectodomains determine the efficiency of cd4+ t lymphocyte depletion in simian-human immunodeficiency virus-infected macaques. *The Journal of experimental medicine*. 1998;188:1159-1171

68. Kondo N, Marin M, Kim JH, Desai TM, Melikyan GB. Distinct requirements for hiv-cell fusion and hiv-mediated cell-cell fusion. *The Journal of biological chemistry*. 2015;290:6558-6573

Chapter 5 Single-cell RNA-seq reveals activation of latent oncogenes and pluripotency genes as a consequence of stem cell-parenchymal cell fusion

Elements of this work will be published as:

Freeman BT, Jung PJ, Ogle BM. Single-cell RNA-seq reveals activation of latent oncogenes and pluripotency genes as a consequence of stem cell-parenchymal cell fusion. (Submitted)

5.1 Abstract

Fusion of donor mesenchymal stem cells with parenchymal cells of the recipient can occur in the brain, liver, intestine and heart following transplantation. The therapeutic benefit or detriment of resultant hybrids is unknown. Here we sought to obtain a global view of phenotypic diversification of mesenchymal stem cell-cardiomyocyte hybrids and associated time course. Using single-cell RNA-seq, we found hybrids can express a transcriptome similar to individual fusion partners, but can also acquire distinct expression profiles in one day. Some hybrids underwent reprogramming, expressing pluripotency and cardiac precursor genes latent in parental cells. Other hybrids differentially expressed genes associated with ontologic cancer sets and two hybrids clustered with breast cancer cells, expressing critical oncogenes and lacking tumor suppressor genes. Rapid transcriptional diversification of this type garners consideration in

the context of cellular transplantation to damaged tissues, those with viral infection or other microenvironmental conditions that might promote fusion.

Non-standard Abbreviations and Acronyms

hMSC: human mesenchymal stem cells

mMSC: mouse mesenchymal stem cells

BiFC: Bimolecular Fluorescence Complementation

hSLAM: human signaling lymphocytic activation molecule

F: fusion protein

H: hemagglutinin

GFP: green fluorescent protein

HC: hierarchal clustering

PCA: principal component analysis

5.2 Introduction

Mesenchymal/multipotent stem/stromal cells (MSCs) can fuse with parenchymal cells of the brain[1], liver[2], small intestine[3] and heart[1, 4-9] following transplantation. Fusion of this type might be tightly controlled and restricted to certain cell types as with sperm-egg fusion and skeletal myoblast fusion. However, it is more likely that regulation of fusion is bypassed in the context of transplantation and the altered tissue environment of damaged or diseased tissue. So-called “accidental cell fusion” can result from cell stress

including nutrient deprivation and hypoxia which can render cell membranes leaky or unstable[10, 11]. Unstable cell membranes are biophysically susceptible to membrane fusion[12]. It may be for this reason that cell fusion appears to occur more readily in the context of hypoxia than normoxia[13, 14]. Accidental cell fusion can also be mediated by viral fusogenic proteins of an active virus or activated elements of an endogenous virus[15-23]. It is estimated that more than 17 of 29 virus families that infect human cells have elements capable of fusing cells[15].

We and others have proposed that accidental cell fusion can give rise to fusion products capable of acquiring phenotypic and functional properties of either or both fusion partners[2, 24-32]. The beneficial effects of such an outcome include cell fusion between myeloma cells and B cells to form hybridomas and associated monoclonal antibodies[33]. Similarly, fusion between dendritic cells and tumor cells augments secretion of paracrine factors and can be used as anti-tumor immunotherapy[34]. Return of liver function has been reported after fusion between transplanted bone marrow MSCs and diseased hepatocytes[2, 25, 35] and endogenous c-kit+ cells can form cardiomyocytes in an infarcted murine heart as a result of cell fusion[36].

Accidental cell fusion might also enable catastrophic events including the development of tumor cells and/or metastatic spread of tumor cells. Spontaneous fusion has been reported between normal breast epithelium and breast cancer cells[37, 38], among breast tumor cells themselves[39, 40], and between breast cancer epithelium and tumor stromal cells including MSCs[41,

42]. *In vitro* studies of hybrids formed between normal breast epithelium (M13SV1-EGFP-Neo) and breast cancer cells (HS578T-Hyg) showed increased "locomotory activity" compared to the normal parental line[43]. Fusion-enhanced migration was associated with altered CCL21/CCR7 signaling, which was previously linked to metastatic spreading of breast cancer to lymph nodes. Increased metastatic potential of hybrids was also observed *in vivo* when breast cancer cell variants (MDA-MB-231) with tropism for either lung or bone injected in nude mice gave rise to hybrids capable of metastases to both organs[39].

Here we probe the extent of transcriptional diversification of hybrids formed between MSCs and cardiomyocytes, and the beneficial or detrimental outcomes of diversification at the single cell level. We probe this particular cell pairing as hybrids of this type have been most frequently reported in the context of MSC transplantation to the heart. We utilize single-cell RNA-seq since each hybrid is predicted to be transcriptionally distinct and hence population analyses may mute unique expression profiles.

5.3 Materials and Methods

Human MSCs (hMSC), mouse bone marrow MSCs (mMSC) and HL-1 cardiomyocytes (HL1cm) were expanded and cultured as previously described [44, 45]. hMSCs were used only in **Figure 5-2** to confirm specificity of the measles virus system. mMSCs were used for single-cell RNA-seq experiments. The first five fusion products were detected via the inducible bimolecular fluorescence complementation (BiFC) system[46]. The remaining twenty-three

hybrids were detected via the more commonly used two-color fluorescence methodology. Briefly, GFP was constitutively expressed in HL1cms and mCherry in mMSCs. Hybrids in this case are dual-labeled with both GFP and mCherry. BiFC positive (GFP) cells or dual-labeled cells were sorted using FACS. Sorted, single-cell, fusion products were captured on chips using the Fluidigm C1 system. mRNA libraries were constructed using the Illumina Nextera XT according to the manufacturer's protocol and sequenced on the Illumina Miseqv3 (**Figure 5-1**). RNA-seq data has been uploaded to the Gene Expression Omnibus (GEO) database and can be accessed via confidential link (to be made accessible to public at time of publication, http://www.ncbi.nlm.nih.gov/geo/query/acc.cgi?token=ylkbseoaxpkjxsd&acc=GSE69926). RNA-seq data was confirmed with qPCR analysis on the cDNA from the Fluidigm C1 chip for selected genes.

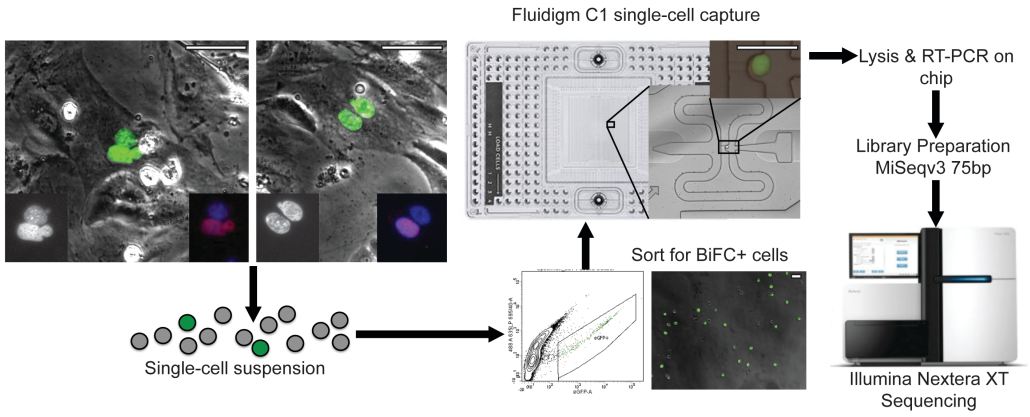

Figure 5-1. Workflow for identification, isolation and RNA-seq of mMSC-cardiomyocyte fusion products and associated controls, Related to Experimental Procedures.

Fusion products were identified via detection of green fluorescence associated with the intact BiFC construct or dual color expression of both GFP and mCherry (and therefore cell fusion) via fluorescence microscopy, upper left panel. Merged image of bright field (to discern cell membranes) and BiFC (green). Scale bar = 50 μm. After identification, cells were removed from culture dishes and sorted for GFP^+ cells using FACS. Sorted cells were injected into the Fluidigm C1 chip and again visualized via fluorescence microscopy to ensure successful capture and to confirm cell viability (cells were also stained with DEAD cell viability assay). Cells of interest were lysed and RNA extraction and cDNA synthesis were performed on the chip. Library preparation followed using Illumina Nextera XT and then sequencing using MiSeqv3.

5.3.1 Cell Culture

Human MSCs derived from human embryonic stem cells (hMSCs from WA-01), a gift of Dr. Peiman Hematti (University of Wisconsin-Madison) were expanded and cultured as previously described [44]. Also, mouse bone marrow mesenchymal stem cells (mMSCs) were purchased (3 month-old male C57BL mice, Georgia Reagents University, Augusta, GA and expanded and cultured with the same protocol as the hMSCs. Briefly, MSCs were cultured on a 0.1% gelatin (Sigma Aldrich, St. Louis, MO) pretreated flask containing a-minimum essential medium (MEM) complete. Alpha-MEM-complete consisted of a-MEM (Invitrogen, Carlsbad, CA), 10% fetal bovine serum (Hyclone, Logan, UT), 0.1 mM nonessential amino acids (Invitrogen), and 2 mM L-glutamine (Invitrogen). MSC cultures were allowed to grow to 60-70% confluence and were replated at a concentration of 1,500 cells/cm^2. HL-1 cardiomyocytes (HL1cm) (a gift of Dr. William Claycomb) were also expanded and cultured as previously described [45]. HL1cms were cultured on fibronectin/gelatin (1.25 mg fibronectin/100 mL, 0.02% gelatin) (Sigma Aldrich) pretreated flasks containing Claycomb-complete.

Claycomb-complete medium was comprised of Claycomb medium (SAFC Biosciences, St. Louis, MO, USA), 10% fetal bovine serum qualified for CMs (SAFC Biosciences), 100 U/mL: 100 μg/mL penicillin-streptomycin (Lonza, Walkersville, MD, USA), 0.1 mM norepinephrine (Sigma-Aldrich), and 2 mM L-glutamine (Invitrogen). HL1cms were passaged at 100% confluence and split 1:3. HL1cm coating and HL1cm medium was used when the two cell types were co-cultured. Experiments were performed using passages 6 – 11 and 70 – 85 for MSCs and HL1cms, respectively. All cultures were maintained at 37°C in 5% CO_2. hMSCs were used only in **Figure 5-2** to confirm specificity of the measles virus system. mMSCs were used for single-cell RNA-seq experiments.

5.3.2 Cell Fusion Induction and Detection of Fusion

To induce "accidental cell fusion" between MSCs (hMSCs or mMSCs) and HL1cms, we utilized the measles virus to create a recombinant DNA fusion system. The recombinant DNA system contains three components and enables fusion only when the hemagglutinin (H) protein of the virus binds to the human signaling lymphocytic activation molecule (hSLAM) of the human cell, which then forms a trimeric complex with the fusion protein (F) of the virus to initiate fusion. HL1cms are transfected with the receptor component, hSLAM, while MSCs are transfected with the hemagglutinin (H) and fusion (F) proteins (viral fusogens provided by Yoshihiro Kawaoka of the University of Wisconsin-Madison). Fusion only occurs when all three proteins are present and we utilized this ability to induce fusion between MSCs and HL1cms (**Figure 5-2A**). The first five fusion

products (BiFC_D1_F1-5) were detected via the inducible bimolecular fluorescence complementation (BiFC) system [46]. In this system, fluorescence will only be seen in cells that express both the VNH3.1 and YCH3.1 proteins, which are both encoded on separate plasmids and are linked to histones so that the fluorescence will occur in the nucleus. In our system the MSCs were given the YCH3.1 protein and HL1cms were given the VNH3.1 protein, so fluorescence will be detected only after fusion between MSCs and HL1cms. The remaining twenty-three hybrids (DC_D1_F1-16 and DC_D3_F1-7) were detected via the more commonly used two-color fluorescence methodology. Briefly, GFP was constitutively expressed in HL1 cardiomyocytes and mCherry in mMSCs via transfection. Hybrids in this case are dual-labeled with both GFP and mCherry after the HL1cm and mMSC share cytoplasm following fusion. Importantly there were five putative fusion products isolated using the dual color system that were deemed false-positive based on punctate fluorescence of one fluorophore or the other indicating likely endocytosis of cell debris and not bona fide fusion. These five false positive were not included in this manuscript. Transfection was accomplished using the Neon Transfection System (Invitrogen, Carlsbad, CA), according to the manufacturer's protocol. Briefly, 5 x 10^5 HL1cms were transfected with 2 μg of hSLAM and 2 μg of the detection system plasmid (VNH3.1 BiFC or pCAGS-GFP) with one 1,300 V pulse for 30 msec and plated into 6-well plates (Falcon, Fisher Scientific, Forest Lawn, NJ) containing Claycomb-complete medium without penicillin-streptomycin as per Neon Transfection System protocol. The HL1cm electroporation was repeated and

added to the same well to obtain approximately 1 x 10^6 total cells transfected. Eighteen hours later, fresh Claycomb-complete medium without penicillin-streptomycin was added to the transfected HL1cm and 5 x 10^5 MSCs were transfected with 2 μg of F-H and 2 μg of the detection system plasmid (YCH3.1 BiFC plasmid or pCAGS-mCherry) with one 1,500 V pulse for 20 msec and plated directly onto the previously electroporated HL1cms in the 6-well plate. The co-culture was allowed to incubate overnight and the fusion products were analyzed at 24 and 72 hours and identified using fluorescence microscopy for GFP or dual GFP and mCherry.

5.3.3 Immunocytochemistry

To confirm delivery of the vectors as well as detection of human nuclei, electroporated hMSCs and HL1cms were plated for 24 hours and immunocytochemistry (ICC) was performed to detect the H protein in MSCs, the hSLAM protein in HL1cms, or human nuclei in fusion products. We did not probe for the F protein because of the bicistronic nature of the F-H construct. Briefly, cells were washed with two rinses and two incubations of 1X PBS. Cell fixation was performed with 4% PFA for 15 min, followed by another set of washes, and probed with the 1:25 dilution of mouse anti-hemagglutinin antibody (35-614, ProSci Incorporated, Poway, CA), mouse anti-hSLAM antibody (ab2604, Abcam, Cambridge, MA) or mouse anti-human nuclear antigen (MAB1281, Millipore, Temecula, CA) in a dilution buffer of 5% bovine serum albumin (Hyclone, Logan, UT), 2% goat serum (MP Biomedical, Solon, OH), 1% glycine (Sigma Aldrich, St.

Louis, MO), and 0.1% triton-X (MP Biomedical, Solon, OH). Forty microliters of this antibody solution were placed on fixed co-cultures overnight at 4°C. Sections were washed with 1X PBS and incubated for 45 minutes at 4°C with 40 µL of a 1:200 dilution of the secondary antibody (AF647 donkey anti-mouse, Invitrogen, Carlsbad, CA) in dilution buffer. Cultures were washed a final time and mounted in DABCO/DAPI mounting medium (2.5% 1,4-diazabicyclo[2.2.2]octane (Sigma-Aldrich), 50% glycerol (Fisher Scientific, Forest Lawn, NJ, USA), and 0.005% 4′,6-diamidino-2-phenylindole (Sigma-Aldrich) in PBS). Fluorescence emission was detected on an IX71 inverted deconvolution fluorescence microscope (Olympus, Center Valley, PA). Images were acquired with a 20X UPlanFluor objective (NA = 0.5), using Metamorph software (Molecular Devices, Sunnyvale, CA) and analyzed with ImageJ (Fiji; open source software, http://pacific.mpi-cbg.de/wiki/index.php/Fiji). Background fluorescence was determined using a secondary antibody only control.

5.3.4 Flow Cytometry Analysis

To test the specificity of the system, two separate populations of HL-1 cardiomyocytes were transfected with the bicistronic H-F, bicistronic F-H, hSLAM, or no construct. Co-cultures were generated containing HL-1 cardiomyocytes transfected with each combination and monitored for seven days. Transfected HL-1 cardiomyocytes were trypsinized (0.25% trypsin, Mediatech, Inc. Manassas, VA) and fixed with 4% paraformaldehye in suspension after seven days in culture. The DNA content was analyzed via DAPI staining (0.005% 4',6-diamidino-2-

phenylindole in PBS) with flow cytometry and DNA content of experimental co-cultures (H-F/hSLAM and F-H/hSLAM) was compared to coculture controls (no fusogen/no fusogen, H-F/no fusogen, F-H/no fusogen, and hSLAM/no fusogen). The unfused cells should have normal diploid (2n) DNA content, but any cell that is undergoing division or has fused will result in DNA content greater than 2n. The percent of cells greater than 2n was quantified by setting a threshold past the 2n peak in the negative control histogram.

5.3.5 Single-cell Capture and RNA-seq

For the first five fusion products isolated (BiFC_D1_F1-5), co-cultures of transfected mMSCs and HL1cms were trypsinized after 18 hours and suspended in 1X PBS. For the twenty-three dual color hybrids isolated, co-cultures of transfected mMSCs and HL1cms were trypsinized after 18 hours (DC_D1_F1-16) or 72 hours (DC_D3_F1-7) and suspended in 1X PBS. BiFC positive (GFP^+) or dual color positive cells (GFP^+ and $mCherry^+$) were sorted using FACS (Aria II, BD Biosciences) into Claycomb-complete medium in a 6-well plate. The sorted cells were imaged with phase-contrast and fluorescent microscopy to confirm the BiFC or dual color signal. The sorted cells (approximately 300-1000 cells) were centrifuged and resuspended in 5 μL of Claycomb-complete medium for addition to the capture chip. Sorted, single-cell, BiFC-positive or dual color-positive, fusion products were captured on a large-sized (17-25 μm cell diameter) chip using the Fluidigm C1 system. Cells were loaded into the chip at approximately 20-50 cells/μL. The BiFC fusion products were stained for viability (DEAD cell

viability assay; Molecular Probes, Life Technologies, Grand Island, NY). Captured fusion products were imaged with phase-contrast and fluorescence microscopy to confirm cell number, viability and BiFC or dual color positivity at each capture point. Only single, live, BiFC or dual color positive cells were included in the fusion analysis. mMSCs and HL1cms controls without co-culture were captured in a separate Fluidigm C1 device with the HL1cm labeled with a green cytoplasmic dye (1 μm CellTracker Green CMFDA, Molecular Probes, Eugene, OR). Fifteen single, live cells of each control were selected for analysis (mMSC_1-15 and HL1cm_1-15). Also, five mMSCs and five HL1cms that were captured in the same chip as the dual color day one fusion products and were selected for analysis (mMSC_D1_1-5 and HL1cm_D1_1-5). These ten controls underwent co-culture for 24 hours after transfection without fusing. Once cells were captured in the device, cDNAs were prepared from each cell on the chip using the SMARTer Ultra Low RNA kit for Fluidigm C1 System (Clontech, Mountain View, CA). RNA spike-in Mix (Ambion, Life Technologies) was added to the lyses reaction and processed along side to cellular mRNA. mRNA library was constructed using the Illumina Nextera XT preparation kit (Illumina, San Diego, CA) according to the manufacturer's protocol and sequenced on the Illumina MiSeqv3 using paired end reads with a length of 75 bp to a depth of 18 to 22 million reads with the Multiplex on one MiSeq lane to create *.fastq files. For each experiment, a bulk population RNA control of both mMSCs and HL1cm was run in parallel to the single-cell samples. In addition, a population containing a mixture of both parental cells and fusion products obtained 24 hours after co-

culture was included (Mix_D1). Single-cell capture, cDNA preparation and RNA-seq was performed with the help of Kenneth Beckman, Adam Hauge and Jerry Daniel of the University of Minnesota Genomics Center.

5.3.6 Gene Expression Analysis

Gene expression analysis was performed with Galaxy software (Minnesota Supercomputing Institute (MSI), University of Minnesota, Minneapolis, MN). Reads were processed and aligned to the mouse reference genome (mm10_genes_2012_05_23.gtf and canonical_mm10.fa) using Tophat (version 2.0.12, open source software, http://ccb.jhu.edu/software/tophat/index.shtml). The default options supplied with the software were used and the aligned read files produced by Tophat were processed using Cufflinks software (version 2.2.1, open source software, http://cole-trapnell-lab.github.io/cufflinks/), for further analysis, including assembling transcripts, estimating their abundance, and testing for the differential expression between single-cell RNA-seq samples. Read counts were normalized to FPKM according to the gene length and total mapped reads. Genes with a $\log_2$ fold change greater than 1 from the control cells to the fusion products and had a false discovery rate (FDR)-adjusted *P*-value (also called *Q*-value) of less than 0.05 were considered “differentially expressed” and further analyzed for gene ontology. Gene ontology and Kyoto Encyclopedia of Genes and Genomes (KEGG) pathway enrichment analyses were performed with DAVID informatics resources 6.7 of the National Institute of Allergy and Infectious Diseases (NIAID) and of the National Institutes of Health

(NIH). RNA-seq data was analyzed with the assistance of Josh Baller and John Garbe of the Minnesota Supercomputing Institute (MSI, University of Minnesota-Twin Cities).

5.3.7 Gene cluster analysis

Up-stream filtering of the data was done in the SingulaR package. A threshold of 1 FPKM was set as the limit of detection. Outlier analysis was then performed in SingulaR with the identifyOutliers() command. No outliers were identified based on the gene expression. Over 12,000 differentially expressed genes were used to obtain the HC analysis in **Figure 5-3A and 5-3B**. Average linkage hierarchical clustering of gene expression intensity was performed using the Pearson distance to measure distance between gene and single cells. SingulaR (Fluidigm, San Francisco, CA) was used to compute and create the hierarchical clustering and principle component analysis plots.

5.3.8 Statistical Analysis

For comparison of DNA content and significant gene changes per chromosome a normal distribution was assumed and one-way analyses of variance and post-hoc test (Least Significant Difference, LSD) were used. To determine association between day of co-culture and phenotypic tendency to cardiomyocyte or mMSC (two by two table) the Yates corrected Chi-squared test was used. Data were analyzed with Microsoft Excel (Microsoft, Redmond, WA, USA). RNA-seq data was analyzed with the Cuffdiff or SingulaR programs.

5.3.9 Quantitative real-time polymerase chain reactions (qRT-PCR)

Complementary DNA (cDNA) was synthesized following the instructions from the Maxima First Strand cDNA Synthesis Kit (cat# K1642, Thermo Scientific). The cDNA was amplified from the cDNA from the single-cell reaction performed in the Illumina chip. Primers of qRT-PCR were purchased from Biorad (Hercules, CA) and the sequence of *Gapdh* primers (FOR: CATGGCCTTCCGTGTTCCTA, REV: CCTGCTTCACCACCTTCTTGAT) was obtained from a previous reported. Primer efficiencies were extracted from RealPlex^2 software and verified with melting curves. The comparative C_t method was employed to determine the relative changes in gene expression. For comparison to the single-cell RNA-seq results, each gene's FPKM values were normalized to each cell's *Gapdh* FPKM value, which was then normalized to that of the control cells. *Nkx2-5* and *Nanog* were also probed for expression via qPCR analysis but were not detected in any cell probed. This may reflect the fact that PCR was conducted on residual cDNA from the RNA-seq procedure. In cases where qRT-PCR outcompetes RNA-seq in sensitivity, sequencing reads are limited and PCR amplification is conducted on an alternate cell of a given population.

5.3.10 Normalization of FPKM Values

For comparison of single cells between multiple experiments, FPKM values for each cell were normalized to the *Gapdh* FPKM value for each cell. This normalization step allowed for direct comparison between samples in **Figures 5-**

3 and 5-7. However, for **Figure 5-6** the gene ontology was performed without this normalization due to limitations of the cuffdiff program input in the Galaxy software.

5.4 Results and Discussion

5.4.1 Accidental Fusion via Measles Virus Fusogens

Here we take the case of fusion of MSCs with cardiomyocytes, which has been detected by multiple investigators *in vivo*[1, 4-9]. Single-cell transcriptome analysis of hybrids by RNA-seq should enable direct comparison of individual fusion products with parental cells to determine the degree of programming/reprogramming in hybrid cells toward one or both of the parental cells, the rapidity with which programming/reprogramming occurs and the extent to which unique advantageous or deleterious transcriptome features emerge. To this end we developed means to efficiently induce accidental cell fusion between MSCs and cardiomyocytes *in vivo* (previously published[9]) and *in vitro* (shown here) via expression of viral fusogens. The *in vitro* system mimics the measles virus and associate receptor and enables fusion only when the hemagglutinin (H) protein binds to the human signaling lymphocytic activation molecule (hSLAM), which then forms a trimeric complex with the fusion protein (F) to initiate fusion. To test the specificity of the system, two separate populations of HL1cm were transfected with a bicistronic H-F, bicistronic F-H, hSLAM, or no construct. Cocultures were generated containing HL1cm transfected with each combination (i.e., H-F/hSLAM, F-H/hSLAM, H-F/no construct, etc.) and monitored for seven

days. When all three parts of the fusion system were delivered (either H-F/hSLAM or F-H/hSLAM, **Figure 5-2A, B**), the percentage of cells with DNA content greater than 2n increased from about 30% in controls to 59.1% ± 26.6% (not significant, $P = 0.226$) and 69.5% ± 16.7% ($^*P = 0.044$) respectively, which confirms the specificity of the system.

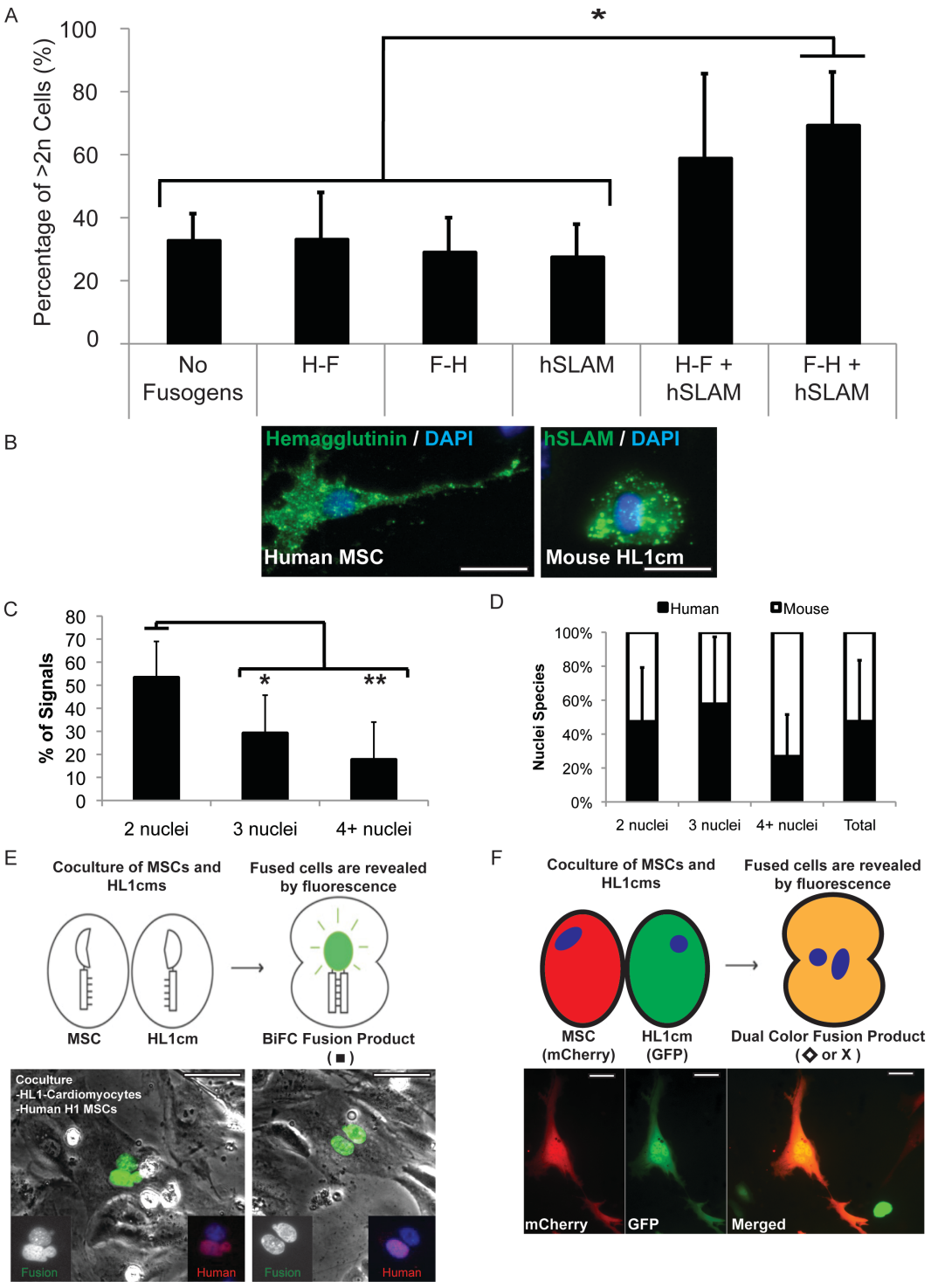

Figure 5-2. Induction and detection of cell fusion via the measles virus system and bimolecular fluorescence complementation (BiFC) and dual-color fluorescence, respectively. A. DNA content of HL1cm was analyzed via DAPI staining with flow

cytometry and DNA content of experimental cocultures (H-F/hSLAM and F-H/hSLAM) was compared to coculture controls (no fusogen/no fusogen, H-F/no fusogen, F-H/no fusogen, and hSLAM/no fusogen) (*p < 0.05). Data are represented as mean ± standard deviation (SD). B. Immunocytochemistry for hemagglutinin (H) on hMSC (green) and hSLAM on HL1cm (green). Nuclei stained with DAPI (blue). Scale bar = 50 mm. C. Greater than 50% of detected fusion products contained 2 nuclei. Data are represented as mean ± SD. (*p < 0.05, **p < 0.01). D. Approximately 50% of the total nuclei of fusion products were of human origin, supporting the specificity of the system. E. Schematic for the bimolecular fluorescence complementation (BiFC) system. Fusion products were detected with fluorescence microscopy for BiFC (green). Cells were then labeled for human nuclear antigen (HNA, red, only present in the hMSC nuclei). Representative fusion products were detected with BiFC (green), HNA (red), and nuclei detected with DAPI (blue). Scale bar = 50 mm. F. Schematic for the dual color fluorescence system. Fusion products were detected with fluorescence microscopy for dual expression of GFP from HL1cm and mCherry from mMSC. Representative fusion product is shown below schematic. Scale bar = 50 mm.

To ensure that fusion occurred between two discrete fusion partners, we induced fusion between mouse HL1cm and human H1 MSCs (hMSC) and detected fusion products using a bimolecular complementation (BiFC)-based reporter assay we previously described[46] (**Figure 5-2E**). This technique is a powerful tool for detecting fusion *in vitro* and its use was essential for these studies to ensure that single-cell transcriptomes emerged from bona fide fusion products due to the inducible nature of the signal. After identifying fusion products via fluorescence microscopy (**Figure 5-2E**), cells were fixed and stained for human nuclear antigen (HNA; present on hMSCs and not HL1cm). Over half of the detected fusion products had two nuclei (53.3% ± 15.7%, *P = 0.027 vs. three nuclei and **P = 0.003 vs. 4+ nuclei) (**Figure 5-2C**). Of the fusion products with two nuclei, 47.2% ± 32.0% were of human origin confirming the ability of the

fusion system to merge at least one cell of each type (i.e., MSCs and HL1cm) in any given fusion product (**Figure 5-2D**). Together, these data confirm the ability of the measles virus-based system to promote accidental cell fusion between hMSCs and cardiomyocytes and of the BiFC-based detection method to robustly identify hybrids. To ensure that the BiFC complex did not introduce transcriptional bias unrelated to fusion, we also used a two-color approach wherein different fluorescence reporter genes were expressed in each fusion partner (**Figure 5-2F**).

5.4.2 Transcriptome Diversification of MSC-Cardiomyocyte Fusion Products

Single-cell RNA-seq was performed on isolated mMSC-HL1cm hybrids. Hierarchical clustering (HC) and principal component analysis (PCA) were executed to compare transcripts of five fusion products (BiFC_D1_F1-5, 24 hours) identified using BiFC, twenty-three fusion products (DC_D1_F1-16, 24 hours; DC_D3_F1-7, 72 hours) identified using dual color (DC) expression of GFP and mCherry, the parental controls, and the population controls (mMSC_PC and HL1cm_PC). Parental controls included 15 cells of each parental type isolated prior to co-culture (mMSC_1-15 and HL1cm_1-15) and 5 cells of each parental cell type isolated 24 hours after co-culture (mMSC_D1_1-5 and HL1cm_D1_1-5). In addition, a population containing a mixture of both parental cells and fusion products obtained 24 hours after co-culture was included (Mix_D1). Resulting HC (**Figure 5-3A**, shown are top ~12,000 differentially

expressed genes, which include all genes with Fragments Per Kilobase of transcript per Million mapped reads (FPKM) >1 for any sample) and PCA plots (**Figure 5-3B**) showed population-level controls correlated with the average of the single cells of that population supporting the accuracy of the single-cell data. The Mix_D1 population control was positioned approximately midway between parental cells reflecting the higher relative fraction of parental cells to fusion products in this population. Analysis of fusion products revealed extensive heterogeneity with ten expressing a unique transcriptome, seven clustering closely with cardiomyocytes and eleven clustering more closely with mMSCs (**Figure 5-3A and 5-3B**). Gain or loss of gene expression did not favor particular chromosomes in a substantive way, though minor nuances were noted (**Figures 5-4 and 5-5**).

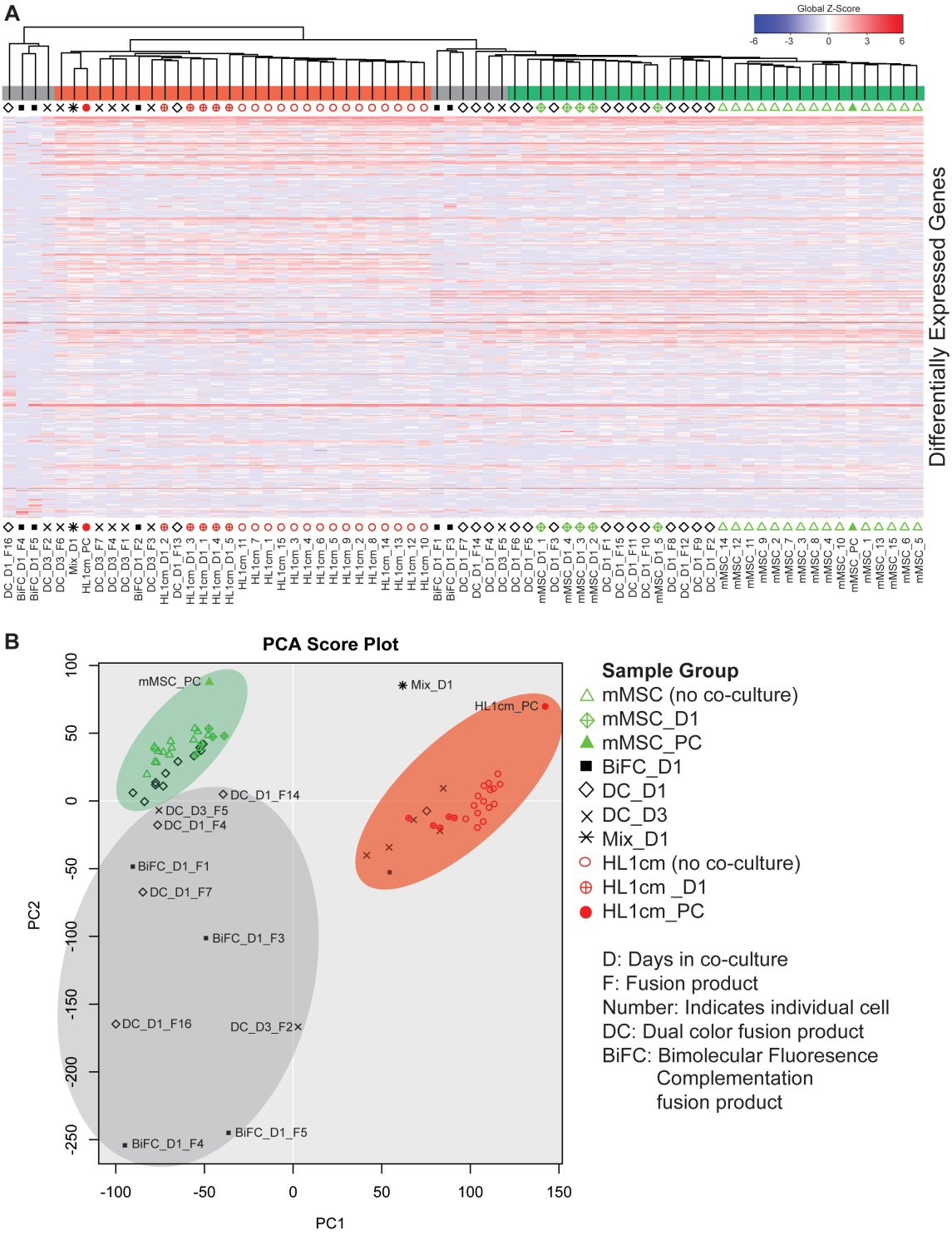

Figure 5-3. Hierarchal clustering (HC) and principal component analysis (PCA) of differentially expressed genes between mMSC-cardiomyocyte fusion products and parental controls. A. A global view of differential gene expression between hybrids

(BiFC_D1_F1-5, DC_D1_F1-16, and DC_D3_F1-7), parental cells (mMSC_1-15, mMSC_D1_1-5, HL1cm_1-15, and HL1cm_D1_1-5) and population controls (mMSC_PC, HL1cm_PC, and Mix_D1). Global Z-Score reflects the number of standard deviations away from the mean of expression of all genes in the display. Gene expression is shown in fragments per kilobase of exon per million fragments mapped (FPKM). Differential expression was defined as a $\log_2$ fold change of greater than 1 and a false discovery rate (FDR)-adjusted *P*-value below 0.05. B. PCA analysis of hybrids, parental cells and population controls.

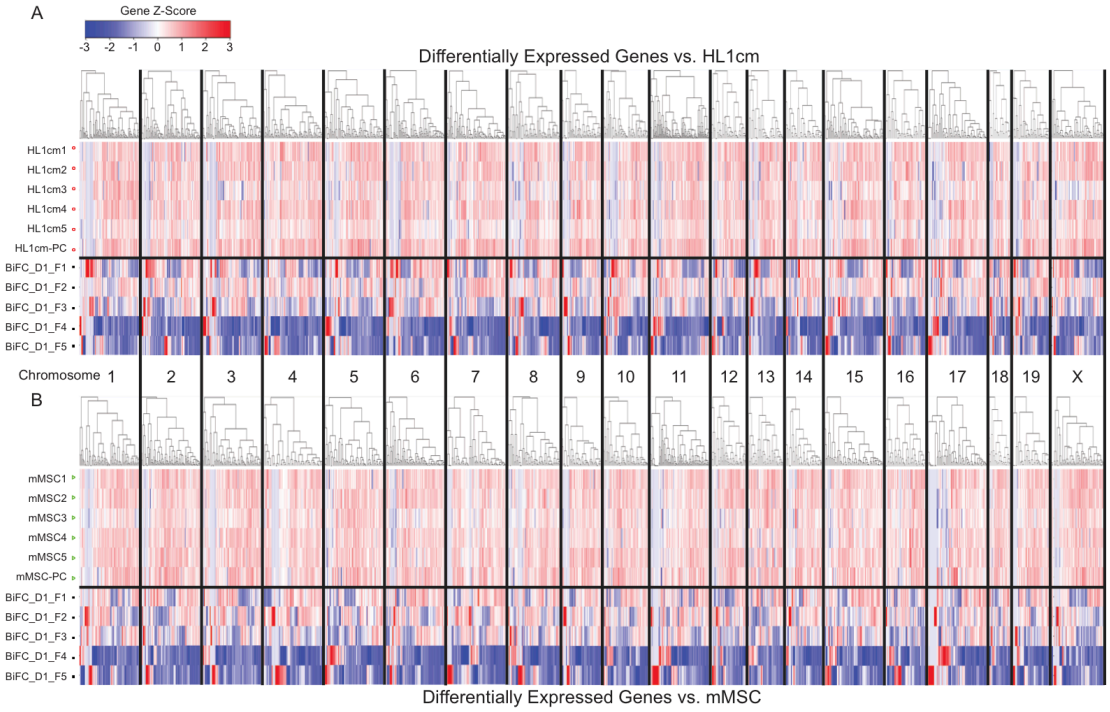

Figure 5-4. Hierarchal clustering of differentially expressed genes of individual hybrids organized according to chromosome. To determine whether gain or loss of gene expression between parental cells and fusion products favored particular chromosomes we plotted differentially expressed genes as a function of chromosome number for BIFC_D1_F1-5 hybrids. Differentially expressed genes of fusion products versus HL1cms (A) or mMSCs (B) were organized into chromosomal groups and hierarchal clustering was performed. There were no specific chromosome(s) that

experienced extensive increase or decrease in FPKM per gene, but BIFC_D1_F4 and BIFC_D1_F5 displayed global reduction of FPKM of many genes on most chromosomes compared to the parental controls and even the other three BiFC fusion products.

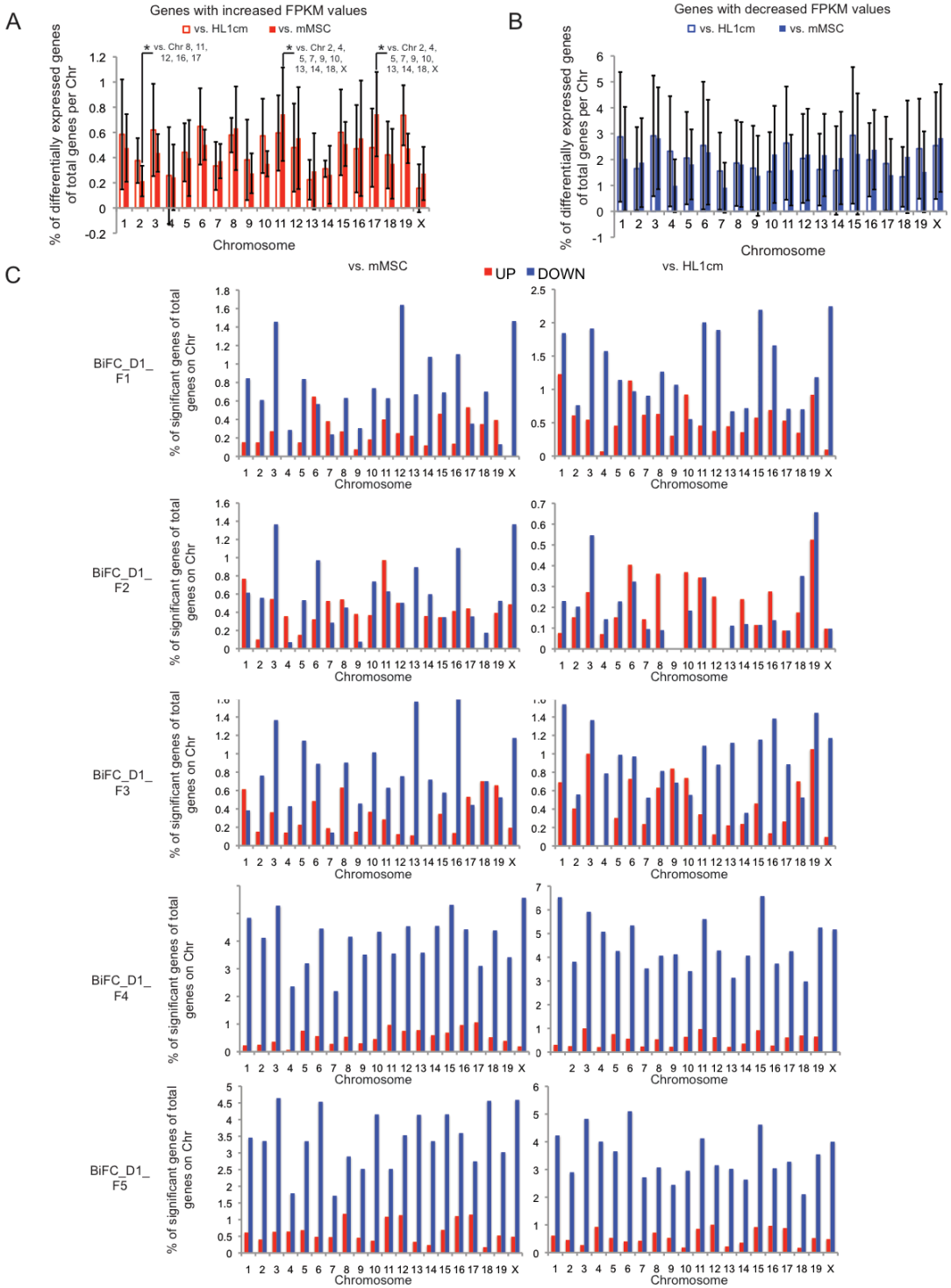

Figure 5-5. Differentially expressed genes of individual hybrids organized according to chromosome. Total number of increased FPKM values (red) or decreased FPKM values (blue) were normalized to the total number of genes on each chromosome for each fusion product (vs. HL-1cm: open bars, vs. mMSC: closed bars). Increases in FPKM values varied from chromosome to chromosome and between hybrids and, as shown in Figure 5-3, occurred most often of chromosomes 2, 11 and 17. Decrease in FPKM values was universal and not chromosome specific. (*$P < 0.05$ via LSD post-hoc analysis). Data are represented as mean ± SD.

To identify enriched function-related gene groups and to isolate interacting proteins of BiFC fusion products (individual) and the ten hybrids with unique transcriptomes (combined) relative to parental cells, we used the Database for Annotation, Visualization and Integrated Discovery (DAVID) bioinformatics resources. Significant genes were identified relative to parental controls and separated according to increased or decreased FPKM values. From the large list of functional clusters that emerged from our analysis certain trends were identified. All five BiFC fusion products realized significant increase of ribosomal genes (**Figure 5-6A**). This was coupled with an almost universal decrease in FPKM values associated with non membrane bounded organelles, membrane enclosed lumen, and the cytoskeleton suggesting that fusion products detect increased cytoplasmic mass following fusion and as a consequence might prepare to recalibrate protein synthesis (**Figure 5-6B**). In addition, many cellular maintenance functions are decreased during the first 24 hours after fusion as noted by the decrease in FPKM values of the genes associated with the cell cycle, translation, and generation of precursor metabolites and energy. Also dominant was an increase in FPKM values of genes associated with methylation

including genes associated with nucleotide binding proteins (*Gng11*, *Gbp2*), histone related genes (*H3f3a*, *Hnrnph1*, *Hnrpdl*, *Hist2h2bb*, *Hist1H3f*, *H3f3b*, *H2afy*) and other genes affecting gene expression (*Runx1*, *Rhob*, *Ubb*, *Ubl3*, *Nras*, *Piwil4*). This result supports the large number of genes with decreased FPKM observed in HC (**Figure 5-3A, Figures 5-4 and 5-5**). Analysis of the ten combined hybrids showed conservation of primary ontologic outcomes of individual hybrids including an increase in FPKM values associated with ribosomes and antigen processing and presentation (**Figure 5-6C**). This conservation also occurred for ontologic groups with decreased FPKM values associated with generation of precursor metabolites and energy, membrane enclosed lumen/intracellular organelle lumen, and chromosomes. The combination of decreased metabolism with increased ribosomes is perhaps counterintuitive, but could reflect a shift of priorities in the cell such that the hybrids emphasize production of ribosomes while downregulating the expression of other genes with a net reduction in energy demands. Generally, combining hybrids for this analysis resulted in loss or muting of differentially expressed genes and associated ontology. Interestingly, the fusion products with a unique transcriptome combined showed a decrease in genes associated with muscle protein, vascular smooth muscle contraction and cytoskeletal binding suggesting a loss of cardiomyocyte contractile function, which was similar to the results found in an *in vitro* functional study of hybrids formed between human MSCs and rat neonatal ventricular myocytes [32].

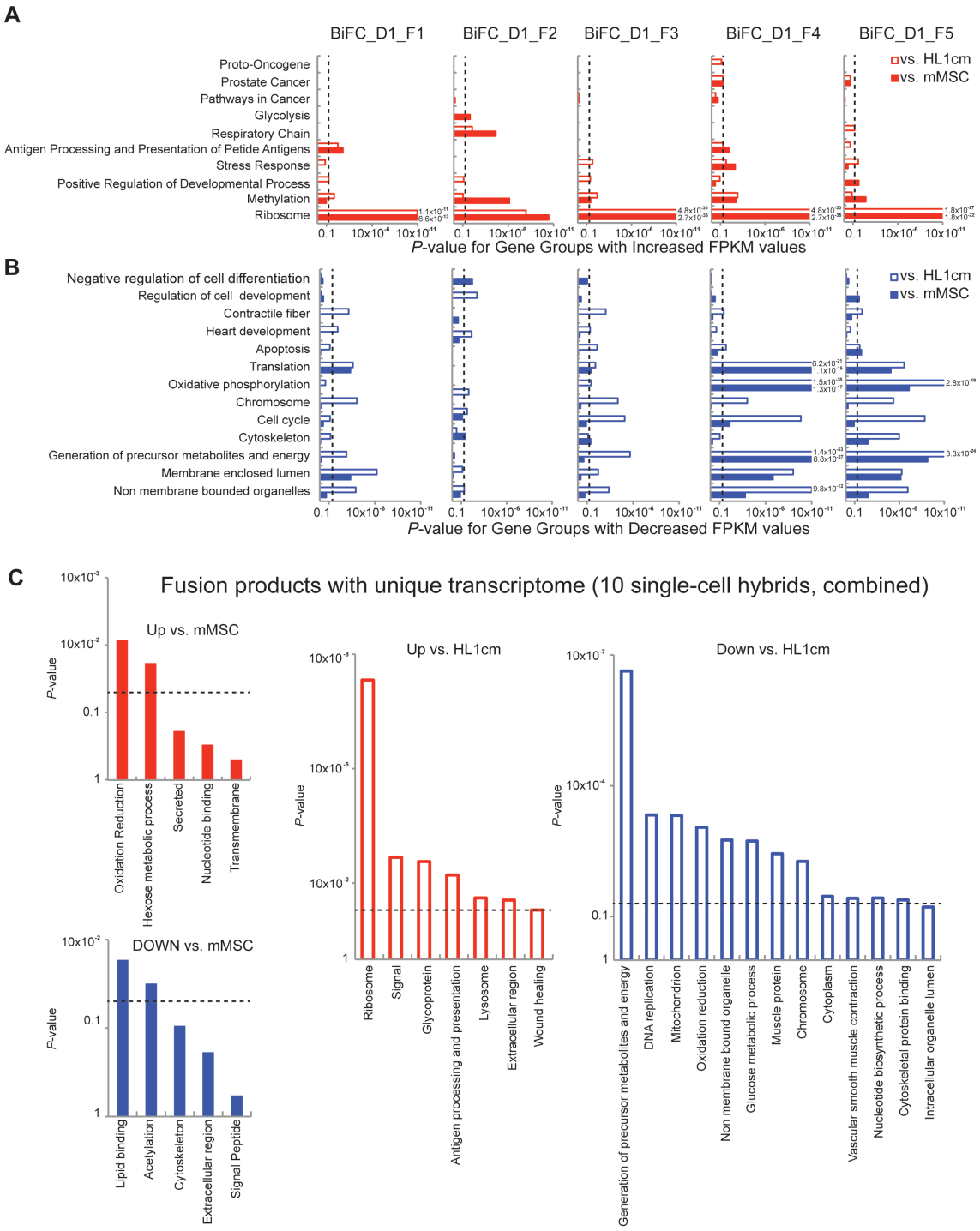

Figure 5-6. Gene Ontology of BiFC Fusion Products and all hybrids with a unique transcriptome. *P*-value of functional annotation for differentially expressed genes (increased FPKM values (A, red) or decreased FPKM values (B, blue)) for each BiFC

fusion product. C. Gene ontology analysis after combining the ten hybrids with unique transcriptomes (vs. HL1cm: open bars, vs. mMSC: closed bars). The dashed line represents a *P*-value of 0.05.

5.4.3 Function-related Gene Groups of Hybrids Can Mirror Parental Groups

To probe more deeply the contribution of parental lines to programming/reprogramming of hybrid transcriptomes, we defined specific genes sets relevant to each parental cell type including genes related to the differentiation of each parental cell (i.e., mesoderm and cardiac precursors for cardiomyocytes and pluripotent cells for MSCs) and, in the case of MSCs, genes related to mesodermal cell types that can arise from MSCs (i.e., adipocytes, osteoblasts, chondrocytes). For the MSC gene set, thirteen of twenty-eight hybrids (BiFC_D1_F1, DC_D1_1-5, 8-12, 15, DC_D3_F5) had a profile quite similar to mMSCs (**Figure 5-7A and 5-7B**). These thirteen expressed genes related to stemness (*Ly6a, CD44, Itgb1, Itgav,* and *Gnl3*) and mesodermal differentiation (*Spp1, Sox9, Col1a1, Scd1* and *Fn1*). RNA-seq data was confirmed with qPCR analysis of *Ly6a* (**Figure 5-7C**). BiFC_D1_F3 and BiFC_D1_F5 (which do not cluster with mMSCs) expressed high levels of the pluripotency gene, *Nanog* (68.8 and 124.5 FPKM in BiFC_D1_F3 and BiFC_D1_F5 respectively). This was unexpected since neither mMSCs (average 1.92 ± 5.34 FPKM) nor HL1cm (average 3.57 ± 6.03 FPKM) express *Nanog* at a high level. *Nanog* is a transcription factor, known for its control of proliferation and self-renewal in the inner cell mass, supporting a reversion or reprogrammed cell state for BiFC_D1_F3 and BiFC_D1_F5. Of note, twelve of the thirteen

hybrids that clustered with mMSCs were obtained one day following co-culture as opposed to those obtained three days after co-culture which either clustered with HL1cm or expressed a unique transcriptome. To explore this trend we next focused on genes associated with cardiomyocyte determination and contractility.

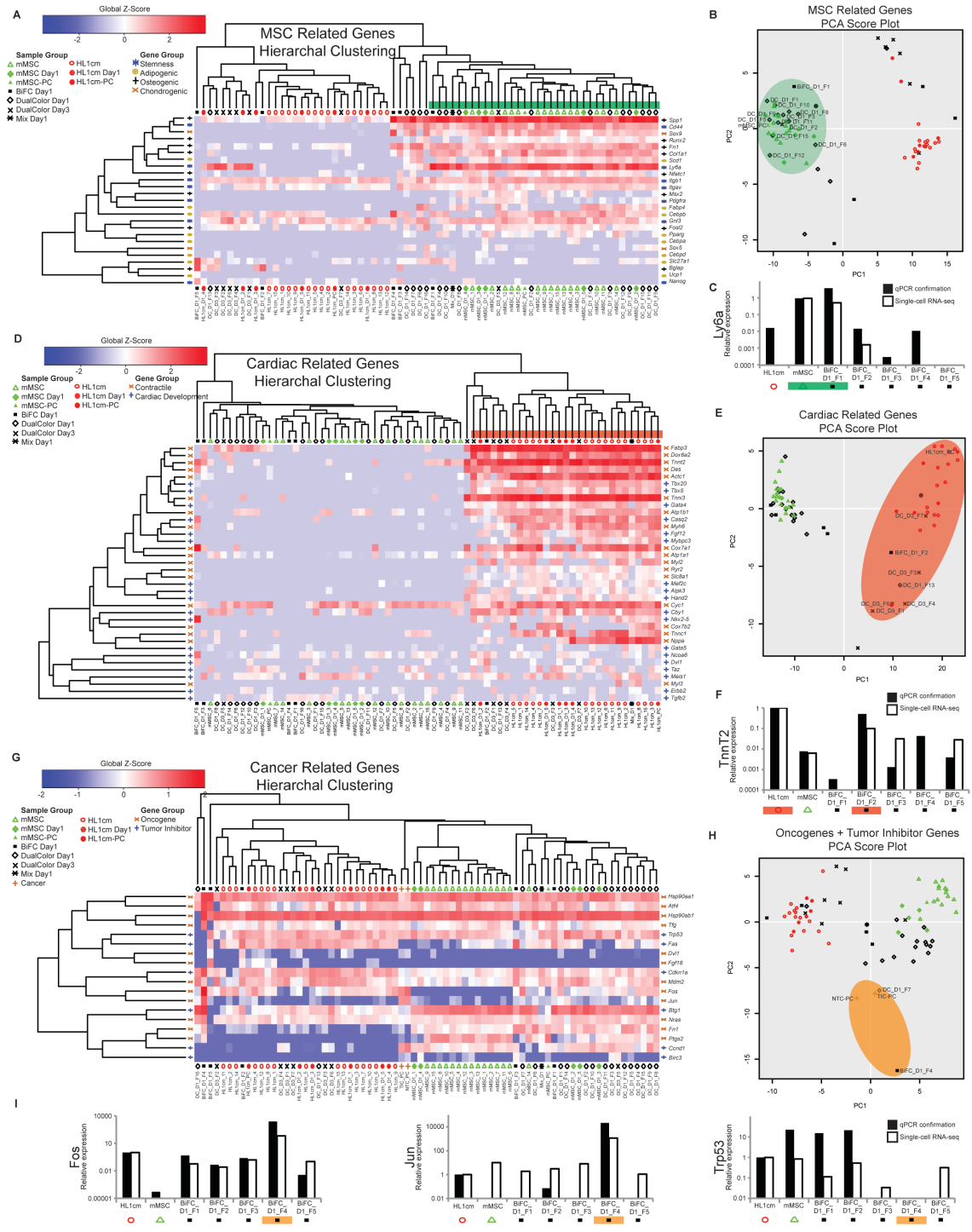

Figure 5-7. mMSC-cardiomyocyte fusion products can express a cardiomyocyte cell-like, stem cell-like or distinct transcriptome. A. HC of fusion products in relation to a set of genes related to stemness (*), adipogenic differentiation (ɵ), osteogenic differentiation (+), or chondrogenic differentiation (x). B. PCA analysis of fusion products and controls. D. HC of fusion products for a set of genes related to cardiac development

(+) or contractile ability (x). E. PCA analysis of fusion products and controls. G. HC of fusion products, a population of tumor initiating cancer cells (TIC-PC), a population of nontumorigenic cancer cells (NTC-PC), and controls for a set of oncogenes and a set of tumor suppressor genes. H. PCA analysis of fusion products, cancer populations and controls for the combined oncogene tumor suppressor gene set. C, F, I. qPCR confirmation of RNA-seq data.

Seven (BIFC_D1_F2, DC_D1_F13, DC_D3_F1, 3, 4, 6, 7) of twenty-eight hybrids had a transcriptome quite similar to the HL1cm (**Figure 5-7D and 5-7E**). Of the seven, five corresponded to hybrids three days after co-culture. These seven expressed genes related to cardiac development to a lesser extent (*Hand2*, *Cby1, Tbx5, Tbx20, and Gata4*) and to contractile machinery to a greater extent (*Actc1*, *Tnni3*, *Cox6a2*, *fabp3*, *Cyc1, Atp1a1, Atp1b1, Des*, *Tnnt2*, and *Myh6*). RNA-seq data was confirmed with qPCR analysis (**Figure 5-7F**). Of particular interest, BiFC_D1_F5 (which clustered far from HL1cm), expressed a vastly different cardiac gene profile overall and unexpectedly expressed mesodermal precursor gene *Nkx2.5* (2545 FPKM) at a level higher than the cardiomyocyte controls (average *Nkx2-5* expression 12.6 $\pm$ 18.2 FPKM) (**Figure 5-7D**). BiFC_D1_F5 also expressed other developmental (*Ncoa6*, *Dvl1*) and contractile genes (*Cox7a1*, *Des*, *Tnnt2* and *Myh6*) at levels comparable to cardiomyocyte controls. Enticing is the possibility that fusion enabled reprogramming to an early mesodermal state.

5.4.4 Cancer-related Gene Groups Prevalent in Some Hybrids

To this point, analyses of transcriptomes of fusion products has been biased toward beneficial outcomes of fusion. Since ten hybrids expressed dramatically diverse and distinct transcriptional features, we reassessed the ontologic outcomes related to cancer fates. Of most critical note, BiFC_D1_F4 saw an increase in FPKM values of genes within three cancer-related ontological gene sets (proto-oncogenes, prostate cancer and pathways of cancer, (**Figure 5-6A**)). As neither parental cell type had a cancer-like phenotype, we conducted further analysis on genes in these sets to discern the degree of tumor susceptibility. These genes were classified into one list containing two gene groups, oncogenes or tumor inhibitors. HC and PCA were performed (**Figure 5-7G, 5-7H, and Figure 5-8**). In addition, we included RNA-seq data from two populations (tumor initiating cells (TIC-PC) and nontumorigenic cancer cells (NTC-PC)) of MMTV-*Wnt-1* murine tumor cells (previously reported, [47]). Interestingly, the PCA plot showed BiFC_D1_F4 and DC_D1_F7 clustered with both TIC-PC and NTC-PC. Of note, BiFC_D1_F4 and DC_D1_F7 showed significantly decreased FPKM values for the tumor suppressor gene, p53 (*Trp53*, no detectable FPKM and 6.65 FPKM, respectively) and increased levels of the proto-oncogenes *Fos* and *Jun*. *Fos* levels were 16952.1 FPKM for BiFC_D1_F4 and 754.0 FPKM for DC_D1_F7. *Jun* levels were 1581.5 FPKM for BiFC_D1_F4 and 14.1 FPKM for DC_D1_F7. Average oncogene levels for parental cell with highest expression (*Fos,* 128.2 ± 111.2 FPKM, HL1cm and *Jun* 3.49 ± 3.62 FPKM, mMSC) were less than levels observed in these two hybrids and *Trp53*

expression (231.5 ± 165.8 FPKM, mMSC; 232.1 ± 144.7 FPKM HL1cm) is reliably detected as opposed to undetected/low levels of these two hybrids. These RNA-seq trends were confirmed with qPCR analysis of *Fos, Jun,* and *Trp53* (**Figure 5-7I**). BiFC_D1_F4 even had higher levels of *Fos* (550.3 and 1201.5 FPKM for TIC-PC and NTC-PC, respectively) and *Jun* (421.1 and 477.0 FPKM for TIC-PC and NTC-PC, respectively) expression than the breast cancer cell populations (accounting in large part for the spread between BiFC_D1_F4 and the TIC/NTC in the PCA score plot, **Figure 5-7H, Figure 5-8**). Thus the increased FPKM values of oncogenes, clustering with tumor-forming cancer cell populations, and decreased or undetected FPKM values of tumor suppressors in some fusion products suggests transcriptome diversity associated with accidental cell fusion can support the emergence of a cancer phenotype.

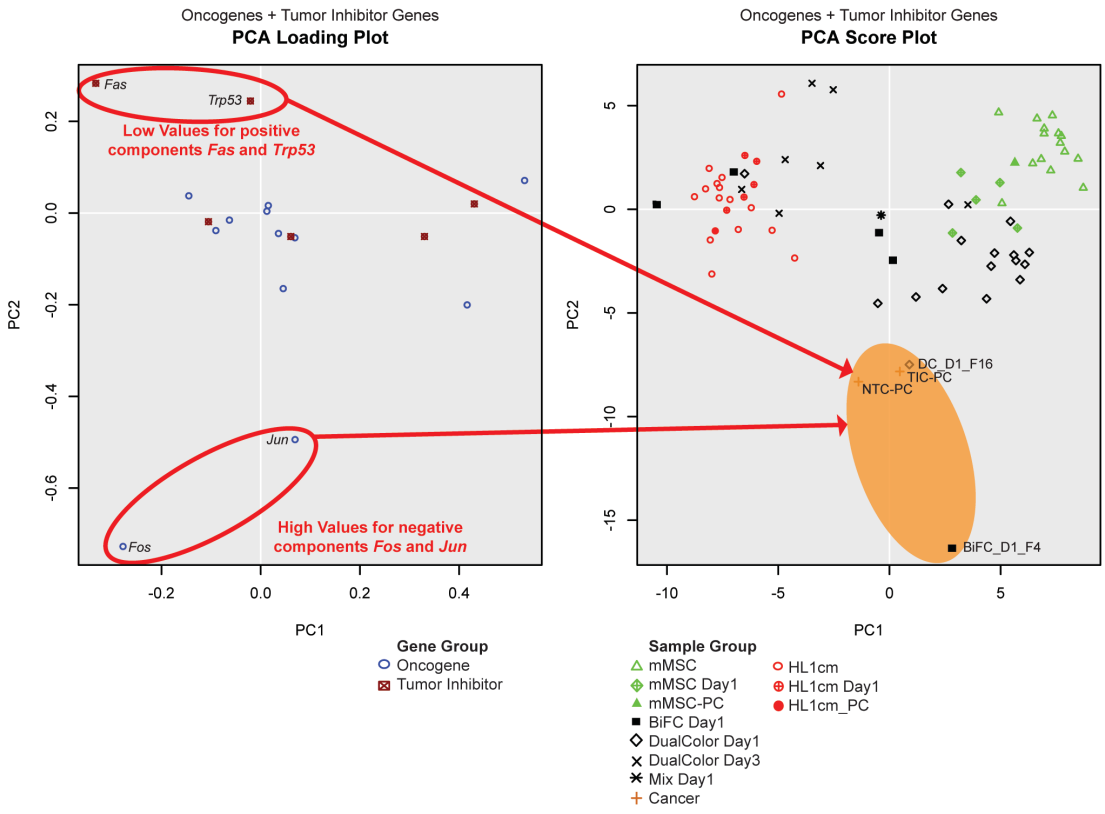

Figure 5-8. PCA loading plot and PCA Score plot for the cancer gene set, The score plot is a summary of the relationship between single-cell samples (or population controls, PC). The loading plot is a summary of the genes and provides a means to interpret patterns seen in the score plot. Genes in the loading plot that fall far from zero on a PC axis are those that most significantly impact on the PC score of individual samples. In this case, *Fos* and *Jun* gene expression have a high negative contribution to the PC2 score, whereas *Fas* and *Trp53* expression have a high positive contribution to PC2. Therefore, if a cell has high expression of *Fos* and *Jun*, but low expression of *Fas* and *Trp53* it will have a negative PC2 value, as seen with BiFC_D1_F4 and DC_D1_F16 and the cancer populations. Interestingly, if BiFC_D1_F4 had lower expression of oncogenes *Fos* and *Jun* and increased expression of tumor suppressor genes *Trp53* and *Fas*, it would cluster more closely with the breast cancer cells on the PCA score plot.

5.5 Conclusions

Thus, here we utilize a robust means to increase accidental cell fusion *in vitro* and an inducible detection system to reliably identify and isolate fusion products subsequently analyzed using single-cell RNA-seq. We found ten hybrids expressed a unique transcriptome, seven clustered closely with cardiomyocytes and eleven clustered more closely with mMSCs supporting the hypothesis that cell fusion is an ingenious means to generate transcriptional diversity. Grouping of hybrids might reflect, in part, the ratio of parental nuclei[48]. **Figure 5-2** indicates approximately 47% of hybrids have more than two nuclei and interestingly 64% of hybrids showed significant similarity to one or the other fusion partner. However, at the later time point (day 3) hybrids appear to tend toward a cardiomyocyte-like phenotype compared to day 1 (Chi-square statistic, 10.73; $P < 0.005$ of HC, **Figure 5-3A**) suggesting such hybrids are more

apt to survive or that numbers of nuclei alone do not dictate phenotypic outcomes. Gene ontology analysis of differentially expressed genes showed that fusion products recalibrate protein synthesis as indicated by increased FPKM values of genes associated with ribosomal proteins and decreased FPKM values of genes associated with cytoplasmic organelles. Gene ontology also showed a significant concentration of genes linked to methylation in the fusion products, supporting the possibility of gene silencing. Some fusion products underwent considerable reprogramming expressing pluripotency and cardiac precursor genes at high levels relative to parental cells. Most interesting was the observation that two hybrids appeared to produce a transcriptome, which aligned closely to that of breast cancer cells, increasing critical oncogenes and decreasing tumor suppressor genes. For these reasons, it will be important to monitor stem cell transplantation and other scenarios that enable membrane instability for the emergence of tumors.

5.6 Acknowledgements

This study was funded by NIH, NHLBI, HL089679; University of Minnesota Genomics Center New Investigator Award; NSF-GRFP, 2010105691.

5.7 References

1. Alvarez-Dolado M, Pardal R, Garcia-Verdugo JM et al. Fusion of bone-marrow-derived cells with Purkinje neurons, cardiomyocytes and hepatocytes. Nature. 2003;425:968-973.

2. Wang X, Willenbring H, Akkari Y et al. Cell fusion is the principal source of bone-marrow-derived hepatocytes. Nature. 2003;422:897-901.

3. Rizvi AZ, Swain JR, Davies PS et al. Bone marrow-derived cells fuse with normal and transformed intestinal stem cells. Proc Natl Acad Sci U S A. 2006;103:6321-6325.

4. Andrade J, Lam JT, Zamora M et al. Predominant fusion of bone marrow-derived cardiomyocytes. Cardiovasc Res. 2005;68:387-393.

5. Kruglyakov PV, Sokolova IB, Zin'kova NN et al. In vitro and in vivo differentiation of mesenchymal stem cells in the cardiomyocyte direction. Bull Exp Biol Med. 2006;142:503-506.

6. Noiseux N, Gnecchi M, Lopez-Ilasaca M et al. Mesenchymal stem cells overexpressing Akt dramatically repair infarcted myocardium and improve cardiac function despite infrequent cellular fusion or differentiation. Mol Ther. 2006;14:840-850.

7. Nygren JM, Liuba K, Breitbach M et al. Myeloid and lymphoid contribution to non-haematopoietic lineages through irradiation-induced heterotypic cell fusion. Nat Cell Biol. 2008;10:584-592.

8. Oh H, Bradfute SB, Gallardo TD et al. Cardiac progenitor cells from adult myocardium: homing, differentiation, and fusion after infarction. Proc Natl Acad Sci U S A. 2003;100:12313-12318.

9. Freeman BT, Kouris NA, Ogle BM. Tracking fusion of human mesenchymal stem cells after transplantation to the heart. Stem cells translational medicine. 2015;4:685-694.

10. McDonald DM, Foss AJ. Endothelial cells of tumor vessels: abnormal but not absent. Cancer metastasis reviews. 2000;19:109-120.

11. Morikawa S, Baluk P, Kaidoh T et al. Abnormalities in pericytes on blood vessels and endothelial sprouts in tumors. Am J Pathol. 2002;160:985-1000.

12. Mondal Roy S, Sarkar M. Membrane fusion induced by small molecules and ions. Journal of lipids. 2011;2011:528784.

13. Paltsyn AA, Manukhina EB, Goryacheva AV et al. Intermittent hypoxia stimulates formation of binuclear neurons in brain cortex- a role of cell fusion in neuroprotection? Exp Biol Med (Maywood). 2014;239:595-600.

14. Lazova R, Chakraborty A, Pawelek JM. Leukocyte-cancer cell fusion: initiator of the warburg effect in malignancy? Adv Exp Med Biol. 2011;714:151-172.

15. Duelli D, Lazebnik Y. Cell-to-cell fusion as a link between viruses and cancer. Nat Rev Cancer. 2007;7:968-976.

16. Kouris NA, Schaefer JA, Hatta M et al. Directed Fusion of Mesenchymal Stem Cells with Cardiomyocytes via VSV-G Facilitates Stem Cell Programming. Stem Cells Int. 2012;2012:414038.

17. Kouris NA, Squirrell JM, Jung JP et al. A nondenatured, noncrosslinked collagen matrix to deliver stem cells to the heart. Regen Med. 2011;6:569-582.

18. Clavel F, Charneau P. Fusion from without directed by human immunodeficiency virus particles. J Virol. 1994;68:1179-1185.

19. Joag SV, Li Z, Foresman L et al. Chimeric simian/human immunodeficiency virus that causes progressive loss of CD4+ T cells and AIDS in pig-tailed macaques. J Virol. 1996;70:3189-3197.

20. Karlsson GB, Halloran M, Schenten D et al. The envelope glycoprotein ectodomains determine the efficiency of CD4+ T lymphocyte depletion in simian-human immunodeficiency virus-infected macaques. J Exp Med. 1998;188:1159-1171.

21. Kondo N, Marin M, Kim JH et al. Distinct requirements for HIV-cell fusion and HIV-mediated cell-cell fusion. J Biol Chem. 2015;290:6558-6573.

22. Gao P, Zheng J. High-risk HPV E5-induced cell fusion: a critical initiating event in the early stage of HPV-associated cervical cancer. Virology journal. 2010;7:238.

23. Hu L, Plafker K, Vorozhko V et al. Human papillomavirus 16 E5 induces bi-nucleated cell formation by cell-cell fusion. Virology. 2009;384:125-134.

24. Lagasse E, Connors H, Al-Dhalimy M et al. Purified hematopoietic stem cells can differentiate into hepatocytes in vivo. Nat Med. 2000;6:1229-1234.

25. Willenbring H, Bailey AS, Foster M et al. Myelomonocytic cells are sufficient for therapeutic cell fusion in liver. Nat Med. 2004;10:744-748.

26. Miller RA, Ruddle FH. Pluripotent teratocarcinoma-thymus somatic cell hybrids. Cell. 1976;9:45-55.

27. Cowan CA, Atienza J, Melton DA et al. Nuclear reprogramming of somatic cells after fusion with human embryonic stem cells. Science. 2005;309:1369-1373.

28. Tada M, Tada T, Lefebvre L et al. Embryonic germ cells induce epigenetic reprogramming of somatic nucleus in hybrid cells. EMBO J. 1997;16:6510-6520.

29. Palermo A, Doyonnas R, Bhutani N et al. Nuclear reprogramming in heterokaryons is rapid, extensive, and bidirectional. FASEB J. 2009;23:1431-1440.

30. Terada N, Hamazaki T, Oka M et al. Bone marrow cells adopt the phenotype of other cells by spontaneous cell fusion. Nature. 2002;416:542-545.

31. Wei HJ, Nickoloff JA, Chen WH et al. FOXF1 mediates mesenchymal stem cell fusion-induced reprogramming of lung cancer cells. Oncotarget. 2014;5:9514-9529.

32. Shadrin IY, Yoon W, Li L et al. Rapid fusion between mesenchymal stem cells and cardiomyocytes yields electrically active, non-contractile hybrid cells. Scientific reports. 2015;5:12043.

33. Milstein C, Cuello AC. Hybrid hybridomas and their use in immunohistochemistry. Nature. 1983;305:537-540.

34. Lindner M, Schirrmacher V. Tumour cell-dendritic cell fusion for cancer immunotherapy: comparison of therapeutic efficiency of polyethylen-glycol versus electro-fusion protocols. Eur J Clin Invest. 2002;32:207-217.

35. Willenbring H, Grompe M. Delineating the hepatocyte's hematopoietic fusion partner. Cell Cycle. 2004;3:1489-1491.

36. van Berlo JH, Kanisicak O, Maillet M et al. c-kit+ cells minimally contribute cardiomyocytes to the heart. Nature. 2014;509:337-341.

37. Dittmar T, Schwitalla S, Seidel J et al. Characterization of hybrid cells derived from spontaneous fusion events between breast epithelial cells exhibiting stem-like characteristics and breast cancer cells. Clinical & experimental metastasis. 2011;28:75-90.

38. Ozel C, Seidel J, Meyer-Staeckling S et al. Hybrid cells derived from breast epithelial cell/breast cancer cell fusion events show a differential RAF-AKT crosstalk. Cell communication and signaling : CCS. 2012;10:10.

39. Lu X, Kang Y. Efficient acquisition of dual metastasis organotropism to bone and lung through stable spontaneous fusion between MDA-MB-231 variants. Proc Natl Acad Sci U S A. 2009;106:9385-9390.

40. Yang JY, Ha SA, Yang YS et al. p-Glycoprotein ABCB5 and YB-1 expression plays a role in increased heterogeneity of breast cancer cells: correlations with cell fusion and doxorubicin resistance. BMC cancer. 2010;10:388.

41. Jacobsen BM, Harrell JC, Jedlicka P et al. Spontaneous fusion with, and transformation of mouse stroma by, malignant human breast cancer epithelium. Cancer Res. 2006;66:8274-8279.

42. Noubissi FK, Harkness T, Alexander CM et al. Apoptosis-induced cancer cell fusion: a mechanism of breast cancer metastasis. FASEB J. 2015.

43. Berndt B, Haverkampf S, Reith G et al. Fusion of CCL21 non-migratory active breast epithelial and breast cancer cells give rise to CCL21 migratory active tumor hybrid cell lines. PLoS One. 2013;8:e63711.

44. Trivedi P, Hematti P. Derivation and immunological characterization of mesenchymal stromal cells from human embryonic stem cells. Exp Hematol. 2008;36:350-359.

45. Steinhelper ME, Lanson NA, Jr., Dresdner KP et al. Proliferation in vivo and in culture of differentiated adult atrial cardiomyocytes from transgenic mice. The American journal of physiology. 1990;259:H1826-1834.

46. Lin HP, Vincenz C, Eliceiri KW et al. Bimolecular fluorescence complementation analysis of eukaryotic fusion products. Biol Cell. 2010;102:525-537.

47. Feng W, Gentles A, Nair RV et al. Targeting unique metabolic properties of breast tumor initiating cells. Stem Cells. 2014;32:1734-1745.

48. Pavlath GK, Blau HM. Expression of muscle genes in heterokaryons depends on gene dosage. J Cell Biol. 1986;102:124-130.

Chapter 6 Future Directions

6.1. *In vivo* Studies

6.1.1 Investigating reprogramming *in vivo*

After obtaining *in vitro* single-cell transcriptional reprogramming data, the next step is to determine if this type of large scale diversification occurs during *in vivo* fusion as well. Based on our studies with the Cre/*LoxP* biophotonic system, fusion is extensive after MSC transplantation. It would be worthwhile to investigate how fusion products are reprogrammed in different organ systems. Hearts, stomachs, intestines, livers and any other organ with detectable fusion could be excised and cellularized. The fusion products would then be sorted out via flow activated cell sorting (FACS) for each organ. The fusion products in each organ could then be captured with the Fluidigm C1 system and undergo single-cell RNA-seq. This study would give useful insight into whether the extensive reprogramming observed *in vitro* varies from organ to organ. I predict that extensive diversification after fusion will be observed across all organ systems. This would match what was observed *in vitro*, however the functionality of fusion products between different organ systems may vary. While fusion between MSCs and cardiomyocytes appears to hinder cardiac functionality seen in our functional study and in an *in vitro* study [1], other studies focusing on fusion in the liver show that fusion between MSC and hepatocytes have a positive affect on liver functionality [2-6]. Fusion in systems outside of the heart

might not be as detrimental if the organ systems are not as metabolically active and electrically active as the heart. Another potential interesting study could involve inserting the BiFC system into a mouse embryoid body and observe how fusion occurs in mouse development. This would allow for live tracking of cell fusion during organogenesis, which could yield important results in the field of developmental cell biology.

Also, the observed activation of latent oncogenes in fusion products suggests the possibility of tumor formation. A few studies have analyzed if reprogramming after fusion between cancer cells and other cells of the body can lead to changes in tumorigenicity [7, 8], but there have not been any investigation into whether fusion between somatic cells can lead to tumors *in vivo*. Our group performed some preliminary studies in which we transplanted fusion products between MSCs and cardiomyocytes into mice in order to determine if the population expressing the oncogenes could form tumors. No tumors have been detected, but these studies were performed with immune competent mice. Further studies with nude mice are still needed to help determine if the fusion products with a cancer-like phenotype has the ability to form tumors.

6.2 *In vitro* Studies

6.2.2 Extended

The next step in studying reprogramming after heterotypic cell fusion would be to examine the transcriptome of fusion products at later time points. In our studies,

we looked at reprogramming up to 3 days after fusion, but a longer study could give a better idea of the affect of cell fusion on reprogramming. Longer studies (weeks to months) would allow the researcher to determine if reprogramming converged to certain transcriptional profiles or whether the diversity seen within one to three days still exists. I predict that at longer time points the fusion products will converge to a certain phenotype/transcriptome that is different that both parental types. The longer fusion products are cultured, the hybrids with the highest proliferation and survival rates will be the cells remaining. Perhaps the hybrids with the oncogenic phenotype would eventually overtake the other hybrids and dominated the culture. Homotypic fusion should also be included in these studies to determine if the transcriptional diversity is merely due to the process of cell fusion or whether heterotypic fusion is the root of the extensive diversity. Increases and/or changes in ploidy (and cell fusion) can be linked to accelerated evolution and possibly cancer. One study suggested that the mechanisms that drive evolution in polyploidy plants could also be the mechanism that drive the evolution of cancerous cells [9]. Lazebnik argues that learning what these mechanisms are would help researchers develop new tools and techniques to potentially prevent cancer. This study also suggests that fusing different types of cells causes a collision of merged cellular systems, resulting in death or leading to emergent phenotypes. This theory directly helps to explain the results seen in the single-cell RNA-seq study. The varied transcriptomes that emerged in the fusion products are a result of the colliding systems.

6.2.4 Epigenic and methylation reprogramming after fusion

Beyond looking at the transcriptome of fusion products, epigenetic and methylation changes after fusion would yield interesting results. This study would help reveal the mechanisms behind the transcriptional changes. A few studies have emerged recently examining this idea. A study by Su et al. started to pull out the mechanisms for reprogramming after cell fusion in tumors [10]. An electrofusion device has also been created to specifically examine epigenetic and methylation changes after cell fusion. These tools could be utilized to further understand reprogramming after somatic cell fusion. Based on the results from our studies, I would predict that fusion products exhibit extensive increases in methylation and consequent silencing of many genes. This epigenetic shift would confirm the increase in methylation associated genes and high level down regulation of genes I observed. Also, to aid in the study a MSC-cardiomyocyte hybrid cell line should be produced. This could be performed by fusing MSCs and cardiomyocytes, sorting and allowing the hybrids to proliferate and stabilize. The hybrids would then undergo testing for proliferation rates, electrical coupling, tumor formation as well as epigenetic/genetic reprogramming. I anticipate that the stabilized cell line would be able to proliferate extensively since the cell line would most likely be composed of the cancer-like hybrids. These cells would be able to electrically couple like the hybrids in the Shadrin et al. study [1], but their contractile ability will be decreased. The hybrids will most likely be able to form

tumors due to their cancer-like phenotype. However, the hybrid tumors may be cleared over time as seen in the Wei at al. study [7].

6.2 References

1. Shadrin IY, Yoon W, Li L et al. Rapid fusion between mesenchymal stem cells and cardiomyocytes yields electrically active, non-contractile hybrid cells. Scientific reports. 2015;5:12043.
2. Wang X, Willenbring H, Akkari Y, Torimaru Y, Foster M, Al-Dhalimy M, Lagasse E, Finegold M, Olson S, Grompe M. Cell fusion is the principal source of bone-marrow-derived hepatocytes. *Nature*. 2003;422:897-901
3. Willenbring H, Bailey AS, Foster M, Akkari Y, Dorrell C, Olson S, Finegold M, Fleming WH, Grompe M. Myelomonocytic cells are sufficient for therapeutic cell fusion in liver. *Nature medicine*. 2004;10:744-748
4. Willenbring H, Grompe M. Delineating the hepatocyte's hematopoietic fusion partner. *Cell cycle*. 2004;3:1489-1491
5. Quintana-Bustamante O, Grueso E, Garcia-Escudero R, Arza E, Alvarez-Barrientos A, Fabregat I, Garcia-Bravo M, Meza NW, Segovia JC. Cell fusion reprogramming leads to a specific hepatic expression pattern during mouse bone marrow derived hepatocyte formation in vivo. *PloS one*. 2012;7:e33945
6. Vassilopoulos G, Wang PR, Russell DW. Transplanted bone marrow regenerates liver by cell fusion. *Nature*. 2003;422:901-904

7. Wei HJ, Nickoloff JA, Chen WH et al. FOXF1 mediates mesenchymal stem cell fusion-induced reprogramming of lung cancer cells. Oncotarget. 2014;5:9514-9529.

8. Zhou X, Merchak K, Lee W, et al. Cell Fusion Connects Oncogenesis with Tumor Evolution. The American Journal of Pathology. 2015;185;7;2049-2060.

9. Lazebnik Y. The shock of being united and symphiliosis: Another lesson from plants? Cell Cycle. 2014;13;15;1-7.

10. Wu W, Qu Y, Hu N, et al. A cell electrofusion chip for somatic cells reprogramming. PLOS ONE. 2015;DOI:10.1371.

Appendices

A1. A Cre-Lox P recombination approach for the detection of cell fusion *in vivo*

Elements of this work have been published as:

Sprangers, A.J., Freeman, B.T., Kouris, N.A., Ogle, B.M. A Cre-Lox P Recombination Approach for the Detection of Cell Fusion In Vivo. J. Vis. Exp. (59), e3581, DOI : 10.3791/3581 (2012).

A1.1 Abstract

The ability of two or more cells of the same type to fuse has been utilized in metazoans throughout evolution to form many complex organs, including skeletal muscle, bone and placenta. Contemporary studies demonstrate fusion of cells of the same type confers enhanced function. For example, when the trophoblast cells of the placenta fuse to form the syncytiotrophoblast, the syncytiotrophoblast is better able to transport nutrients and hormones across the maternal-fetal barrier than unfused trophoblasts [1-4]. More recent studies demonstrate fusion of cells of different types can direct cell fate. The "reversion" or modification of cell fate by fusion was once thought to be limited to cell culture systems. But the advent of stem cell transplantation led to the discovery by us and others that stem cells can fuse with somatic cells in vivo and that fusion facilitates stem cell

differentiation [5-7]. Thus, cell fusion is a regulated process capable of promoting cell survival and differentiation and thus could be of central importance for development, repair of tissues and even the pathogenesis of disease. Limiting the study of cell fusion, is lack of appropriate technology to 1) accurately identify fusion products and to 2) track fusion products over time. Here we present a novel approach to address both limitations via induction of bioluminescence upon fusion (**Figure 1**); bioluminescence can be detected with high sensitivity in vivo [8-15]. We utilize a construct encoding the firefly luciferase (Photinus pyralis) gene placed adjacent to a stop codon flanked by LoxP sequences. When cells expressing this gene fuse with cells expressing the Cre recombinase

protein, the LoxP sites are cleaved and the stop signal is excised allowing transcription of luciferase. Because the signal is inducible, the incidence of false-positive signals is very low. Unlike existing methods which utilize the Cre/LoxP system [16, 17], we have incorporated a "living" detection signal and thereby afford for the first time the opportunity to track the kinetics of cell fusion in vivo. To demonstrate the approach, mice ubiquitously expressing Cre recombinase served as recipients of stem cells transfected with a construct to express luciferase downstream of a floxed stop codon. Stem cells were transplanted via intramyocardial injection and after transplantation intravital image analysis was conducted to track the presence of fusion products in the heart and surrounding tissues over time. This approach could be adapted to analyze cell fusion in any tissue type at any stage of development, disease or adult tissue repair.

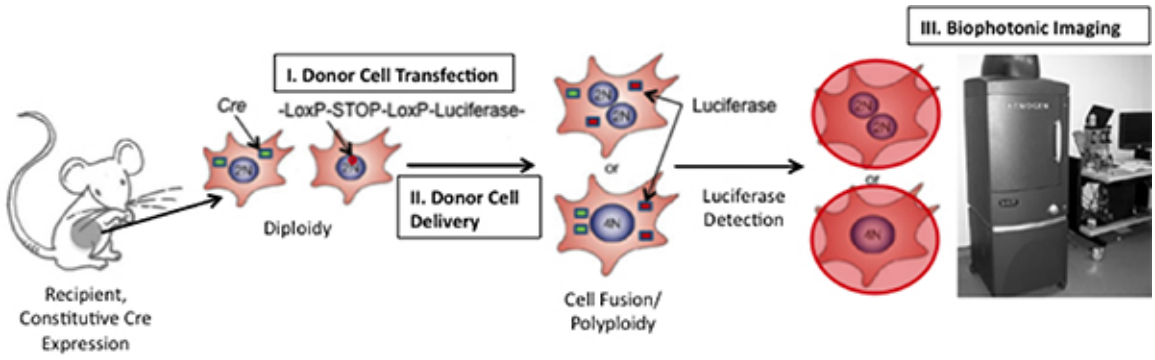

Figure A1-1. Schematic of Technique to Detect Cell Fusion In Vivo. If fusion between Cre-expressing mouse cells and transplanted cells expressing a floxed luciferase plasmid occurs, luciferase will be expressed. Luciferase can be detected by injecting the enzymatic substrate, D-luciferin, into the mouse and then imaging the mouse using a Xenogen Biophotonic Imaging System (Adapted from reference 19).

A1.2 Protocol

A1.2.1 Donor Cell Transfection

1. Harvest mesenchymal stem cells (MSCs, derived from H1 embryonic stem cells kindly donated by Dr. Peiman Hematti; alternatively, any cell type of any species hypothesized to fuse in vivo could be employed) when 70 - 80% confluent with 1X trypsin (Mediatech, Manassas VA) for 5 min. Inactivate trypsin with α-MEM complete medium (antibiotic free, Invitrogen, Carlsbad CA) [18]. Centrifuge at 300 x g for 5 min.

2. Carefully aspirate supernatant and re-suspend pellet in 1 mL of 1X PBS and count cells using a hemacytometer.

3. Transfer 1.5 x 106 cells to a 1.5 mL centrifuge tube. Centrifuge at 300 x g for 5 min.

4. Carefully aspirate supernatant. Resuspend pellet in 300 µL of R Buffer (Neon

Transfection System, Invitrogen) and 6 µg (2 µg / 5.0 x 105 cells) of p231 pCMVe-betaAc-STOP-luc (Addgene, Cambridge, MA). Place 3 mL of E Buffer (Invitrogen) into the electroporation docking port per manufacturer's protocol (Neon Transfection System, Invitrogen).

5. Transfer cell-plasmid solution to a 100 µL Neon pipet tip and electroporate with a pulse duration of 20 ms and a magnitude of 1500 volts. Place electroporated cells into a 15 mL conical tube containing 9.7 mL α-MEM complete medium.

6. Repeat step 1.5 two additional times and pool transfected cells to yield a total volume of 10 mL. Add the 10 mL cell suspension (1.5 x 106 cells) to a T175 flask containing 10 mL α-MEM complete medium. Cell viability after electroporation is approximately 30%, to yield approximately 4.5 x 105 viable cells per T175.

7. Change α-MEM complete medium 24 hours following transfection.

8. Harvest transfected cells when 70 - 80% confluent (~2 - 3 days after electroporation). Perform cell count using a hemacytometer and resuspend the cells at a concentration of 1.0 x 106 cells/50 µL of α-MEM complete medium. Minimize time cells spend in suspension to reduce cell death prior to injection.

A1.2.2 Intramyocardial Injection

1. Induce anesthesia by isoflurane (Phoenix Pharmaceuticals, Inc., St. Joseph, MO) on transgenic mice engineered to constitutively express Cre recombinase in every cell (B6.C-Tg(CMV-cre)1Cgn/J, Jackson Laboratory, Bar Harbor, ME).

2. Remove hair from chest region using hair clippers or chemical hair remover.

3. Intubate with an 18 gauge catheter (Becton Dickinson & Co, Franklin Lakes

NJ) and place on mouse ventilator at 120 - 130 breaths per minute with a stroke volume of 150 µL.

4. Make lateral incision across the fourth intercostal space thereby producing a thoracotomy.

5. Visualizing the heart, make two 25 µL injections of transfected cell suspension using a 1 mL syringe (Temuro Medical Corporation, Somerset, NJ) and 28 gauge needle (Becton Dickinson & Co, Franklin Lakes NJ). To ease the intramyocardial injection and prevent excessive damage to the organ, bend the needle head ~90 degrees.

6. Following injection, use absorbable sutures (e.g., vicryl) to close the ribs and muscle layers. Suture skin closed using 4-0 nylon or silk.

7. Allow mouse to recover from anesthesia and extubate.

8. Control groups should include Cre mice receiving medium injections only, Cre mice receiving the same concentration of untransfected cells and wild type mice receiving transfected cells (alternatively, Cre mice receiving transfected cells not prone to fuse).

A1.2.3 Biophotonic Imaging

1. Five to fifteen minutes before imaging, intraperitoneally (IP) inject 10 µL per gram of mouse body weight of 15 mg/mL D-Luciferin (Caliper Life Sciences, Hopkinton, MA).

2. Induce anesthesia on mice via isoflurane at 4% for induction and 1 - 2% for maintenance.

3. Place mice supine in imaging box with facemask administering 1 - 2% isoflurane for maintenance anesthesia (Xenogen Biophotonic Imaging System, Hopkinton, MA). Several mice can be imaged concurrently. Image sham control mouse with experimental mice for easy comparison of luminescent signal.

4. Using Living Image software (Xenogen), set appropriate exposure time (typically 60 sec, see Results). Set area of image to fit mice and keep area consistent throughout imaging to prevent changes in sensitivity. Set subject height at 4.5 cm.

5. Acquire luminescence intensity signal corresponding to mouse or mice within the view field and save unmodified image files. Process images to remove background signal corresponding to a control or unmanipulated mouse. Intensity values above background correspond to fused cells within the animal. Intensity analysis can be conducted using Living Image software (Xenogen) or open source image analysis software. Typically, a region of interest (ROI) is selected to compare intensity data between animals and experiments.

A1.2.4 Representative Results

To determine the sensitivity of the Xenogen Biophotonic Imaging System, a cell line which constitutively expresses luciferase (231-LUC-D3H1, Xenogen) was delivered to the myocardium of C57/Bl6 mice (Jackson Laboratory). Cells were injected at concentrations of 1 x 106, 1 x 103, or 1 x 101 cells. Six hours after cell delivery, mice were injected intraperitoneally with luciferin and imaged using the Xenogen system. A specific signal could be detected with 1,000 cells (2 of 6 mice

imaged, **Figure 2**), but detection was more reliable with 10,000 cells (6 of 6 mice imaged). Importantly, this study also served to establish a rough correlation between number of luciferase-expressing cells and signal intensity. To demonstrate the utility of the described protocol in detecting and tracking cell fusion, MSCs were transfected with the LoxP-Stop-LoxP-Luciferase plasmid (Addgene) and delivered to the myocardium of Cre-expressing mice. Approximately one week after cell delivery, mice were first imaged using the Xenogen system without D-luciferin injection. As expected, without the enzymatic substrate, no intensity signal was detected (**Figure 3**). Next, D-luciferin was injected intraperitoneally and a signal corresponding to luciferase intensity and thus cell fusion was detected in two of four mice tested. A similar signal was detected one week later (**Figure 3**), suggesting MSC-coupled fusion products can be maintained in vivo. In this case, the study was terminated to allow for evaluation of heart and surrounding tissue, but one could envision longer-term analyses and more frequent imaging to track the maintenance, proliferation and perhaps migration of fusion products in mice.

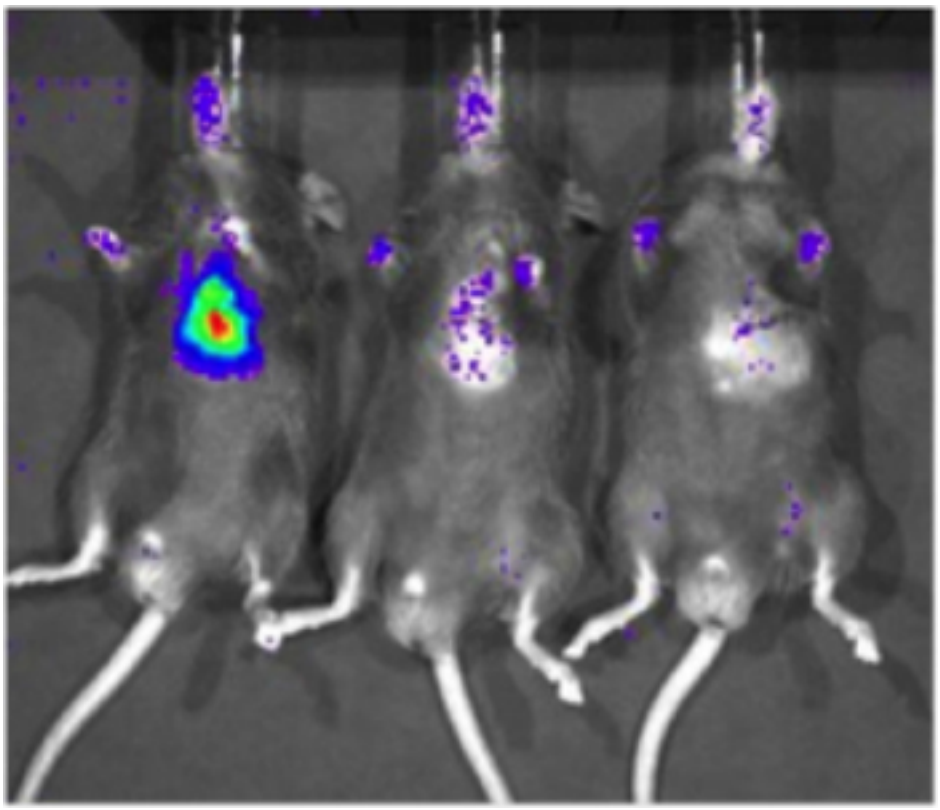

Figure A1-2. Sensitivity of detection of luciferase-expressing cells in cardiac tissue with biophotonic imaging. A cell line which constitutively expresses luciferase (231-LUC-D3H1, Xenogen) was delivered to the intramyocardial space of C57/Bl6 mice at various total cell numbers. Representative images of mice receiving 1 x 106, 1 x 103 and 1 x 101 cells (left to right) are shown, imaging was conducted approximately 6 hours after injection.

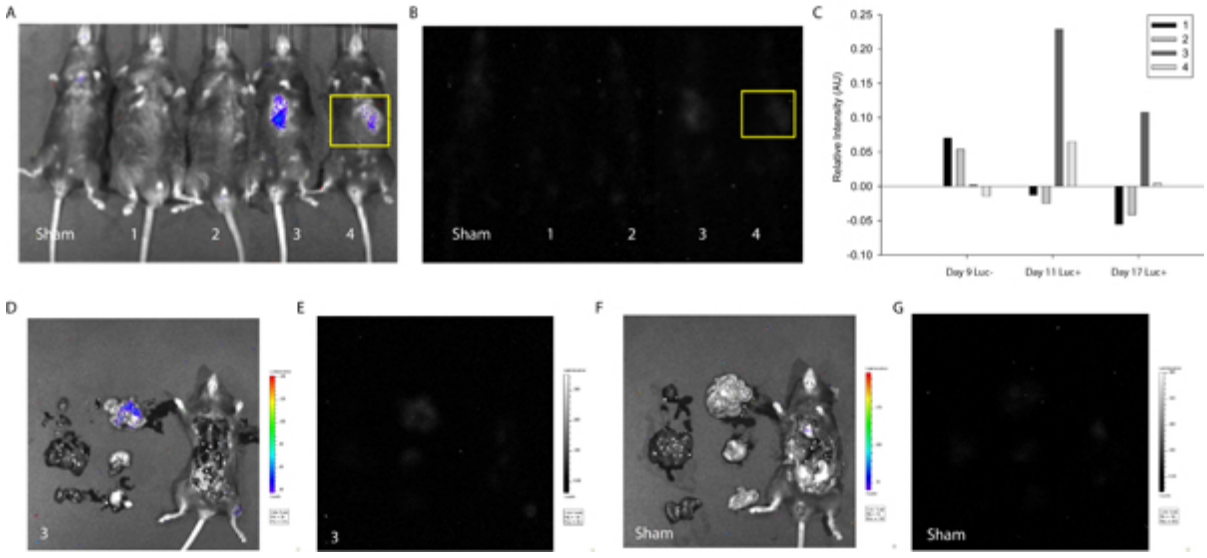

Figure A1-3. Quantification of In Vivo Luminescence Indicative of Cell Fusion. MSCs were transfected with the LoxP-Stop-LoxP-Luciferase plasmid and delivered to the myocardium of Cre-expressing mice. Approximately one week and two weeks after cell delivery, Cre mice were imaged using the Xenogen Biophotonic Imaging System to measure the intensity of luminescence indicative of cell fusion. (A) Overlay of photograph and intensity of luminescence of sham and mice 1-4 (left to right) 17 days after cell delivery. (B) Intensity of luminescence of sham and mice 1-4 (left to right) 17 days after cell delivery. A region of interest was selected (yellow) corresponding to the injection site and intensity levels were determined using ImageJ (free source) software20. (C) Intensity of luminescence was normalized to the same region of interest on sham mouse for all experimental conditions. At one week, mice 3 and 4 showed positive luminescence signal suggesting spontaneous fusion of a mouse cell and transplanted MSC. The signal persisted in mouse 3 at two weeks. To determine organ-specific localization of the signal corresponding to mouse 3, the thoracic cavity was exposed and primary organs excised and imaged. (D) Overlay of photograph and intensity of luminescence of mouse 3. Note localization of intensity signal in the small intestine. (E) Intensity of luminescence of mouse 3. (F) Overlay of photograph and intensity of luminescence of sham mouse. (G) Intensity of luminescence of sham mouse.

A1.3 Discussion

The method described here allows, for the first time, discrete identification and temporal analysis of cell fusion in organisms, including small animals. The

approach combines Cre-LoxP recombination with subsequent biophotonic image analysis. The approach is amenable to tracking not only cell-cell fusion, but also virus-cell fusion and so could prove useful for tracking viral infections. Image analysis is rapid and it is possible to image multiple small animals simultaneously. Detection of fusion is limited by the frequency of fusion of particular cell partners in their corresponding microenvironments and by the efficiency of transfection of the LoxP-Stop-LoxP-Luciferase plasmid. Thus, optimum results would be obtained with fusion partners containing an integrated form of the LoxP-Stop-LoxP-Luciferase sequence. In addition, the organisms must be stationary to image and so anesthesia is required for small animals.

A1.4 Acknowledgements

The authors would like to thank Dr. Peiman Hemmati (Department of Medicine, University of Wisconsin-Madison) for generously providing the H1 MSCs, and Dr. Tim Hacker, Dr. Gouqing Song and Ms. Jill Koch of the University of Wisconsin Cardiovascular Physiology Core Facility for performing mouse surgeries. This work was supported by the National Science Foundation through a Graduate Research Fellowship to Brian Freeman and NIH R21 HL089679.

A1.5 References

1. Bernirschke, K.K., P. Pathology of the Human Placenta. Springer, New York, (2000).
2. Hoshina, M., Boothby, M., & Boime, I. Cytological localization of chorionic

gonadotropin alpha and placental lactogen mRNAs during development of the human placenta. J. Cell. Biol. 93, 190-198 (1982).

3. Johansen, M., Redman, C.W., Wilkins, T., & Sargent, I.L. Trophoblast deportation in human pregnancy--its relevance for pre-eclampsia. Placenta. 20, 531-539 (1999).
4. Redman, C.W. & Sargent, I.L. Placental debris, oxidative stress and pre-eclampsia. Placenta. 21, 597-602 (2000).
5. Ogle, B.M., et al. Spontaneous fusion of cells between species yields transdifferentiation and retroviral transfer in vivo. FASEB. J. 18, 548-550 (2004).
6. Nygren, J.M., et al. Bone marrow-derived hematopoietic cells generate cardiomyocytes at a low frequency through cell fusion, but not transdifferentiation. Nat. Med. 10, 494-501 (2004).
7. Nygren, J.M., et al. Myeloid and lymphoid contribution to non-haematopoietic lineages through irradiation-induced heterotypic cell fusion. Nat. Cell. Biol. 10, 584-592 (2008).
8. Kutschka, I., et al. Adenoviral human BCL-2 transgene expression attenuates early donor cell death after cardiomyoblast transplantation into ischemic rat hearts. Circulation. 114, I174-180 (2006).
9. Min, J.J., et al. In vivo bioluminescence imaging of cord blood derived mesenchymal stem cell transplantation into rat myocardium. Ann. Nucl. Med. 20, 165-170 (2006).
10. Malstrom, S.E., Tornavaca, O., Meseguer, A., Purchio, A.F., & West, D.B.

The characterization and hormonal regulation of kidney androgen-regulated protein (Kap)-luciferase transgenic mice. Toxicol. Sci. 79, 266-277 (2004).

11. Weir, L.R., et al. Biophotonic imaging in HO-1.luc transgenic mice: real-time demonstration of gender-specific chloroform induced renal toxicity. Mutat. Res. 574, 67-75 (2005).
12. Rajashekara, G., Glover, D.A., Banai, M., O'Callaghan, D., & Splitter, G.A. Attenuated bioluminescent Brucella melitensis mutants GR019 (virB4), GR024 (galE), and GR026 (BMEI1090-BMEI1091) confer protection in mice. Infect. Immun. 74, 2925-2936 (2006).
13. Kadurugamuwa, J.L., et al. Noninvasive biophotonic imaging for monitoring of catheter-associated urinary tract infections and therapy in mice. Infect. Immun. 73, 3878-3887 (2005).
14. Ryan, P.L., Youngblood, R.C., Harvill, J., & Willard, S.T. Photonic monitoring in real time of vascular endothelial growth factor receptor 2 gene expression under relaxin-induced conditions in a novel murine wound model. Ann. N.Y. Acad. Sci. 1041, 398-414 (2005).
15. Zhu, L., et al. Non-invasive imaging of GFAP expression after neuronal damage in mice. Neurosci. Lett. 367, 210-212 (2004).
16. Noiseux, N., et al. Mesenchymal stem cells overexpressing Akt dramatically repair infarcted myocardium and improve cardiac function despite infrequent cellular fusion or differentiation. Mol. Ther. 14, 840-850 (2006).
17. Ajiki, T., et al. Composite tissue transplantation in rats: fusion of donor muscle to the recipient site. Transplant. Proc. 37, 208-209 (2005).

18. Trivedi, P. & Hematti, P. Derivation and immunological characterization of mesenchymal stromal cells from human embryonic stem cells. Exp. Hematol. 36, 350-359 (2008).

19. Ogle, B.M., Cascalho, M., & Platt, J.L. Biological implications of cell fusion. Nat. Rev. Mol. Cell. Biol. 6, 567-575 (2005).

20. Collins, T.J. ImageJ for microscopy. BioTechniques. 43, 25-30 (2007).

A2. Single-cell RNA-seq of bone marrow-derived mesenchymal stem cells reveals unique profiles of lineage priming

Elements of this work have been published as:

Freeman BT, Jung PJ, Ogle BM. Single-cell RNA-seq of murine bone-marrow mesenchymal stem cells reveals unique profiles of lineage priming. ***PLoS ONE*****, 10(9): e0136199. doi:10.1371/journal.pone.0136199. 2015.**

A2.1 Abstract

The plasticity and immunomodulatory capacity of mesenchymal stem cells (MSCs) have spurred clinical use in recent years. However, clinical outcomes vary and many ascribe inconsistency to the tissue source of MSCs. Yet unconsidered is the extent of heterogeneity of individual MSCs from a given tissue source with respect to differentiation potential and immune regulatory function. Here we use single-cell RNA-seq to assess the transcriptional diversity of murine mesenchymal stem cells derived from bone marrow. We found genes associated with MSC multipotency were expressed at a high level and with consistency between individual cells. However, genes associated with osteogenic, chondrogenic, adipogenic, neurogenic and vascular smooth muscle differentiation were expressed at widely varying levels between individual cells.

Further, certain genes associated with immunomodulation were also inconsistent between individual cells. Differences could not be ascribed to cycles of proliferation, culture bias or other cellular process, which might alter transcript expression in a regular or cyclic pattern. These results support and extend the concept of lineage priming of MSCs and emphasize caution for *in vivo* or clinical use of MSCs, even when immunomodulation is the goal, since multiple mesodermal (and even perhaps ectodermal) outcomes are a possibility. Purification might enable shifting of the probability of a certain outcome, but is unlikely to remove multilineage potential altogether.

A2.2 Introduction

Mesenchymal/multipotent stem/stromal cells (MSCs) are utilized in stem cell therapy for treatment of a variety of diseases including myocardial infarction, cancer, lung fibrosis, spinal cord injury, bone and cartilage repair, and muscular dystrophy(1-4). MSCs are clinically beneficial due in part to the ability to home to sites of injury(5, 6), differentiate to mesenchymal cell types, suppress immune responses(7) and modulate angiogenesis(8-10). In addition, MSCs are easy to isolate and expand and can be derived from multiple different tissue sources including bone-marrow, fat, placenta, synovium, periosteum, and tooth(2).

The large variety of tissue sources and species from which MSCs can be isolated have spurred efforts to characterize and compare each MSC isolate. The approach has been to identify a protein marker, or series of markers unique to MSCs and then to validate multipotency via differentiation protocols. For

example, human MSCs are typically isolated from bone-marrow by selecting for adherent cells then confirming expression of $CD73^{+}/CD90^{+}/CD105^{+}/CD34^{-}/CD14^{-}/CD19^{-}/CD45^{-}$ for MSC characterization(11). Use of the entire panel is inconsistent, as are the subsets selected by individual investigators(12, 13). A similar trend occurs with isolation and characterization of murine MSCs derived from bone marrow. In this case, more than thirty different surface markers have been used with varying subsets over the past 15 years(14). It is challenging to determine whether subset selection indicates an assumption by investigators that each subset reflects the whole or that a given isolate does not in fact express certain markers. But we do know that inconsistent use of MSC biomarkers to isolate “pure” populations can lead to variable levels of differentiation potential and ability to self renew(15, 16).

More perplexing is the fact that *consistent* use of biomarkers, can also lead to variable *in vitro* and *in vivo* outcomes between research groups. For example, murine bone marrow-derived MSCs sorted via immunodepletion of CD11b and CD45 for treatment of acute lung injury showed increased survival across studies but associated mechanisms were varied and sometimes contradictory(17-20). Gupta et al., showed elevation of IL-10 and no change in neutrophil infiltration relative to controls(18), while Xu et al., showed no change in IL-10 production, but a decrease in neutrophil infiltration(17). In addition, retention of water in the lungs was significantly decreased only after 48 hours in the study by Gupta et al., while in Xu et al., water retention was only observed at 24 hours and lost by 48. Some of this variation has been attributed to age or

disease of the organism at the time of MSC isolation(21). More likely however, is the fact that a handful of proteins cannot adequately describe the varied members of MSCs between species, between tissues and even perhaps between cells of a given population. Advanced molecular approaches including microarray(22), qPCR(23) and RNAseq(12, 13, 24-29) have allowed extensive characterization of 100s to 10,000s of transcripts of MSC populations. Results of these studies suggest heterogeneity of MSC populations could be ascribed to populations containing a varied mixture of undifferentiated MSCs primed(12, 30) for multiple pathways. Lineage priming has been observed with hematopoietic stems cells using single cell RT-PCR(31) and microarray(32, 33). Transcription factors from both erythroid and myeloid differentiation pathways were expressed at a variety of levels in hematopoietic stems cells, suggesting that these stem cells could differentiate effectively down either pathway. Delorme et al., proposed that a similar process might occur with MSCs, but the study was conducted on clonal populations using qPCR and therefore a limited number of transcripts(12).

Until recently, cell-by-cell, whole-transcriptome analysis of MSCs has not been possible. However, advances in microfluidics and small volume cDNA synthesis now allow single-cell RNA-seq of individual MSCs(34). Using this approach we find that individual MSCs exhibit multilineage priming, but priming is not uniform and appears to favor one and sometimes two lineages even while maintaining multipotency. In addition, a limited, but measureable degree of heterogeneity is observed in expression of genes associated with

immunomodulation in the absence of immune stimulation. These results point to an as yet unappreciated source of heterogeneity of MSCs from a single tissue source.

A2.3 Materials and Methods

A2.3.1 Cell Culture

Mouse bone marrow mesenchymal stem cells (mMSCs) were purchased (3 month-old male C57BL mice, Georgia Reagents University, Augusta, GA, all procedures approved by the Institutional Care and Use Committee, Medical College of Georgia(35)) and expanded and cultured as previously described(36). Briefly, MSCs were cultured on a 0.1% gelatin (Sigma Aldrich, St. Louis, MO) pretreated flask containing α-minimum essential medium (MEM) complete. Complete alpha-MEM consisted of α-MEM (Invitrogen, Carlsbad, CA), 10% fetal bovine serum (Hyclone, Logan, UT), 0.1 mM nonessential amino acids (Invitrogen), and 2 mM L-glutamine (Invitrogren). MSC cultures were allowed to grow to 60-70% confluence and were replated at a concentration of 1,500 cells/cm^2. Experiments were performed using passages 6 – 11 for mMSCs. As a control, HL-1 cardiomyocytes (HL-1cm) (a gift of Dr. William Claycomb) were also expanded and cultured as previously described(37). All cultures were maintained at 37°C in 5% CO_2.

A2.3.2 Single-cell Capture and RNA-seq

mMSCs were trypsinized and suspended in phosphate buffered saline (PBS). The mMSCs were centrifuged and resuspended in 5 μL of complete alpha-MEM medium for addition to the capture chip. mMSCs were captured on a large-sized (17-25 μm cell diameter) chip using the Fluidigm C1 system. Cells were loaded into the chip at approximately 2000 cells/μL and stained for viability (DEAD cell viability assay; Molecular Probes, Life Technologies, Grand Island, NY) and imaged with phase-contrast and fluorescence microscopy to confirm cell number and viability at each capture point. mMSCs and the HL-1cm controls were captured in the same Fluidigm C1 device with the HL-1cm labled with a green cytoplasmic dye (1 μm CellTracker Green CMFDA, Molecular Probes, Eugene, OR). 16 single, live mMSCs and 5 single, live HL1cm were selected for analysis. Once cells were captured in the device, cDNAs were prepared from each cell on the chip using the SMARTer Ultra Low RNA kit for Fluidigm C1 System (Clontech, Mountain View, CA). RNA spike-in Mix (Ambion, Life Technologies) was added to the lyses reaction and processed with cellular mRNA. mRNA library was constructed using the Illumina Nextera XT preparation kit (Illumina, San Diego, CA) according to the manufacturer's protocol and sequenced on the Illumina MiSeqv3 using paired end reads with a length of 75 bp to a depth of 18 to 22 million reads with the Multiplex on one MiSeq lane to create *.fastq files. A bulk population RNA control of both mMSCs and HL-1cm was run in parallel to the single-cell samples.

A2.3.3 Gene Expression Analysis

Gene expression analysis was performed with Galaxy software (Minnesota Supercomputing Institute (MSI), University of Minnesota, Minneapolis, MN). Reads were processed and aligned to the mouse reference genome (mm10_genes_2012_05_23.gtf and canonical_mm10.fa) using Tophat (version 2.0.12, open source software, http://ccb.jhu.edu/software/tophat/index.shtml)(38). The default options supplied with the software were used and the aligned read files produced by Tophat were processed using Cufflinks software (version 2.2.1, open source software, http://cole-trapnell-lab.github.io/cufflinks/), for further analysis, including assembling transcripts, estimating their abundance, and testing for the differential expression between single-cell RNA-seq samples(38). Read counts were normalized to fragments per kilobase of exon per million mapped reads (FPKM) according to the gene length and total mapped reads. Genes with a $\log_2$ fold change greater than 1 from the control cells to the fusion products and had a *P* value of less than 0.05 were considered “differentially expressed” and further analyzed for gene ontology. Gene ontology and Kyoto Encyclopedia of Genes and Genomes (KEGG) pathway enrichment analyses were performed with DAVID informatics resources 6.7 of the National Institute of Allergy and Infectious Diseases (NIAID) and of the National Institutes of Health (NIH)(39, 40).

A2.3.4 Gene cluster analysis

Average linkage hierarchical clustering of gene expression intensity was performed using the Pearson distance to measure distance between gene and single cells. SingulaR (Fluidigm, San Francisco, CA) was used to compute and create the hierarchal clustering and principle component analysis plots.

A2.3.5 Statistical Analysis

Data were analyzed with Microsoft Excel (Microsoft, Redmond, WA, USA). RNA-seq data was analyzed with the Cuffdiff or SingulaR programs.

A2.3.6 Quantitative real-time polymerase chain reactions (qRT-PCR)

Complementary DNA (cDNA) was synthesized following the instructions from the Maxima First Strand cDNA Synthesis Kit (cat# K1642, Thermo Scientific). The cDNA was amplified from the cDNA from the single-cell reaction performed in the Illumina chip. Primers of qRT-PCR were purchased from Biorad (Hercules, CA) and the sequence of *Gapdh* primers (FOR: CATGGCCTTCCGTGTTCCTA, REV: CCTGCTTCACCACCTTCTTGAT) was obtained from (41). Primer efficiencies were extracted from RealPlex^2 software and verified with melting curves. The comparative C_t method(42) was employed to determine the relative changes in gene expression. For comparison to the single-cell RNA-seq results, each gene's FPKM values were normalized to each cells *Gapdh* FPKM value, which was then normalized to the control cells.

A2.4 Results

A2.4.1 Bone marrow-derived mMSCs express genes associated with MSC multipotency

To begin characterization of the transcriptome of bone marrow-derived MSCs, sixteen mouse mesenchymal stem cells (mMSC1-mMSC16) were individually sequenced using single-cell RNA-seq. Also, a population control (PC) containing thousands of cells (mMSC-PC) were sequenced in parallel with the single cells. Next, a gene set was assembled that included published markers indicative of MSC multipotency. Hierarchal clustering (HC) and principal component analysis (PCA) analysis were then conducted using this gene set. HL-1 cardiomyocytes (HL1cm) were used as a negative control for this analysis and *Gapdh* was used to represent basal expression of a housekeeping gene. The mMSCs all clustered together far from the HL-1cm controls (**Figure A2-1A and A2-1B**). Of note, all mMSCs and mMSC-PC exhibited high expression of MSC stemness-associated markers previously shown to be upregulated in mouse MSCs (*Ly6a*, *Cd9, Cd44, Sdc4, Lamp2)* and low expression of MSC stemness-associated markers previously shown to be downregulated in mouse MSCs (*Anpep, Itgam, Eng, Nt5e, Pecam1, Nanog)(14)*. In addition, mMSCs exhibited inconsistent expression of markers reported to have variable expression in mMSCs (*Pdgfra, Cd80, Cd34, Tfrc)(14)*. The HL1cm control cells expressed MSC markers at a much lower level, but with similar levels of *Gapdh* expression, demonstrating the specificity of the gene set for mMSCs. RNA-seq data was confirmed with qPCR analysis of *Ly6a* showing similar relative

expression between mMSCs and low expression in the HL1cm control (**Figure A2-1C**).

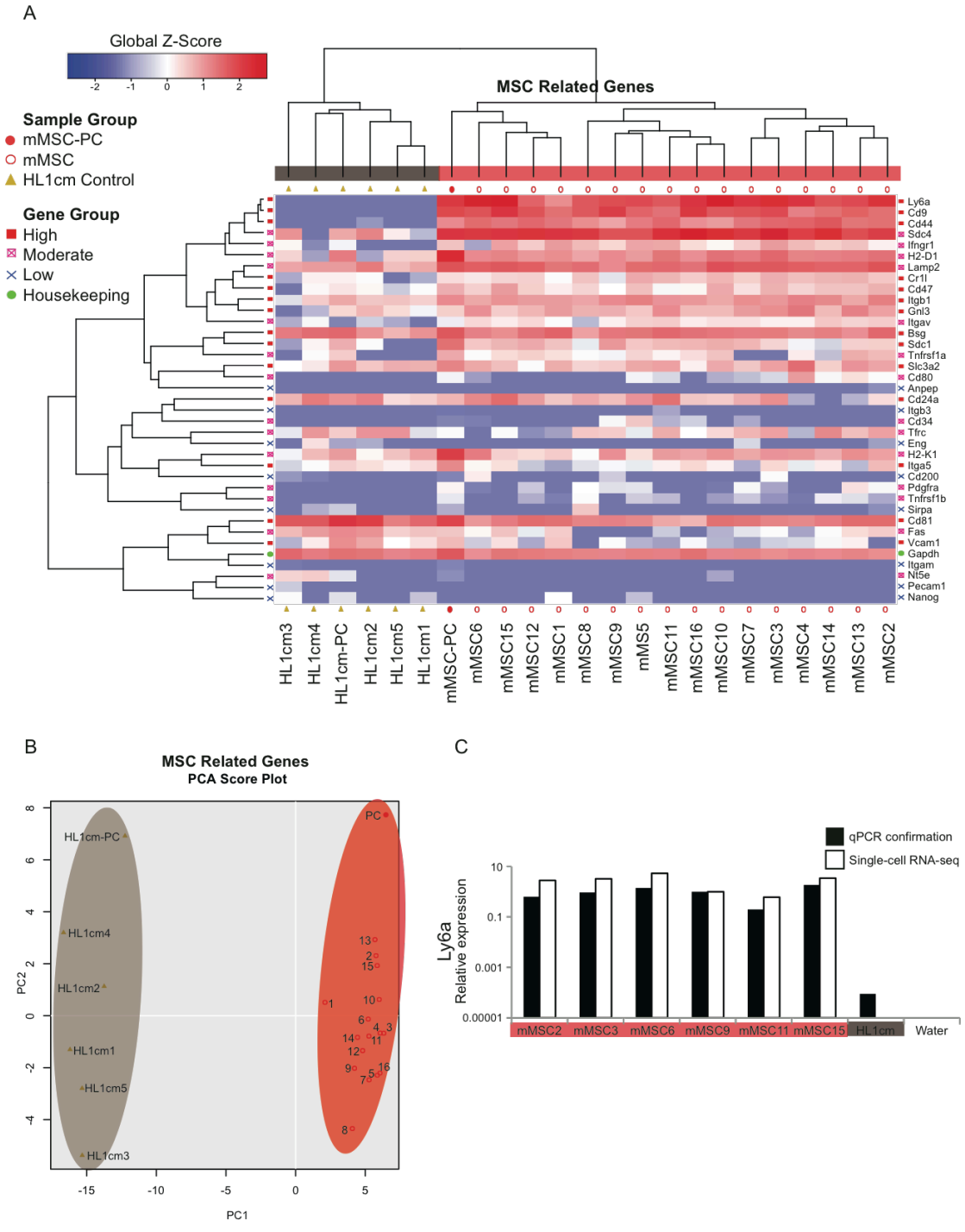

Figure A2-1. Single-cell mMSCs express genes associated with MSC multipotency **A.** Hierarchal clustering (HC) of mMSCs for a set of genes related to MSC multipotency. Genes are organized either by genes expressed highly in mMSCs (red), genes expressed moderately/heterogeneously in mMSCs (pink), genes that are lowly expressed in mMSCs (blue) or housekeeping genes (green). Global Z-Score reflects the number of standard deviations away from the mean of expression in the reference. **B.** Principal component analysis (PCA) analysis of single cell mMSCs (1-16) (red), negative control single cells (HL1cm1-HL1cm5) (brown), and population controls (PC and HL1cmPC). **C.** Quantitative reverse transcriptase polymerase chain reaction (qPCR) confirmation of RNA-seq data.

A2.4.2 Multilineage priming of individual bone marrow-derived mMSCs

To determine whether differentiation potential could account, at least in part, for varied *in vivo* outcomes, we generated gene sets corresponding to mesenchymal specification. The gene list included early stage (e.g. transcription factors) and late stage (e.g. functional proteins) markers for osteogenic, chondrogenic, adipogenic, vascular smooth muscle and neurogenic lineages. Using this set, HC and PCA analyses were conducted on single-cell mMSCs and the mMSC-PC (**Figure A2-2A through A2-2C**). The mMSC-PC control correlated with the average of the single mMSCs supporting the accuracy of the single-cell data. In addition, the population control contained transcripts corresponding to early and late markers of multiple lineages at variable levels, a finding perhaps attributable to the mixing of multiple lineage-committed or lineage-primed populations. The profile of the mMSC-PC control was similar to that of each single-cell mMSC (**Figure A2-2A**). Individual mMSCs did not express markers of a single lineage, but instead showed expression of early

stage markers of at least three differentiation pathways *simultaneously* (**Figure A2-2E** and **Figure A2-3**). Since it was previously established that all mMSCs used in this study were still expressing high levels of multipotency-associated genes (**Figure A2-1A and A2-1B**), this was quite surprising. The separation of individual MSCs in the PCA plot was due to variable expression of genes from all five lineages. Cells at the top of the PCA score plot had higher levels of a few osteogenic (*Ogn* and *Wisp2*) and adipogenic (*Fabp4* and *Cebpb*) markers, cells on the right had higher levels of vascular smooth muscle markers (*Acta2, Cnn1* and *Tagln*), *Tubb* (neurogenic), *Slco2a1* and *Angptl4* (most often associated with adipogenesis) (**Figure A2-2C**). In an attempt to more easily visualize the varied linage propensities of individual mMSCs, one key transcription factor for each lineage (*Runx2, Sox9, Cebpb, Gata6* and *Nr4a2*) was selected and normalized to *Gapdh* expression for all sixteen cells and the population control (**Figure A2-2E**). The population control revealed a similar profile to that seen for the clonal populations of the Delorme study(12), but surprisingly each individual mMSCs exhibited much more varied profiles. Seven of the sixteen mMSCs expressed all five transcription factors, six mMSCs expressed four of the transcription factors and three mMSCs expressed three of the transcription factors. These data were confirmed with qPCR of a gene highly expressed in all mMSCs (*Ly6a*) (**Figure A2-1C)** and a gene with high variability of expression in individual mMSCs (*Fabp4*) (**Figure A2-2D**).

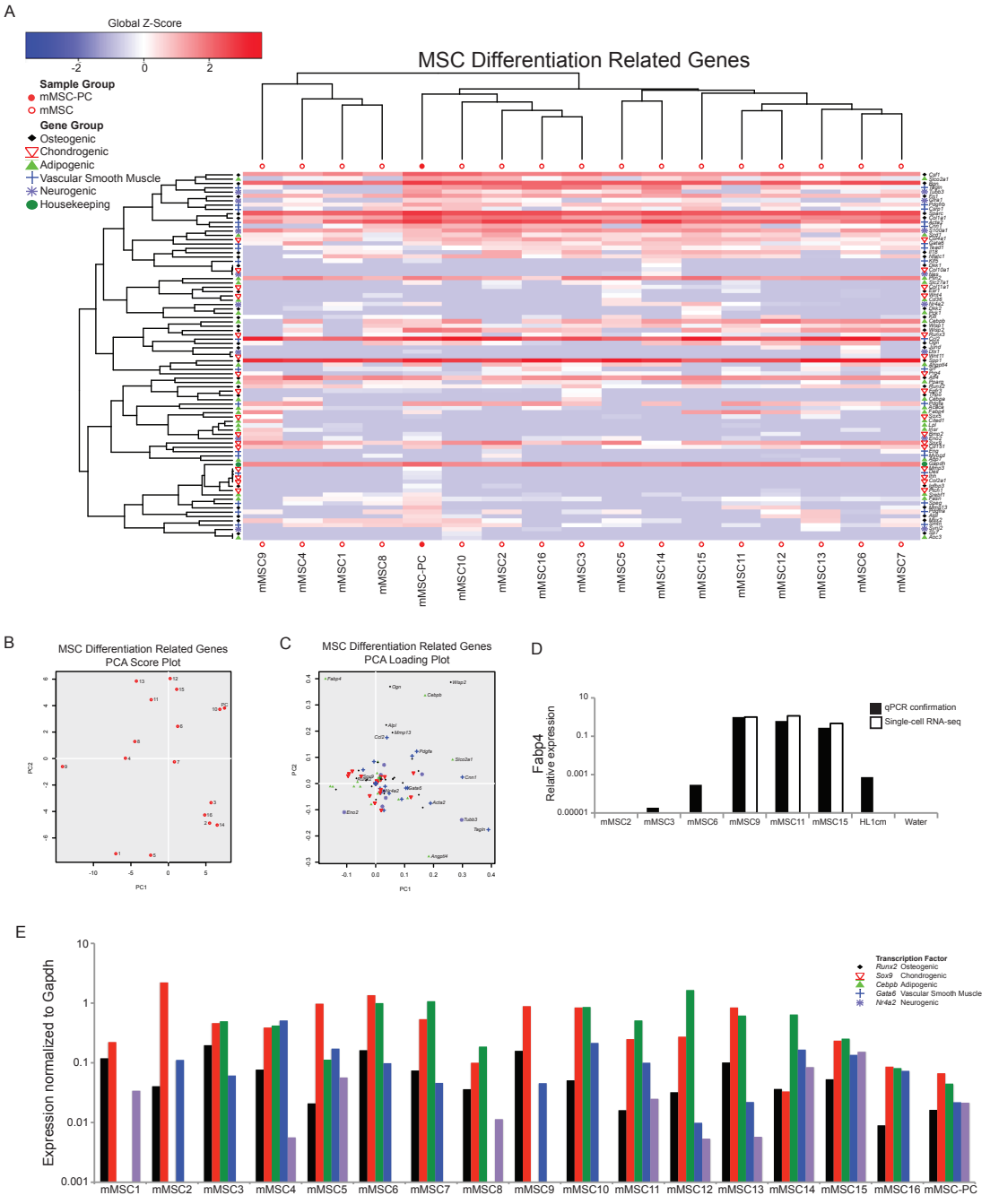

Figure A2-2. Individual mMSCs express genes from multiple differentiation pathways. A. HC of single cell mMSCs and mMSC population control (mMSC-PC) for a set of genes related to osteogenesis, chondrogenesis, adipogenesis, vascular smooth muscle, neurogenesis, and housekeeping genes. **B.** PCA analysis of single cell mMSCs (1-16) and population control (PC). **C**. PCA loading plot showing individual differentiation genes represented in **B**. **D.** qPCR confirmation of RNA-seq data. **E.** A key transcription

factor was selected for each differentiation lineage and expression was normalized to *Gapdh* for each sample.

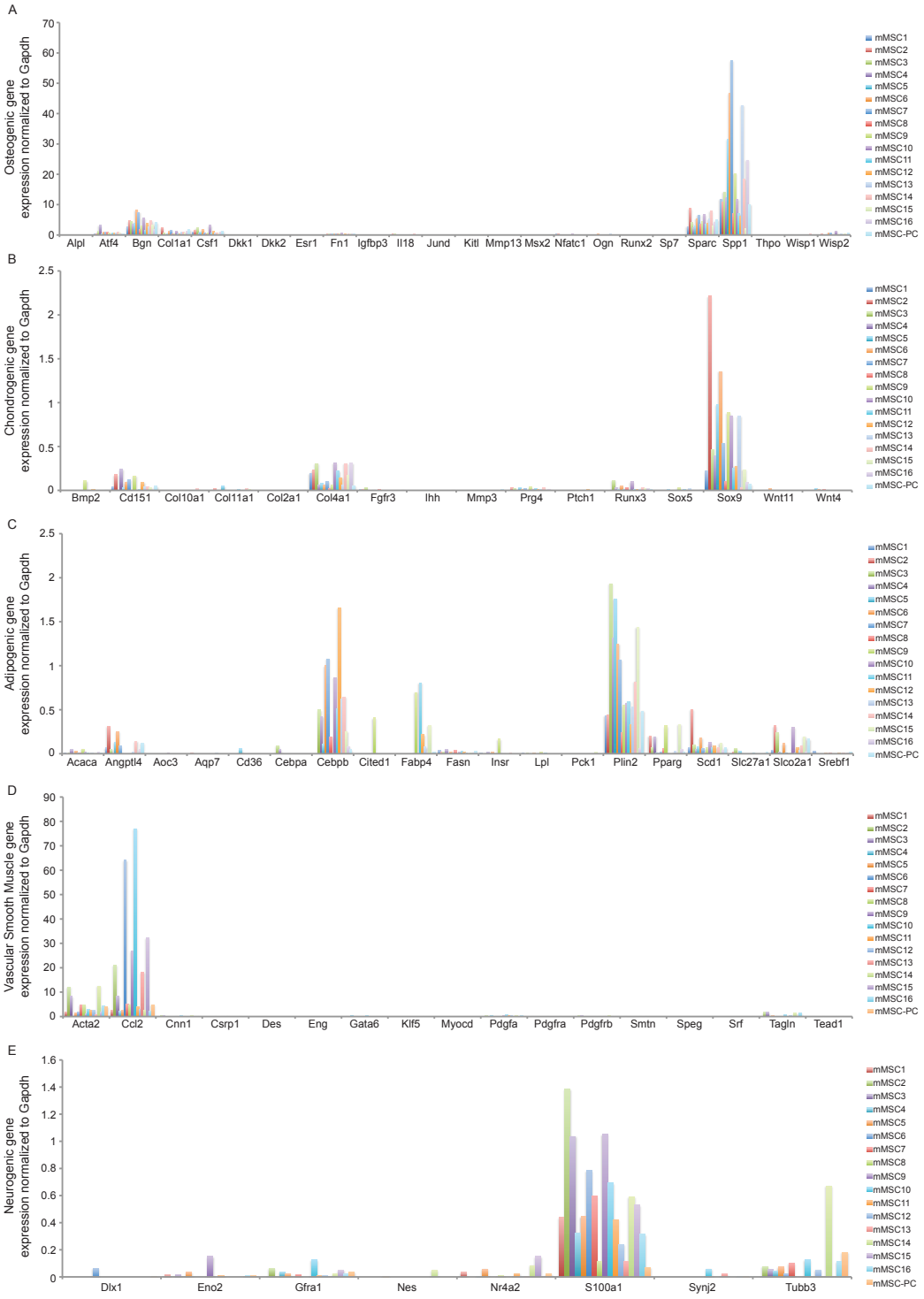

Figure A2-3. Expression of each lineage gene normalized to *Gapdh*. A. Osteogenic gene profile. **B.** Chondrogenic gene profile. **C**. Adipogenic gene profile. **D**. Vascular smooth muscle gene profile. **E**. Neurogenic gene profile

A2.4.3 Basal immunomodulatory capacity of individual bone marrow-derived mMSCs

To determine whether basal immunomodulatory capacity could also account for varied MSC behavior *in vitro* and *in vivo*, we generated a gene set containing soluble, immunoregulatory factors known to be produced by MSCs *in vitro* and *in vivo* (**Figure A2-4A**). Individual cells were largely the same with the exception of *Il6* expression. Indeed variability in the expression of this gene accounted almost solely for the population spread on the PCA score plot (**Figure A2-4B, A2-4C**). The significance of this difference was further probed via global analysis of differentially expressed genes.

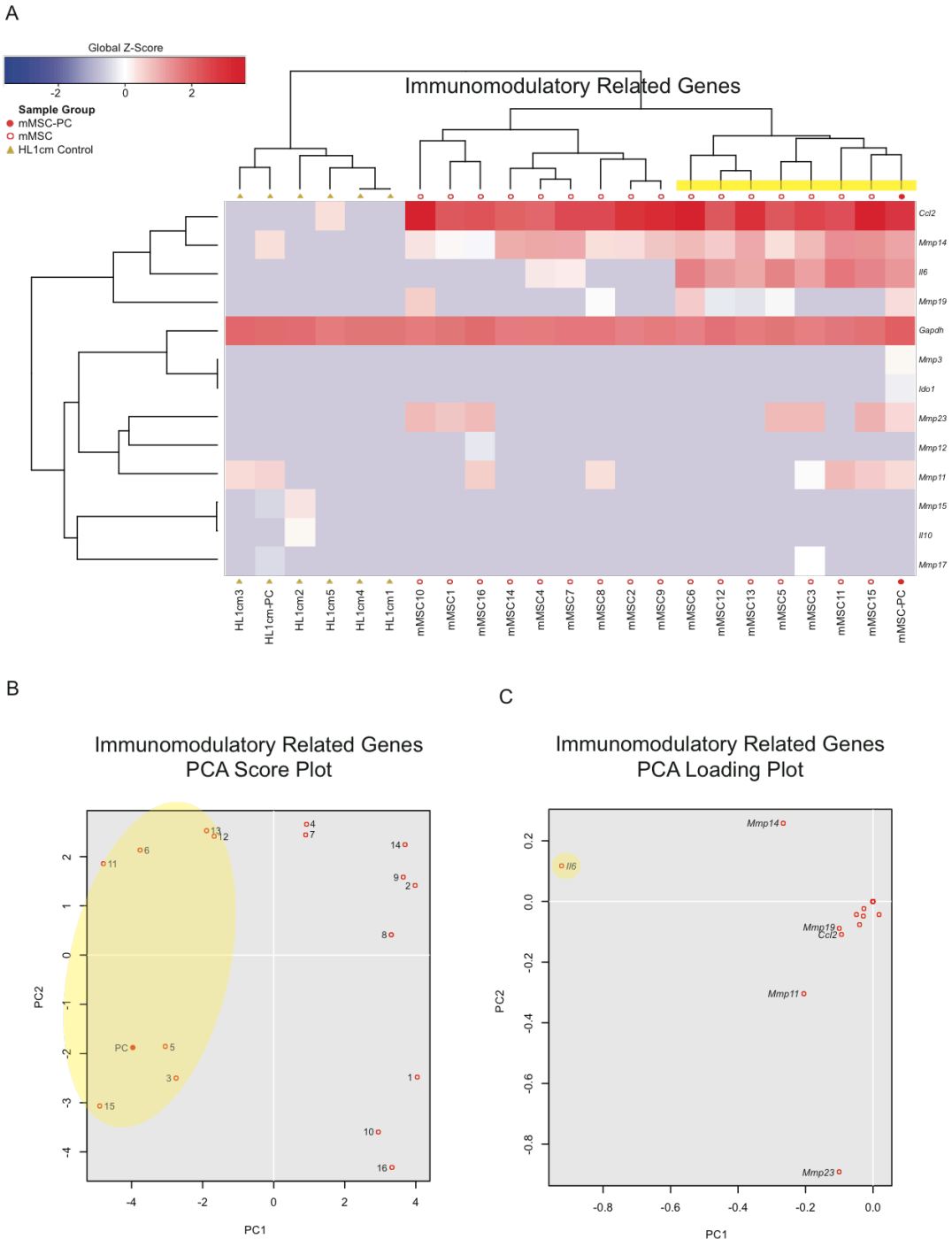

Figure A2-4. **Single cell mMSCs exhibit minimal but measureable differences in expression of immunomodulatory genes. A.** HC of single cell mMSCs, negative control single cells (HL1cm1-5), and population controls (mMSC-PC and HL1cmPC) for a set of genes related to immunomodulatory function. **B.** PCA analysis of single cell

mMSCs (1-16) and population control (PC). **C**. PCA loading plot showing individual differentiation genes represented in **B**. *Il6* expressing cells clustered together (yellow).

A2.4.4 Transcriptome Heterogeneity of mMSCs

To more comprehensively delineate differences in the transcriptome that might augment findings related to lineage priming and support/refute subtle differences in immunomodulatory function, we identified all differentially expressed genes between each mMSC as well as the population control. Differential expression was defined as a $\log_2$ fold change of greater than 1 and a *P* value below 0.05. Over 9,000 differentially expressed genes were identified and displayed using HC (**Figure A2-5A**) and PCA score plot (**Figure A2-5B**). Results indicate global heterogeneity of single mMSCs arguably expected of mesenchymal progenitors (**Figure A2-5A and A2-5B).** Despite the heterogeneity, five different clusters emerged and are designated with different color labels. At first glance, we suspected clusters might represent different types and levels of lineage commitment of mesenchymal progenitors. To test this possibility, gene ontology analysis was conducted on the differentially expressed genes to determine whether each cluster aligned with specific mesenchymal differentiated cell types (e.g., osteogenic, adipogenic, chondrogenic).

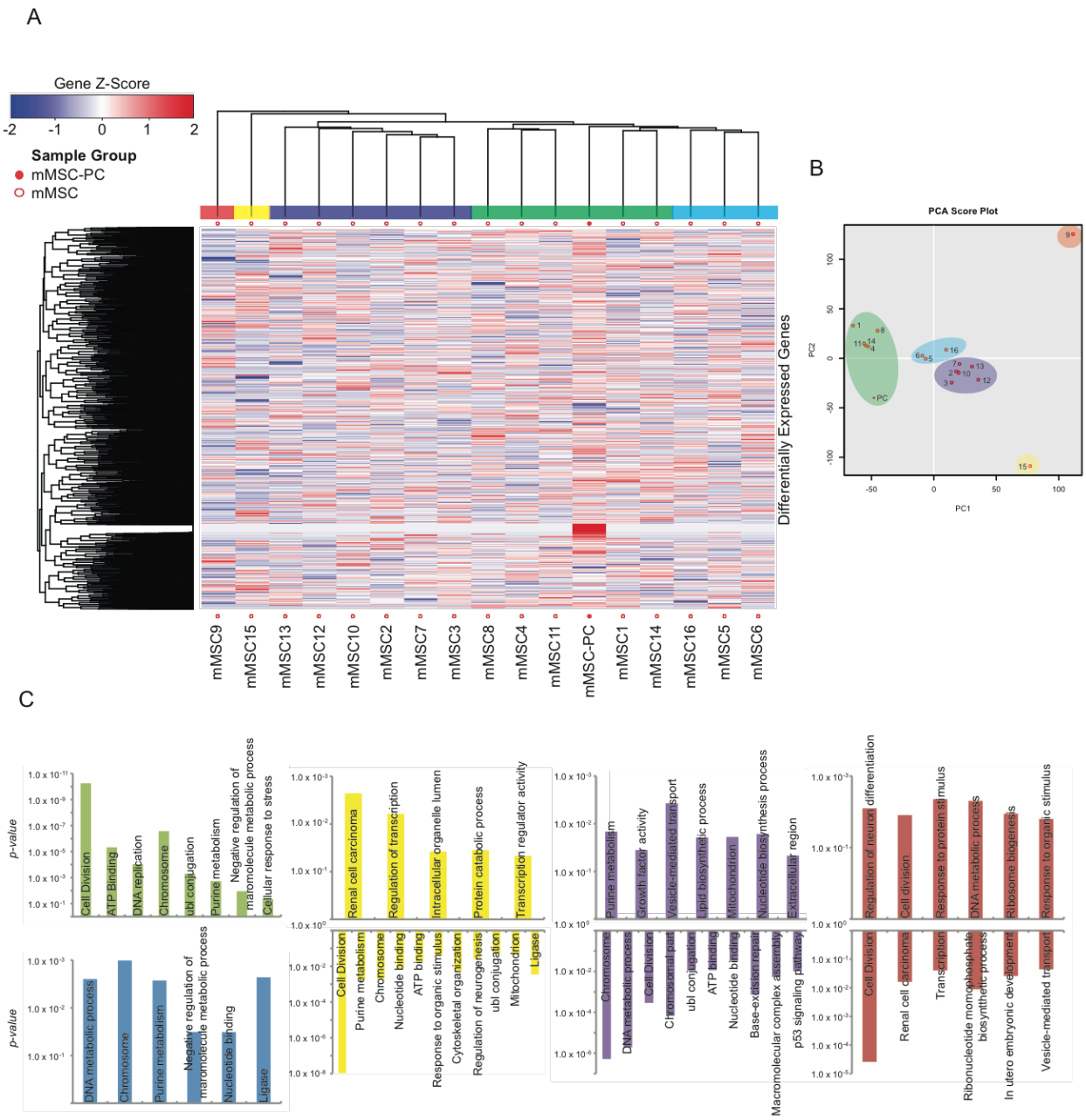

Figure A2-5. HC and PCA of mMSCs show transcriptome heterogeneity and gene ontology of subpopulations. A. A global view of differential gene expression between single cell mMSCs and the population control (mMSC-PC). Gene Z-Score reflects the number of standard deviations away from the mean of expression in the reference. **B.** PCA analysis of single cell mMSCs (1-16) and population control (PC). **C.** Gene onotology of five subpopulations of single-cell mMSCs (green, blue, yellow, purple and red clusters). Ontology groups are plotted with the *P* value on the y-axis. Upregulated

groups have bars extending in the positive y-direction and down regulated groups have bars extending in the negative y-direction.

DAVID bioinformatics resource was utilized to define function-related gene groups associated with each cluster of MSCs. Differentially expressed genes were isolated for each cluster of MSCs and separated according to up- or down-regulation. The significance of each concentrated gene group was plotted on a negative log scale with upregulated gene groups extending upward and downregulated gene groups extending downward (**Figure A2-5C**). Only gene groups with a *P* value below 0.05 were included in the graph and surprisingly only one was related to differentiation. The first cluster (green) contained upregulation of genes involved in cell division, ATP binding, DNA replication, and chromosomes which suggests that this cluster of five cells (along with the population control) was in active proliferation at the time of cell capture. The ratio of cells (5 of 16, ~30%) matches our data and literature reports of the percentage of cells actively dividing in a healthy population of bone marrow-derived MSCs(43). The blue cluster showed upregulation of genes associated with DNA metabolic process, chromosomes, purine metabolism and nucleotide binding. The blue cluster did not contain genes upregulated with cell division, but these three cells do appear to be preparing DNA for future division. The cell of the yellow cluster (mMSC15) upregulated genes associated with regulation of transcription and protein catabolic process, while downregulating genes associated with cell division and regulation of neurogensis. The purple cluster also downregulated genes linked to cell division, but upregulated genes involved with growth factor activity, vesicle-mediated transport, lipid biosynthetic process

and the extracellular region. This cluster could perhaps represent active paracrine signaling corresponding to the immunomodulatory capacity of MSCs. If active paracrine signaling is defined as augmented *Il6* production (**Figure A2-4,** mMSC 3, 6, 5, 11, 12, 13, 15), then there is an insignificant relationship between active paracrine signaling and association with the purple cluster (Chi-square statistic 0.15, $P = 0.70$). Though a relationship with similar strength exists between proliferation and downregulation of *Il6* (Chi-square statistic 2.14, $P = 0.14$). Instead, the purple cluster could represent a subpopulation of mMSCs with advanced commitment to adipogenesis, since this cluster also shows an upregulation of the lipid biosynthetic process. However, cross reference of cells of this group (mMSC2, 3, 7, 10, 12 and 13) to the differentiation analysis (**Figure A2-2A** and **A2-2B**), shows each falls in different regions of the PCA plot suggesting they each have unique lineage priming, not significantly tending toward adipogenesis. The cell of the red cluster (mMSC 9) showed an unexpected upregulation of genes involved with the regulation of neuronal differentiation and ribosome biogenesis, suggesting priming for neurogenesis which has been reported in isolated instances for MSCs(44-46). In sum, mMSCs clusters primarily correspond to proliferating cells (green and blue clusters) and quiescent cells (yellow, purple and red clusters). Importantly proliferation status does not correlate with the level or number of lineage commitment or immune regulatory genes expressed per cell.

A2.5 Discussion

In this study the transcriptomes of individual, bone marrow-derived mMSCs were analyzed via RNA-seq. Using this approach, a new perspective on the heterogeneity of MSCs emerges. First, MSCs were found to express varied levels of early markers of multiple mesenchymal lineages extending the definition of lineage priming of this unique cell type. Importantly, differences in level or number of lineage commitment genes expressed did not correlate with proliferation or other cellular process, which might alter transcript expression in a regular or cyclic pattern. Second, basal expression of genes associated with immunomodulation were quite uniform aside from *Il6* in gene set analyses and categories related to immunomodulation did not emerge from ontology analyses suggesting cell-to-cell variation for immunomodulation is present but less pronounced than lineage commitment.

Since there was no clear functional clustering of the mMSCs based on gene ontology (aside from proliferating/nonproliferating), we also scanned for gene markers that could be used to represent the clustered populations (**Figure A2-2**) and perhaps correspond to lineage priming. A previous report on mouse MSCs subpopulations found that *Cd200* expression level indicated osteogenic potential and *Pdgfra* expression indicated adipogenic potential(14). However, mMSC3, mMSC6, and mMSC9 were the only mMSCs with detectable *Cd200* expression and indeed these three mMSCs did not cluster in either the global analyses (**Figure A2-5**) or gene list analyses with markers of differentiation (**Figure A2-2**). *Pdgfra* expression also failed to aid clustering of the eleven mMSCs that had detectable expression (mMSC2, 3, 5, 6, 7, 8, 9, 10, 12, 13, 14).

The discrepancy between our work and previous reports suggests an environmental trigger was necessary to promote particular cell fates and therefore that marker expression alone (at least in these two cases) is not enough to predict single cell propensities. We also note, based on the results presented here, that inter-lineage plasticity is likely very high. And that, even if an MSC "commits" to a particular lineage, conversion to another might not entail the set up of whole molecular programs, but instead upregulation of a few components(47).

Of note, one cell upregulated expression of neurogenic transcript for *Eno2*. This is not the first report of an MSC expressing transcripts considered specific to ectodermal lineage. In multiple reports Foudah *et al.* demonstrate that neuronal makers *Tubb* and *NeuN* are spontaneously expressed by a high percentage of undifferentiated MSCs from multiple tissues from both human and rat(44-46). Thus, while the relative fraction of MSCs capable of expressing early transcripts of neurogenesis and of giving rise to bona fide neurons is not known, single cell analysis suggests plasticity to this lineage may be possible.

A2.6 Conclusions

In sum, this study confirms and augments the concept of multi-lineage priming of MSCs by showing that MSCs typically express early (and sometimes even late) markers of more than one mesenchymal lineage *simultaneously*. Moreover, expression levels are quite distinct between cells, suggesting MSCs,

despite being primed to multiple fates, might prefer one fate over the other. In other words, even if an MSC is environmentally triggered for one lineage, it might easily be switched if even a weak signal comes along for the preferred lineage. Immunomodulation of MSCs on the other hand, appears to be relatively consistent between cells of a given population. Even so, these results emphasize caution for *in vivo* or clinical use of MSCs, even when immunomodulation is the goal, since multiple mesenchymal (and even perhaps ectodermal) outcomes are a possibility. Purification might enable shifting of the probability of a certain outcome, but can never remove multilineage potential altogether.

A2.7 Acknowledgements

We thank Kenneth Beckman, Adam Hauge and Jerry Daniel of the University of Minnesota Genomics Center for technical assistance with the single-cell capture, cDNA preparation and RNA-seq, and Josh Baller and John Garbe of the Minnesota Supercomputing Institute at the University of Minnesota-Twin Cities for assistance with analysis of RNA-seq data. The present study was supported by the NIH (award HL089679), National Science Foundation Graduate Research Fellowship Program (NSF-GRFP 2010105691), National Science Foundation (CAREER, award 0844537).

A2.8 References

1. Barry FP, Murphy JM. Mesenchymal stem cells: clinical applications and biological characterization. The international journal of biochemistry & cell biology. 2004 Apr;36(4):568-84. PubMed PMID: 15010324.
2. Deans RJ, Moseley AB. Mesenchymal stem cells: biology and potential clinical uses. Experimental hematology. 2000 Aug;28(8):875-84. PubMed PMID: 10989188.
3. Ren G, Chen X, Dong F, Li W, Ren X, Zhang Y, et al. Concise review: mesenchymal stem cells and translational medicine: emerging issues. Stem cells translational medicine. 2012 Jan;1(1):51-8. PubMed PMID: 23197640. Pubmed Central PMCID: 3727691.
4. Williams AR, Hare JM. Mesenchymal stem cells: biology, pathophysiology, translational findings, and therapeutic implications for cardiac disease. Circulation research. 2011 Sep 30;109(8):923-40. PubMed PMID: 21960725. Pubmed Central PMCID: 3604746.
5. Mouiseddine M, Francois S, Semont A, Sache A, Allenet B, Mathieu N, et al. Human mesenchymal stem cells home specifically to radiation-injured tissues in a non-obese diabetes/severe combined immunodeficiency mouse model. The British journal of radiology. 2007 Sep;80 Spec No 1:S49-55. PubMed PMID: 17704326.
6. Nagaya N, Fujii T, Iwase T, Ohgushi H, Itoh T, Uematsu M, et al. Intravenous administration of mesenchymal stem cells improves cardiac function in rats with acute myocardial infarction through angiogenesis and myogenesis.

American journal of physiology Heart and circulatory physiology. 2004 Dec;287(6):H2670-6. PubMed PMID: 15284059.

7. Djouad F, Bouffi C, Ghannam S, Noel D, Jorgensen C. Mesenchymal stem cells: innovative therapeutic tools for rheumatic diseases. Nature reviews Rheumatology. 2009 Jul;5(7):392-9. PubMed PMID: 19568253.
8. Zacharek A, Chen J, Cui X, Li A, Li Y, Roberts C, et al. Angiopoietin1/Tie2 and VEGF/Flk1 induced by MSC treatment amplifies angiogenesis and vascular stabilization after stroke. Journal of cerebral blood flow and metabolism : official journal of the International Society of Cerebral Blood Flow and Metabolism. 2007 Oct;27(10):1684-91. PubMed PMID: 17356562. Pubmed Central PMCID: 2796470.
9. Bian S, Zhang L, Duan L, Wang X, Min Y, Yu H. Extracellular vesicles derived from human bone marrow mesenchymal stem cells promote angiogenesis in a rat myocardial infarction model. J Mol Med (Berl). 2014 Apr;92(4):387-97. PubMed PMID: 24337504.
10. Nassiri SM, Rahbarghazi R. Interactions of mesenchymal stem cells with endothelial cells. Stem Cells Dev. 2014 Feb 15;23(4):319-32. PubMed PMID: 24171705.
11. Dominici M, Le Blanc K, Mueller I, Slaper-Cortenbach I, Marini F, Krause D, et al. Minimal criteria for defining multipotent mesenchymal stromal cells. The International Society for Cellular Therapy position statement. Cytotherapy. 2006;8(4):315-7. PubMed PMID: 16923606.

12. Delorme B, Ringe J, Pontikoglou C, Gaillard J, Langonne A, Sensebe L, et al. Specific lineage-priming of bone marrow mesenchymal stem cells provides the molecular framework for their plasticity. Stem cells. 2009 May;27(5):1142-51. PubMed PMID: 19418444.
13. Kaltz N, Ringe J, Holzwarth C, Charbord P, Niemeyer M, Jacobs VR, et al. Novel markers of mesenchymal stem cells defined by genome-wide gene expression analysis of stromal cells from different sources. Experimental cell research. 2010 Oct 1;316(16):2609-17. PubMed PMID: 20599957.
14. Rostovskaya M, Anastassiadis K. Differential expression of surface markers in mouse bone marrow mesenchymal stromal cell subpopulations with distinct lineage commitment. PloS one. 2012;7(12):e51221. PubMed PMID: 23236457. Pubmed Central PMCID: 3517475.
15. Pevsner-Fischer M, Levin S, Zipori D. The origins of mesenchymal stromal cell heterogeneity. Stem cell reviews. 2011 Sep;7(3):560-8. PubMed PMID: 21437576.
16. Roobrouck VD, Ulloa-Montoya F, Verfaillie CM. Self-renewal and differentiation capacity of young and aged stem cells. Experimental cell research. 2008 Jun 10;314(9):1937-44. PubMed PMID: 18439579.
17. Xu J, Woods CR, Mora AL, Joodi R, Brigham KL, Iyer S, et al. Prevention of endotoxin-induced systemic response by bone marrow-derived mesenchymal stem cells in mice. Am J Physiol Lung Cell Mol Physiol. 2007 Jul;293(1):L131-41. PubMed PMID: 17416739.

18. Gupta N, Su X, Popov B, Lee JW, Serikov V, Matthay MA. Intrapulmonary delivery of bone marrow-derived mesenchymal stem cells improves survival and attenuates endotoxin-induced acute lung injury in mice. J Immunol. 2007 Aug 1;179(3):1855-63. PubMed PMID: 17641052.
19. Rojas M, Xu J, Woods CR, Mora AL, Spears W, Roman J, et al. Bone marrow-derived mesenchymal stem cells in repair of the injured lung. Am J Respir Cell Mol Biol. 2005 Aug;33(2):145-52. PubMed PMID: 15891110. Pubmed Central PMCID: 2715309.
20. Ortiz LA, Dutreil M, Fattman C, Pandey AC, Torres G, Go K, et al. Interleukin 1 receptor antagonist mediates the antiinflammatory and antifibrotic effect of mesenchymal stem cells during lung injury. Proc Natl Acad Sci U S A. 2007 Jun 26;104(26):11002-7. PubMed PMID: 17569781. Pubmed Central PMCID: 1891813.
21. Griffith LM, Pavletic SZ, Tyndall A, Gratwohl A, Furst DE, Forman SJ, et al. Target populations in allogeneic hematopoietic cell transplantation for autoimmune diseases--a workshop accompanying: cellular therapy for treatment of autoimmune diseases, basic science and clinical studies, including new developments in hematopoietic and mesenchymal stem cell therapy. Biology of blood and marrow transplantation : journal of the American Society for Blood and Marrow Transplantation. 2006 Jun;12(6):688-90. PubMed PMID: 16737943.
22. Jeong JA, Hong SH, Gang EJ, Ahn C, Hwang SH, Yang IH, et al. Differential gene expression profiling of human umbilical cord blood-derived

mesenchymal stem cells by DNA microarray. Stem cells. 2005 Apr;23(4):584-93. PubMed PMID: 15790779.

23. Phinney DG, Hill K, Michelson C, DuTreil M, Hughes C, Humphries S, et al. Biological activities encoded by the murine mesenchymal stem cell transcriptome provide a basis for their developmental potential and broad therapeutic efficacy. Stem cells. 2006 Jan;24(1):186-98. PubMed PMID: 16100003.
24. De Luca A, Roma C, Gallo M, Fenizia F, Bergantino F, Frezzetti D, et al. RNA-seq analysis reveals significant effects of EGFR signalling on the secretome of mesenchymal stem cells. Oncotarget. 2014 Nov 15;5(21):10518-28. PubMed PMID: 25344915. Pubmed Central PMCID: 4279390.
25. Roson-Burgo B, Sanchez-Guijo F, Del Canizo C, De Las Rivas J. Transcriptomic portrait of human Mesenchymal Stromal/Stem cells isolated from bone marrow and placenta. BMC genomics. 2014;15:910. PubMed PMID: 25326687. Pubmed Central PMCID: 4287589.
26. Tsai MS, Hwang SM, Chen KD, Lee YS, Hsu LW, Chang YJ, et al. Functional network analysis of the transcriptomes of mesenchymal stem cells derived from amniotic fluid, amniotic membrane, cord blood, and bone marrow. Stem cells. 2007 Oct;25(10):2511-23. PubMed PMID: 17556597.
27. Eirin A, Riester SM, Zhu XY, Tang H, Evans JM, O'Brien D, et al. MicroRNA and mRNA cargo of extracellular vesicles from porcine adipose tissue-

derived mesenchymal stem cells. Gene. 2014 Nov 1;551(1):55-64. PubMed PMID: 25158130. Pubmed Central PMCID: 4174680.

28. Jaager K, Fatkina A, Velts A, Orav E, Neuman T. Variable expression of lineage regulators in differentiated stromal cells indicates distinct mechanisms of differentiation towards common cell fate. Gene. 2014 Jan 1;533(1):173-9. PubMed PMID: 24103479.
29. Li J, Ma Y, Teng R, Guan Q, Lang J, Fang J, et al. Transcriptional profiling reveals crosstalk between mesenchymal stem cells and endothelial cells promoting prevascularization by reciprocal mechanisms. Stem cells and development. 2015 Mar 1;24(5):610-23. PubMed PMID: 25299975. Pubmed Central PMCID: 4333618.
30. Charbord P. Bone marrow mesenchymal stem cells: historical overview and concepts. Human gene therapy. 2010 Sep;21(9):1045-56. PubMed PMID: 20565251.
31. Hu M, Krause D, Greaves M, Sharkis S, Dexter M, Heyworth C, et al. Multilineage gene expression precedes commitment in the hemopoietic system. Genes & development. 1997 Mar 15;11(6):774-85. PubMed PMID: 9087431.
32. Huang S. Reprogramming cell fates: reconciling rarity with robustness. BioEssays : news and reviews in molecular, cellular and developmental biology. 2009 May;31(5):546-60. PubMed PMID: 19319911.

33. Huang S, Guo YP, May G, Enver T. Bifurcation dynamics in lineage-commitment in bipotent progenitor cells. Developmental biology. 2007 May 15;305(2):695-713. PubMed PMID: 17412320.

34. Kalisky T, Quake SR. Single-cell genomics. Nature methods. 2011 Apr;8(4):311-4. PubMed PMID: 21451520.

35. Zhang W, Ou G, Hamrick M, Hill W, Borke J, Wenger K, et al. Age-related changes in the osteogenic differentiation potential of mouse bone marrow stromal cells. J Bone Miner Res. 2008 Jul;23(7):1118-28. PubMed PMID: 18435580. Pubmed Central PMCID: 2679384.

36. Trivedi P, Hematti P. Simultaneous generation of CD34+ primitive hematopoietic cells and CD73+ mesenchymal stem cells from human embryonic stem cells cocultured with murine OP9 stromal cells. Exp Hematol. 2007 Jan;35(1):146-54. PubMed PMID: 17198883. Epub 2007/01/03. eng.

37. Delcarpio JB, Lanson NA, Jr., Field LJ, Claycomb WC. Morphological characterization of cardiomyocytes isolated from a transplantable cardiac tumor derived from transgenic mouse atria (AT-1 cells). Circ Res. 1991 Dec;69(6):1591-600. PubMed PMID: 1954678.

38. Trapnell C, Roberts A, Goff L, Pertea G, Kim D, Kelley DR, et al. Differential gene and transcript expression analysis of RNA-seq experiments with TopHat and Cufflinks. Nat Protoc. 2012 Mar;7(3):562-78. PubMed PMID: 22383036. Pubmed Central PMCID: 3334321.

39. Huang da W, Sherman BT, Lempicki RA. Bioinformatics enrichment tools: paths toward the comprehensive functional analysis of large gene lists.

Nucleic Acids Res. 2009 Jan;37(1):1-13. PubMed PMID: 19033363. Pubmed Central PMCID: 2615629.

40. Huang da W, Sherman BT, Lempicki RA. Systematic and integrative analysis of large gene lists using DAVID bioinformatics resources. Nat Protoc. 2009;4(1):44-57. PubMed PMID: 19131956.
41. Tsujita Y, Muraski J, Shiraishi I, Kato T, Kajstura J, Anversa P, et al. Nuclear targeting of Akt antagonizes aspects of cardiomyocyte hypertrophy. Proc Natl Acad Sci U S A. 2006 Aug 8;103(32):11946-51. PubMed PMID: 16882732. Pubmed Central PMCID: 1567678.
42. Livak KJ, Schmittgen TD. Analysis of relative gene expression data using real-time quantitative PCR and the 2(-Delta Delta C(T)) Method. Methods. 2001 Dec;25(4):402-8. PubMed PMID: 11846609.
43. Baksh D, Yao R, Tuan RS. Comparison of proliferative and multilineage differentiation potential of human mesenchymal stem cells derived from umbilical cord and bone marrow. Stem cells. 2007 Jun;25(6):1384-92. PubMed PMID: 17332507.
44. Foudah D, Monfrini M, Donzelli E, Niada S, Brini AT, Orciani M, et al. Expression of neural markers by undifferentiated mesenchymal-like stem cells from different sources. Journal of immunology research. 2014;2014:987678. PubMed PMID: 24741639. Pubmed Central PMCID: 3987801.
45. Foudah D, Redondo J, Caldara C, Carini F, Tredici G, Miloso M. Expression of neural markers by undifferentiated rat mesenchymal stem cells. Journal of

biomedicine & biotechnology. 2012;2012:820821. PubMed PMID: 23093867. Pubmed Central PMCID: 3474592.

46. Foudah D, Redondo J, Caldara C, Carini F, Tredici G, Miloso M. Human mesenchymal stem cells express neuronal markers after osteogenic and adipogenic differentiation. Cellular & molecular biology letters. 2013 Jun;18(2):163-86. PubMed PMID: 23430457.
47. Chateauvieux S, Ichante JL, Delorme B, Frouin V, Pietu G, Langonne A, et al. Molecular profile of mouse stromal mesenchymal stem cells. Physiological genomics. 2007 Apr 24;29(2):128-38. PubMed PMID: 17179208.
48. Kolf CM, Cho E, Tuan RS. Mesenchymal stromal cells. Biology of adult mesenchymal stem cells: regulation of niche, self-renewal and differentiation. Arthritis research & therapy. 2007;9(1):204. PubMed PMID: 17316462. Pubmed Central PMCID: 1860068.
49. Brambrink T, Foreman R, Welstead GG, Lengner CJ, Wernig M, Suh H, et al. Sequential expression of pluripotency markers during direct reprogramming of mouse somatic cells. Cell Stem Cell. 2008 Feb 7;2(2):151-9. PubMed PMID: 18371436. Pubmed Central PMCID: 2276627.
50. Funari VA, Day A, Krakow D, Cohn ZA, Chen Z, Nelson SF, et al. Cartilage-selective genes identified in genome-scale analysis of non-cartilage and cartilage gene expression. BMC genomics. 2007;8:165. PubMed PMID: 17565682. Pubmed Central PMCID: 1906768.

51. James CG, Stanton LA, Agoston H, Ulici V, Underhill TM, Beier F. Genome-wide analyses of gene expression during mouse endochondral ossification. PLoS One. 2010;5(1):e8693. PubMed PMID: 20084171. Pubmed Central PMCID: 2805713.

52. Ng F, Boucher S, Koh S, Sastry KS, Chase L, Lakshmipathy U, et al. PDGF, TGF-beta, and FGF signaling is important for differentiation and growth of mesenchymal stem cells (MSCs): transcriptional profiling can identify markers and signaling pathways important in differentiation of MSCs into adipogenic, chondrogenic, and osteogenic lineages. Blood. 2008 Jul 15;112(2):295-307. PubMed PMID: 18332228.

53. Park KW, Waki H, Kim WK, Davies BS, Young SG, Parhami F, et al. The small molecule phenamil induces osteoblast differentiation and mineralization. Mol Cell Biol. 2009 Jul;29(14):3905-14. PubMed PMID: 19433444. Pubmed Central PMCID: 2704753.

54. Tanaka T, Yoshida N, Kishimoto T, Akira S. Defective adipocyte differentiation in mice lacking the C/EBPbeta and/or C/EBPdelta gene. EMBO J. 1997 Dec 15;16(24):7432-43. PubMed PMID: 9405372. Pubmed Central PMCID: 1170343.

55. Zaidi M. Skeletal remodeling in health and disease. Nat Med. 2007 Jul;13(7):791-801. PubMed PMID: 17618270.

56. English K, Barry FP, Mahon BP. Murine mesenchymal stem cells suppress dendritic cell migration, maturation and antigen presentation. Immunology letters. 2008 Jan 15;115(1):50-8. PubMed PMID: 18022251.

57. English K, French A, Wood KJ. Mesenchymal stromal cells: facilitators of successful transplantation? Cell stem cell. 2010 Oct 8;7(4):431-42. PubMed PMID: 20887949.

58. English K, Mahon BP. Allogeneic mesenchymal stem cells: agents of immune modulation. Journal of cellular biochemistry. 2011 Aug;112(8):1963-8. PubMed PMID: 21445861.